U.S. Department of Energy, Office of Fossil Energy

Produced Water and Waste Heat-aided Blowdown Water Treatment: Using Chemical and Energy Synergisms for Value Creation

Project Final Report

Principal Investigator:
Lian-Shin (Lance) Lin, PhD
Professor, Civil and Environmental Engineering
West Virginia University
lianshin.lin@mail.wvu.edu
304-293-9935

Co-Investigators
Harry Finklea (WVU, Chemistry)
Hailin Li (WVU, Mechanical and Aerospace Engineering)
Fernando Lima (WVU, Chemical Engineering)
Paul Ziemkiewicz (WV Water Research Institute)

West Virginia University Research Corporation DUN's Number: 191510239 886 Chestnut Ridge Road, P.O. Box 6845 Morgantown, WV 26506-6845

Submitted to:
U.S. Department of Energy
National Energy Technology Laboratory

July 30, 2022

Executive Summary

The project objective was to develop a cooling blowdown water (BDW) treatment process utilizing produced water (PW) and low-grade heat to maximize water reuse and saleable by-product generation while reducing chemical and energy footprints of the treatment. The proposed treatment process consists of mixing, softening, organics and suspended solids removal, reverse osmosis (RO), thermal desalination, and brine electrolysis. BDW samples collected from a local coal-fired power plant and PW samples from two shale gas production wells were used in this study. Each treatment unit was first designed and tested to quantify its treatment efficiency, and its chemical and energy requirements. In addition, a process model was developed and model simulations were conducted based on the experimental results and literature data to optimize the treatment process. A techno-economic analysis was conducted to quantify chemical and energy savings as well as production of 10-lb brine as a saleable product.

With the field-collected BDW and PW samples, mixing experiments determined a volumetric mixing ratio 10:1 (BDW:PW) resulted in the best performance of multivalent ions removal and largest chemical savings for softening. Softening of the BDW/PW mixtures using alkaline chemicals (Na₂CO₃ and NaOH) achieved 95%-100% removal of scaling-forming cations (Ca, Mg, Fe, Ba, Sr) and 60% of silicon, and 10% of total organic carbon (TOC). The mixing and softening treatments yielded an effluent with total dissolved solids (TDS) concentration of 23 g/L. Activated carbon (AC) filtration removed TOC to a low level (< 3 mg/L) and further removed remaining scale-forming divalent metals and silica from the softened water. The AC filtration resulted in a slight reduction of TDS from 23 g/L to 20 g/L, leaving behind only mostly monovalent ions (i.e., sodium and chloride) in the filtered water. These pretreatments yielded a feed water that met the criteria of the downstream reverse osmosis (RO) to prevent membrane fouling.

A cross-flow RO system was used to further concentrate the TDS of the AC effluent. Various factors including TDS, pH, and applied pressure were examined and optimal conditions were determined for the co-treatment process. An integrated process consisting of mixing, softening, AC filtration and RO was used to treat a continuous flow (0.25-1.2 L/min, or 0.07-0.32 gpm) and successfully generated RO permeate as product water (TDS < 0.5 g/L) for reuse in cooling operation, and a concentrate (TDS ~ 45 g/L) to be further treated in a thermal desalination unit. These flow rates meet the FOA's criterion of 0.01-1 gpm. Overall, the co-treatment of BDW/PW allowed shorter ramp-up time compared to treatment of BDW alone. It resulted in 40% and 55% savings of Na₂CO_{3(s)} and NaOH, respectively, compared to treating the BDW and PW individually for the same level of softening. The co-treatment also resulted in a 29% energy saving compared to treatment of BDW only for the level of TDS concentration.

A thermal desalination system was designed using CFD simulations and manufactured in the WVU Innovation Hub for further treatment of the RO concentrate to generate 10-lb brine. The system has a design flow rate of 2 gpm and has been successfully tested. A bench-scale brine electrolysis system was developed for on-site generation of chlorine/hypochlorite (Cl₂/OCl⁻) and caustic soda (NaOH) as useful chemicals for the co-treatment process. Using salt solutions (0.5 M and 1 M), the system achieved faradaic efficiencies of 93%-97% and 70%-77% for caustic soda and chlorine/hypochlorite generation, respectively. An economic analysis showed that the

electricity costs for on-site generation of these chemicals were significantly lower than the chemical prices offered by suppliers.

An industrial-scale process model consisting of mixing, softening, AC filtration, RO, thermal desalination, and brine electrolysis was developed using the Aspen Plus V9 in conjunction with Aspen Custom Modeler V9. The model serves as a solvable Aspen Plus model and as basis to form the costing infrastructure. In addition, techno-economic analysis considering capital, operating, and transportation costs was conducted. An optimization solution showed that produced water for mixing is still advantageous in low quantities. The optimum solution approaches a leveled cost of water (LCW) of 2 \$/m³ which becomes cost competitive with nominal water treatment prices.

Table of Contents

Executive Summary	1
Task 1.0 – Project Management and Planning	8
Task 1.1 Project Management Plan	8
Task 1.2 Technology Maturation Plan	8
Task 2.0 – Produced water-aided blowdown water treatment with alkaline chemicals	8
Task 3.0 – Removal of organics and suspended solids using activated carbon filtration	12
Task 4.0 – Product water and concentrate generation using reverse osmosis	14
Task 4.1 – Electrodialysis for RO concentrate treatment (additional work beyond the origonal scope of the project)	_
Task 5.0 – Waste heat-aided thermal desalination to generate 10-lb brine	26
5.1. Design and objectives of the thermal desalination system	27
5.2. Preliminary examination of thermal desalination system	29
5.3. Preliminary design of the shell-tube heat exchanger	30
5.4. Simulation of the shell-tube heat exchanger using CFD	30
5.5. Shell-tube heat exchanger fabrication and testing	32
5.6. Thermal desalination system assembling	34
Task 6.0 – Brine electrolysis for caustic soda and chlorine production	36
Task 7.0 – Integration of treatment units	43
Task 8.0 – Process Modeling and Simulations	49
8.1. Process Modeling and Simulations Objective	
8.2. Solution Approach	50
8.3. Modeling and Simulation Strategies	51
8.3.1. Software Implementation	51
8.3.2. Process Scale	52
8.3.3. Defining Water Properties	
8.3.4. Softening and Filtration	54
8.3.5. Reverse Osmosis	54
8.3.6. Thermal Desalination	56
8.3.7. Electrolysis	58
8.3.8. Summary	59
8.4. Process Analysis	60
8.4.1. Techno-Economic Analysis	60

8.4.2. Sustainability Assessment
8.5. Optimization
8.5.1. Optimization Strategy
8.6. Results and Conclusions
References74
List of Figures
Figure 2-1. Laboratory-scale softening treatment unit
treatment
Figure 4-1. (A) Laboratory-scale RO system and (B) schematic of the RO system
function of current

Figure 5-5. Fluid zones in Ansys mesh
Figure 5-6. Temperature distribution on the cross section of the shell-tube heat exchanger 3
Figure 5-7. Velocity distribution in the designed heat exchanger
Figure 5-8. Heat flux distribution in the designed heat exchanger
Figure 5-9. Heat Exchanger Design in Solidworks Environment
Figure 5-10. Heat exchanger undergoing pressure testing (top left), stainless steel tubes befor
assembly (top right), and internal frame of the heat exchanger (bottom)
Figure 5-11. Steam canner for steam generation
Figure 5-12. Condensing coil bucket
Figure 5-13. Schematic diagram of the integrated thermal desalination system
Figure 5-14. Photo of the fabricated thermal desalination system
Figure 6-1. Galvanodynamic scans for the cell with the N2050WX membrane. (A) 0.5 M Nac
catholyte, 0.5 M NaCl + 0.2 M NaHCO $_3$ anolyte; (B) 1.0 M NaCl catholyte, 1.0 M NaCl + 0.
M NaHCO ₃ anolyte. Scan from 0 to 1930 to 0 mA at 20 mA/s. The blue lines are data, an
the orange lines are quadratic fits of voltage to current above 500 mA. Quadratic equation
are (A) $E(V) = (-0.00328)I^2 + (0.8046)I + (1.398)$ and (B) $E(V) = (-0.01442)I^2 + (0.6137)I$
(1.400)
Figure 6-2. Galvanostatic plots of voltage vs time for the N2050WX membrane in two sets of
solutions using a current of 1.936 A (80 mA/cm ²). Catholyte solution compositions ar
shown in the legend; the anolyte solutions also contain 0.2 M NaHCO ₃ 3
Figure 6-3. Galvanostatic plots of voltage vs time for the four membranes in (A) 0.5 M NaCl an
(B) 1.0 M NaCl 4
Figure 6-4. Galvanodynamic scan for membrane N966WX in 1 M NaCl. Scan from 0 to 1930 to
mA at 20 mA/s 4
Figure 6-5. Faradaic efficiencies for production of NaOH (A) and NaOCI (B) in two sets of
solutions4
Figure 6-6. Specific energies for the production of NaOH (A) and NaOCl (B) in two sets of
solutions4
Figure 7-1. The integrated process consists of softening treatment (a), activated carbon filtratio
(b), reverse osmosis (c), and flow diversion from RO concentrate for the therma
desalination unit (d) for continuous treatment
Figure 7-2. TDS concentrations during RO treatment and diverted flow from the RO reject stream
(y1-axis); RO permeate and diverted flow rates (y2-axis) under an applied pressure of 90
psi (62 bar) and continuous operation for (a) the co-treatment of BDW and PW, and (b) th
BDW alone 4
Figure 7-3. RO reject TDS level and permeate flow for a single-pass RO desalination under a
applied pressure of 900 psi (62 bar) for the continuous co-treatment of BD and PW 4
Figure 9.1. Modular process arrangement for water treatment defined in project arranged.
Figure 8-1. Modular process arrangement for water treatment defined in project proposal 5 Figure 8-2. Software workflow integrated with the proposed unit designs. Here software
packages are outlined in dashed boxes and connectivity is shown by solid black lines 5 Figure 8-3. Regression results for determining σ , Ps, and k
Tigure 0-3. Negression results for determining 0, F3, and K

total initial volume of diluate and concentrate (600 mL). Faradaic efficiency is b	
transfer coefficient of Na	
Table 4-7. Specific costs of diluate for the first stage.	25
Table 5-1. TDS of further concentrated rundown water through thermal evaporati	on process.
	29
Table 5-2. Design Parameters	30
Table 5-3. Specifications of the designed shell and tube heat exchanger.	30
Table 5-4. Specifications of the steam canner	
Table 5-5. Condensing coil bucket specifications	
Table 6- 1. Performance metrics for the four Chemours membranes	39
Table 6-2. Average cell ohmic resistance, membrane resistance and membrane vom MA/cm ²	_
Table 6- 3. Estimated cost of production in \$/kg for NaOH and NaOCI.	
Table 7-1. Continuous treatment performance at the steady-state condition.	47
Table 7- 2. Chemicals requirement for the pretreatment of BD-PW mixture and the	eir separate
treatments	47
Table 8-1. Operating costs summary	64
Table 8-2. Capital cost summary	66
Table 8-3. GREENSCOPE indicators selected for sustainable design assessment (Ruiz-	
al., 2012)	67
Table 8-4. Custom indicators added for sustainable design assessment	68
Table 8-5. Decision variables of the process optimization	70

Task 1.0 – Project Management and Planning Task 1.1 Project Management Plan

Approach

This task shall include all work elements required to maintain and revise the Project Management Plan, and to manage and report on activities in accordance with the plan. It shall also include the necessary activities to ensure coordination and planning of the project with DOE/NETL and other project participants. These shall include, but are not limited to, the submission and approval of required National Environmental Policy Act (NEPA) documentation.

Results and Discussion

The Project Management Plan (PMP) - submitted to NETL

Task 1.2 Technology Maturation Plan

Approach

The task developed a Technology Maturation Plan (TMP) that describes the current technology readiness level (TRL) of the proposed technology/technologies, relates the proposed project work to maturation of the proposed technology, and describes known post-project work necessary to further increase the technology TRL level.

Results and Discussion

The Technology Maturation Plan (TMP) – submitted to NETL.

Task 2.0 – Produced water-aided blowdown water treatment with alkaline chemicals Approach

This task was to develop a produced water-aided blowdown water treatment with softening. A range of volumetric mixing ratios of the produced water (PW) and blowdown water (BDW) samples was subjected to Jar tests to measure pH changes and the removal efficiency of scale-forming constituents. The NaOH solution used to raise to the pH of the PW-BD water mixtures to different end points for further removal of scale-forming constituents. The softening treatment will also be conducted with soda ash (Na₂CO₃) addition for comparison. The softened effluent will be analyzed, and the softening efficiency will be quantified as a function of pH end points of the mixture. The softening treatment will be conducted in both batch and continuous modes. Settling characteristics of the chemical precipitates will be examined for designing a continuous softening unit.

Methods and Materials

BDW samples withdrawn from the recirculating cooling operation at the Longview

thermoelectric power plant (Maidsville, Lat: 39.7075 N; Long: -79.9567 W) was collected for the study. PW samples were collected from two local Marcellus Shale gas wells (i) Morgantown Industrial Park (Lat: 39.6090 N; Long: -79.9777 W) and (ii) Northeast Natural Energy Boggess Site (Lat: 39.6671 N; Long: -80.0968 W) in West Virginia. The untreated wastewater samples were analyzed in the lab as received to characterize their chemical composition following the Standard Methods (APHA, 1998).

A range of BDW/PW volumetric ratio (2, 5, and 10) was tested in bench-scale experiments to determine optimal mixing conditions using a mixing tank and another tank for collecting supernatant (**Figure 2-1**). PW were mixed at different volumetric ratios (BD/PW = 2, 5, and 10) to examine removal of divalent ions. Both the supernatant and the chemical precipitates from the mixing of two waters were collected for analyses. Specifically, supernatant samples were analyzed for sulfate and divalent metals (i.e., Al, Ba, Ca, Fe, Mg, Mn, Si, and Sr). The chemical precipitates (solids) were characterized for their morphology, chemical composition using a scanning electron microscopy (SEM, Hitachi, S-4700) equipped with energy dispersive spectroscopy (EDS, PV7746/58 ME, EDAX Inc., Mahwah, NJ, USA) for chemical composition.



Figure 2-1. Laboratory-scale softening treatment unit.

The remaining scale-forming or hardness causing constituents (i.e., Ca, Mg, Ba, Sr, etc.) in the BDW/PW mixtures were removed by chemical softening using sodium carbonate (Na₂CO₃)

and NaOH. Specifically, Na₂CO₃ was added at a molar concentration equal to the total hardness of the mixture water. The total hardness of the sample was calculated as the total of major multivalent cations including calcium, magnesium, barium, strontium, and iron. In addition, a concentrated sodium hydroxide (NaOH, 5M) was used to raise the pH of the BDW/PW mixtures to ~12 to remove magnesium. Our previous study has shown that such a treatment removes major cations in PW including Ca, Mg, Ba, Sr, Mn, and Al through chemical precipitation (Khajouei et al., 2021). The BDW/PW mixtures were then subject to 5-min rapid mixing followed by 60-min slow mixing to promote formation of solid flocs. The solids were then allowed enough time to settle without mixing. The supernatant (i.e., softened water) was sampled and filtered using 0.22μm mixed cellulose ester membranes (GSWP, Millipore Sigma) and analyzed for pH, total dissolved solids (TDS), total organic carbon (TOC, Shimadzu TOC-L), divalent metals, sulfate, chloride, and silica to determine the effectiveness of the softening process.

Results and Discussion

The chemical composition of the BDW and PW samples are listed in **Table 2-1**.

Table 2-1. The chemical composition of cooling blowdown and produced water samples.

Parameters	BDW, Mean ± STD	PW, Mean ± STD
рН	8.1±0.2	6.0±0.4
Total Dissolved Solids (TDS, g/L)	2.5±0.7	249±17
Total organic carbon (TOC, mg/L)	15±7	12±1.7
Sulfate (SO ₄ ²⁻ , mg/L)	800±130	<2.1
Silica (SiO ₂ , mg/L)	14±11	16.0±1.4
Chloride (Cl ⁻ , mg/L)	128±29	80,500 ± 9,400
Calcium (Ca ²⁺ , mg/L)	171±8	20,000 ± 5,000
Magnesium (Mg ²⁺ , mg/L)	46±5	1,900 ± 300
Barium (Ba ²⁺ , mg/L)	0.3±0.4	7,100 ± 1,800
Strontium (Sr ²⁺ , mg/L)	1.3±0.5	4,400 ± 300
Total iron (mg/L)	<0.01	90 ± 10
Aluminum (Al ²⁺ , mg/L)	<0.001	0.1 ±0.1
Manganese (Mn ²⁺ , mg/L)	<0.001	4.2 ± 4.0

Given the mean chemical compositions (**Table 2-1**), a stoichiometric ratio of sulfate to Ba would require approximately 6 volumes of BDW per volume of PW. In one specific example (**Table 2-2**), the stoichiometric ratio of sulfate to Ba would be achieved by mixing 10 volumes of BDW (7.3 mM sulfate) with 1 volume of PW (80.1 mM Ba). The volumetric BDW/PW mixing ratio of 10:1 resulted in the removal of 90% and 70% of barium and sulfate, respectively. Furthermore, it brought the pH to near neutral (*i.e.*, pH = 6.9) and raised the BDW TDS concentration from 1.8 g/L to 23 g/L in the mixture (**Table 2-2**). This ratio consistently produced a mixture TDS

concentration ~20 g/L from different field-collected water samples (data not shown). The softening treatment further removed of the scale-forming divalent cations (95% to ~100%) (i.e., Ca, Mg, Ba, Sr, and Fe) and 60% removal of silicon (60%). The chemical softening only removed ~10% TOC.

Table 2-2. The chemical composition in mixed, softened, and AC filtered water.

Parameter	PW	BDW	Mixing (10:1) ^a	Softening	AC filtration
рН	5.7	7.3	6.9	12.1	10.5
TDS (g/L)	230	1.8	23	~23	20
TOC (mg/L)	13	16	14.5	~15	<3 (90%)
Sulfate (mg/L)	< 0.01	700	215 (70%)	225	202
Calcium (Ca, mg/L)	14,000	160	1,900	2.3 (100%)	0.04 (98%)
Magnesium (Mg, mg/L)	1,600	50	200	0.16 (100%)	0.02 (88%)
Barium (Ba, mg/L)	11,000	0.1	100 (90%)	2.0 (98%)	<0.02 (100%)
Strontium (Sr, mg/L)	4,800	1.6	480	6.0 (99%)	<0.01 (100%)
Iron (Fe, mg/L)	80	< 0.01	4.0	0.2 (95%)	0.15 (15%)
Silicon (Si, mg/L)	10.5	9.0	18	7.0 (60%)	7.0 (60%)
Lithium (Li, mg/L)	30	<0.048	6.0	5.8	2.9 (50%)

Note. Percentages in parentheses are percent removal as a result of the treatment unit. aVolumetric mixing ratio of BDW to PW is 10 to 1. AC filtration was done after the softening treatment.

The results of softening were supported by SEM-EDS analysis (**Figure 2-2**). The SEM micrographs showed more particles attached to the surface of probably carbon particles after softening. According to EDS analysis, an increased abundance of Mg after softening is highly significant.

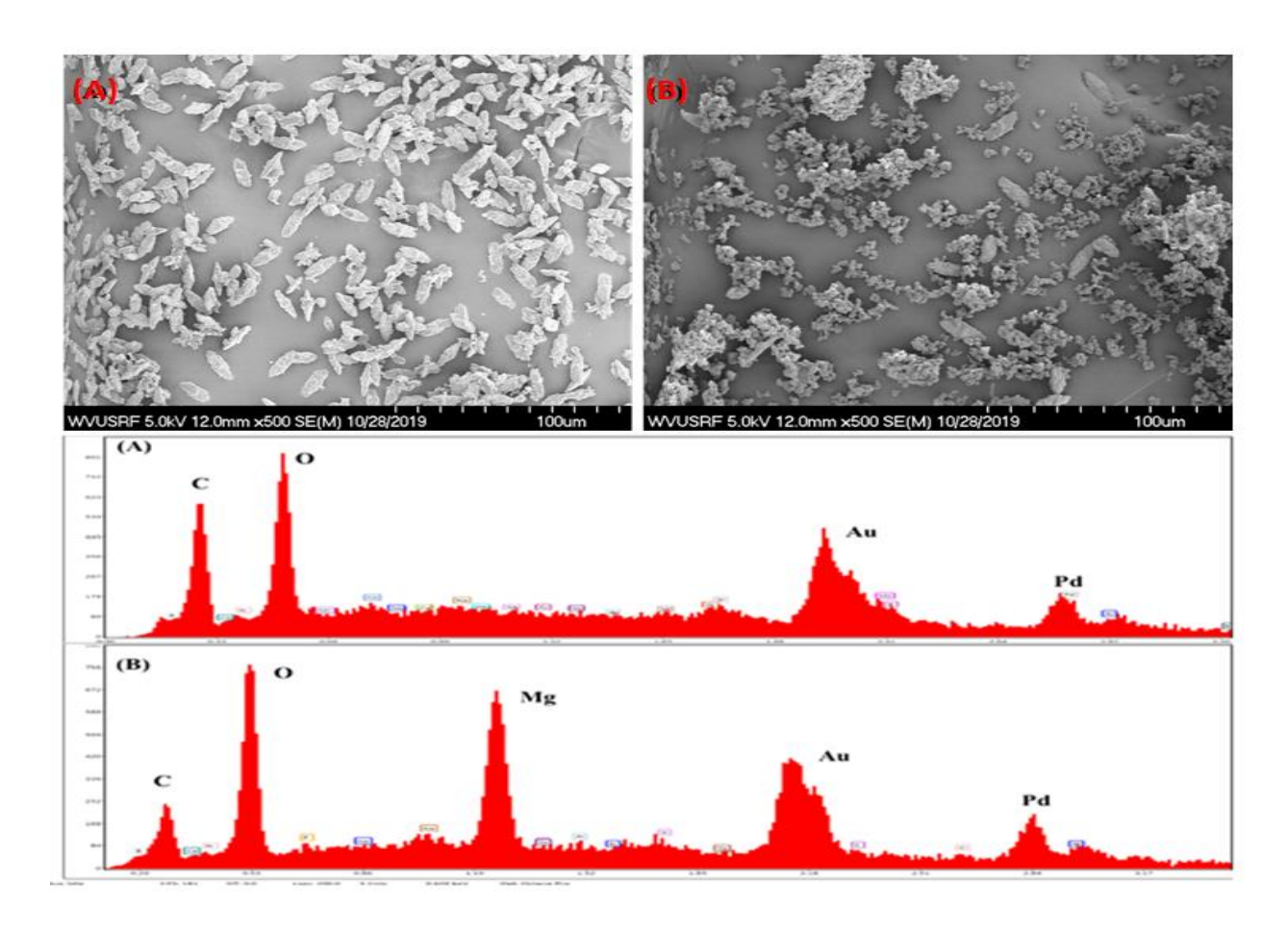


Figure 2-2. EDS-SEM of chemical precipitates generated from BDW and PW mixing at a ratio 10:1 A) before softening and B) after softening.

Products

G. Khajouei, H. I. Park, H. O. Finklea, P. F. Ziemkiewicz, E. F. Peltier, and L.-S. Lin, Produced water softening using high-pH catholyte from brine electrolysis: reducing chemical transportation and environmental footprint, *Journal of Water Process Engineering*, 40, 101911, 2021, https://doi.org/10.1016/j.jwpe.2020.101911.

Task 3.0 – Removal of organics and suspended solids using activated carbon filtration Approach

The softened water (i.e., effluent collected from the softening unit) was treated by activated carbon (AC) to condition the water for downstream RO treatment. Specifically, AC filtration was used to remove remaining suspended solids (SS) and organics to meet the criteria of RO feed water to prevent membrane fouling.

Methods and Materials

Two different activated carbon (AC) filtration systems for batch and continuous operation

were set up for the removal of organic matters. The system for batch operation consisted of five filters (Thermo Scientific Barnstead Organic Removal Cartridge, D0813, 17.5×3.4 in, **Figure 3-1A**) and the softened water was circulated from the supernatant tank into the AC system using a hydraulic pump (Danfoss, APP 2.2). The flow rate was adjusted to 0.35 L/min to provide a retention time of approximately 10 minutes required for reducing the total organic carbon (TOC) concentration of the solution to less than 3 mg/L. This retention time was obtained from preliminary experiments and TOC less than 3 mg/L was one of the criteria for RO feed water.

For the single-pass treatment operation, the system was scaled up and designed based on the 10-minutes retention time and a maximum flow rate of 2 L/min. The scaled-up system consisted of four PVC pipes (4 ft \times 4 in) filled with granular activated carbon (**Figure 3-1B**). The softened water was fed at a flow rate ranged ranging from 0.30 L/min (0.08 gpm) to 0.90 L/min (0.24 gpm) using a commercial pump (Danfoss APP 2.2 Pump). The AC filtered water was collected and analyzed for total organic carbon (TOC) concentration measurement using a total carbon analyzer. In addition, the filtrate was used to determine silt density index (SDI) using a 0.45 μ m membrane filter under a constant applied pressure (30 psi, 0.21 MPa) following the ASTM D 4189-82 Standard Test Method.

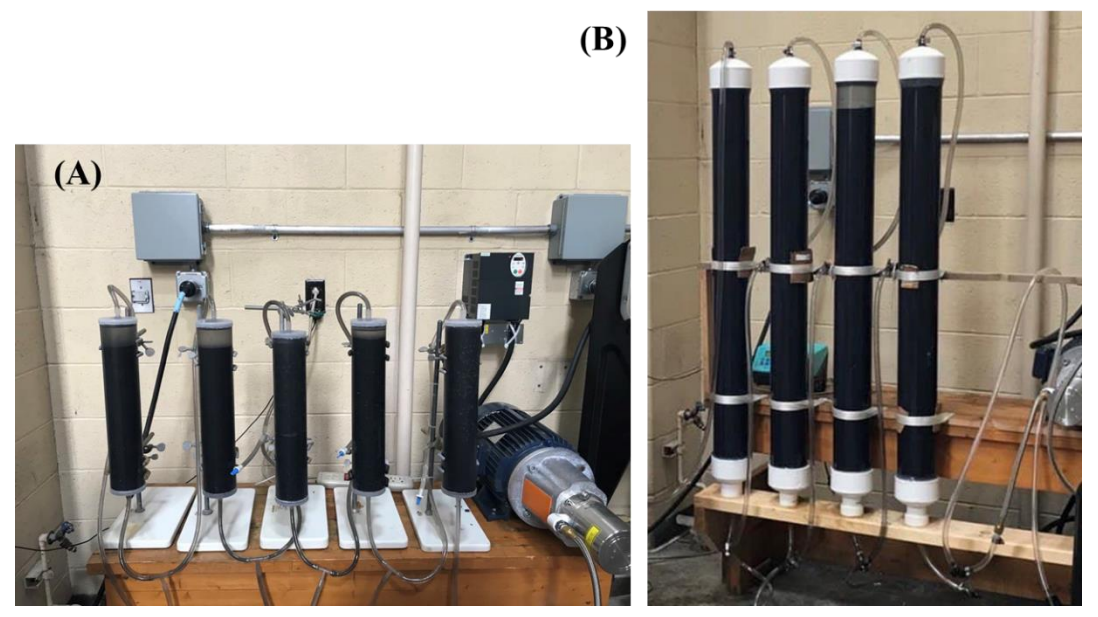


Figure 3-1. Activated carbon filtration system for (A) batch and (B) single-pass continuous water treatment.

Results and Discussion

The AC filtration removed organic compounds from the softened water to a TOC content < 3.0 mg/L (**Table 2-2**). This is critical for the downstream RO treatment as it requires very low TOC content to preventing biofouling on the RO membrane. In addition to TOC removal, the AC

filtration further removed the remaining scale-forming divalent metals and silica from the softened water. The low value of SDI (<5) determined from the rate plugging of AC filtered water indicated the low potential of silt deposition on the membrane surface as well. The AC treatment also resulted in a slight reduction of TDS from 23 g/L to 20 g/L, leaving behind only mostly monovalent ions (i.e., sodium and chloride) in the filtered water.

Task 4.0 – Product water and concentrate generation using reverse osmosis Approach

The effluent from the AC filtration was treated by a laboratory-scale reverse osmosis (RO) unit to generate low-salinity permeate for water reuse and a concentrate stream to be treated by a thermal desalination unit for further water recovery and brine generation.

Method and Materials

A cross-flow RO unit was used for all membrane separation experiments to recover water and concentrate TDS (Figure 4-1). Specifically, a commercial high rejection seawater RO desalination (SWRO) membrane (Applied Membrane, Inc, Model No. M-S2514A) was used. The membrane had the following specifications: maximum operating pressure, 69 bar (1000 psi); maximum operating temperature, 45°C; feedwater pH range, 2-11; continuous operation; maximum feed silt density index (SDI), 5; zero chlorine tolerance; minimum salt rejection, 99.2%; stabilized salt rejection, 99.6%; single element recovery, 2%; and maximum feed flow rate, 1.36 m³/hr (6 gpm). The above benchmark values are based on the following condition: 32,000 mg/L sodium chloride, 55.2 bar (800 psi), 25°C, and pH 8. The RO system consisted of a high-pressure pump (Pentair Hypro 2220B-P) which was spinning at 1725 rpm (feedwater flowrate was around 7.9 L/min), cartridge filter, pressure relief valve, membrane cell, membrane cell holder, highpressure concentrate control valve, pressure indicator, feed tank, permeate collection tank, and connections/tubings. Water temperature in the feed was kept below 30 °C by circulating the water through a spiral stainless-steel tubing placed in a bucket of ice water before entering the RO feed tank. The RO treatment was operated in a recirculating mode in which the concentrate stream was returned to the feed tank and permeate water was collected in a separate tank. The TDS concentration in the feed tank gradually increased during the operation because of the concentration effect and decrease in the volume of the feed tank. The required pressure in the membrane cell was adjusted by the concentrate control valve. Membrane operating pressures tested in this study were 34.5 bar (500 psi), 48 bar (700 psi), and 62 bar (900 psi). Between experiments, the membrane was rinsed by circulating distilled water for one hour, three times. In addition, warm acidic distilled water (pH = 2, T = 40°C) was circulated through the system for one hour followed by a one-hour circulation of warm distilled water (T = 40°C) to remove any scales from the membrane when needed. Both batch and continuous modes of treatment operation were employed in this study. In the batch mode, 70 liters of pre-treated water after softening and AC filtration was stored in the feed tank and fed to the RO unit at a flow rate of ~ 2 gallons per minute (gpm). To study the effect of pH on the RO treatment, a set of experiments with initial pH of 8.5 and applied pressure of 900 psi was conducted to compare with the results of experiments with initial pH of 10.5 under the pressure of 900 psi.

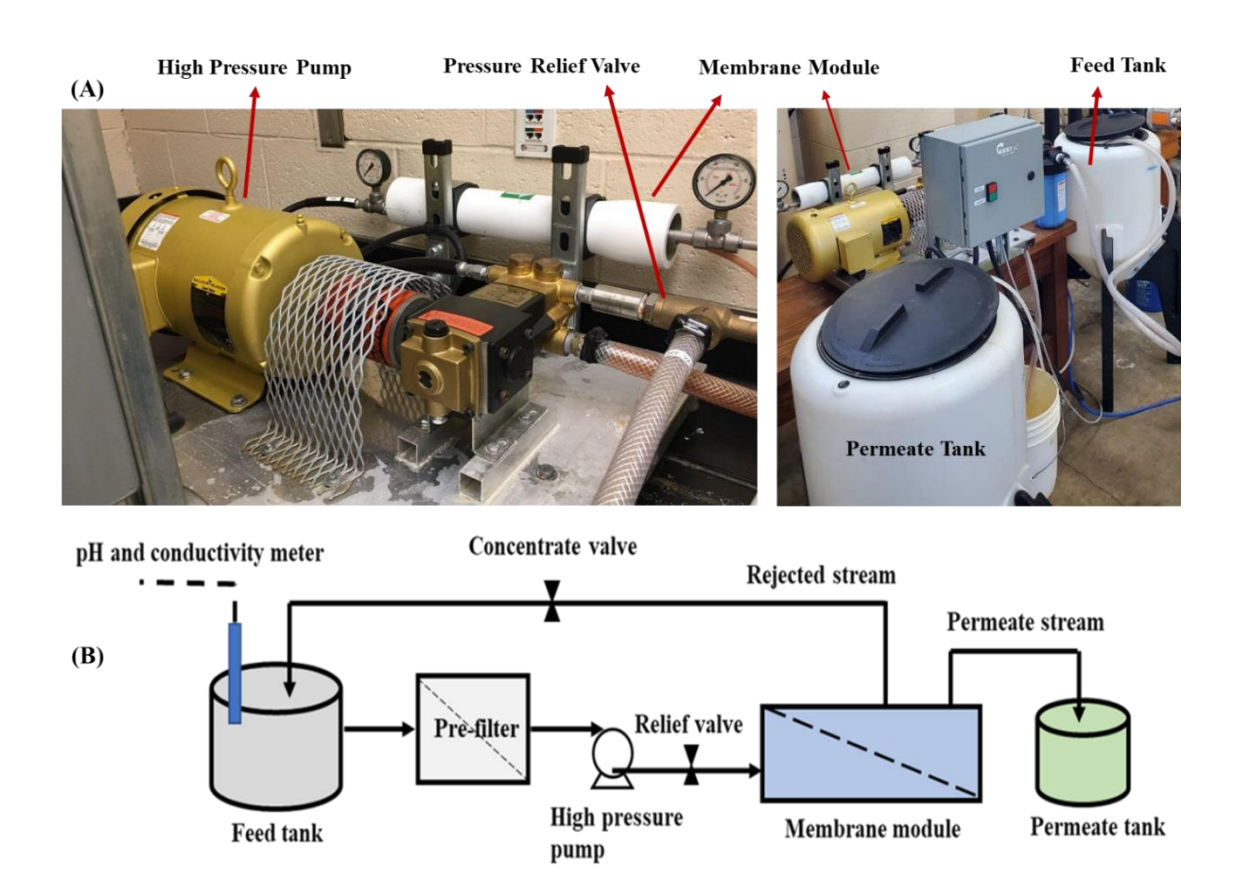


Figure 4-1. (A) Laboratory-scale RO system and (B) schematic of the RO system.

Results and Discussion

BDW/PW mixtures

In all experiments, the initial volume of the pre-treated water was ~70 L. Figure 4-2 shows how TDS increased during the RO treatment of the BDW/PW mixture under different applied pressures. The initial TDS of the mixture was ~17 g/L corresponding to the osmotic pressure of 200 psi and an initial pH of ~ 10.5. As the applied pressure increased, the difference between hydrostatic pressure and osmotic pressure increased. This pressure difference across the membrane is the driving force for the water to move against the natural direction of the osmosis. As the applied pressure increased, the final TDS concentration of the rejected water, as well as the flow rate of permeate water increased (Figure 4-3). Similarly, the TDS of permeate water increased as applied pressure increased due to increased salinity at the membrane surface which resulted in an increase in salt transport through the membrane. The salt rejection (Rs) which is a measure of overall membrane system performance and is calculated by Equation 1, was approximately 99% in all experiments (Table 4-1). However, the concentration factor (ratio of the concentrate TDS to the feed TDS) increased as applied pressure increased and was ~ 3 under feed pressure of 900 psi.

$$R_s = \left(1 - \frac{c_{permeat}}{\frac{c_{feed} + c_{concentrate}}{2}}\right) \times 100$$
 Equation 1

As the RO applied pressure and thus the pressure difference increased, the permeate water flow rate and consequently the overall water recovery of the treatment increased (**Table 4-1**). However, during the operation, the permeate flow gradually decreased as the salinity of the water increased, and consequently, the cross-membrane pressure difference decreased. Also, it was observed that the TDS concentration of the permeate water was slightly higher under higher applied pressure (**Table 4-1**).

RO treatment of BDW/PW continued till the permeate flow rate reached as low as the flow rate of approximately 0.15 L/min. At this point, the rate of TDS increases in concentrate slowed down significantly due to the high osmotic pressure of the water and a significant decrease in pressure difference. It can be noted from **Figure 4-2** that higher applied pressure and thus higher-pressure difference led to the higher rate of TDS increase and shorter operation time.

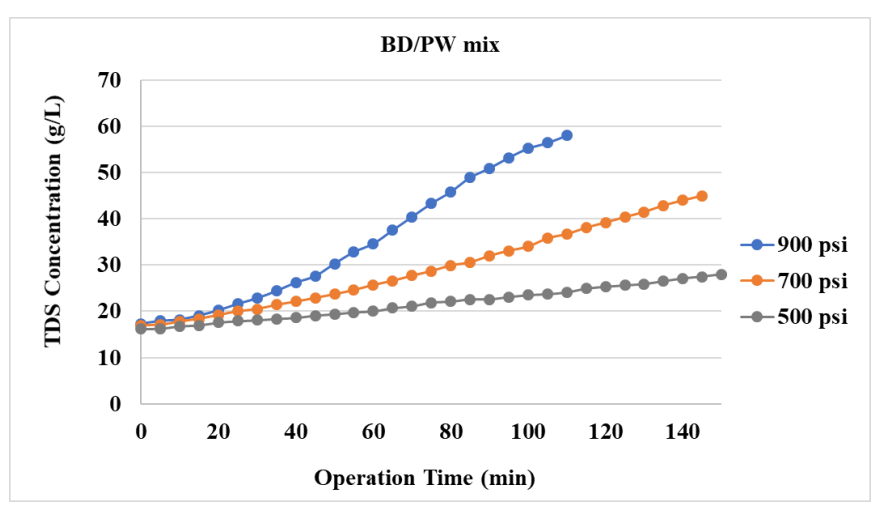


Figure 4-2. TDS concentration of feed water during RO desalination of BDW/PW mixture under applied pressures of 500, 700, and 900 psi.

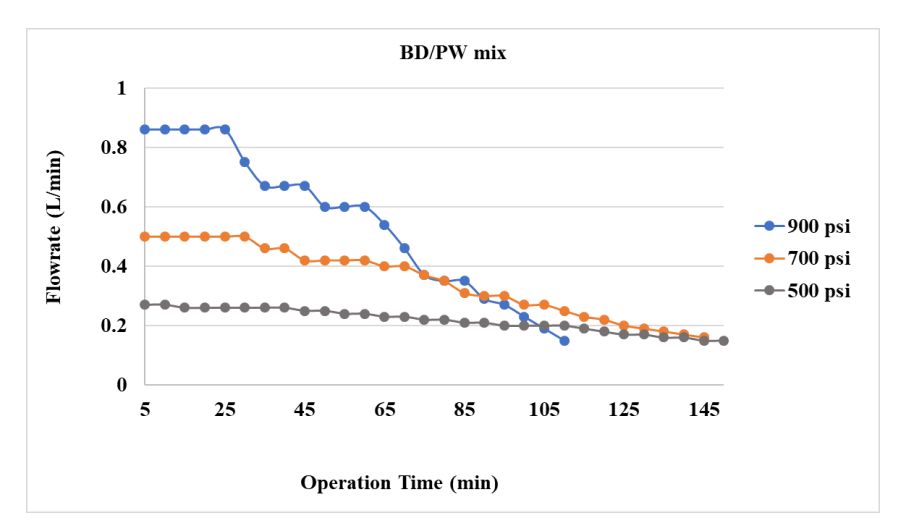


Figure 4-3. Permeate flow rate during RO treatment of BDW/PW mixture under applied pressures of 500, 700, and 900 psi.

The water recovery by the RO system was calculated by dividing the final volume of the permeate water by the initial volume of the feed water. In addition to the overall water recovery, the water recovery during 100 mins and 60 minutes of operation under different applied pressures was calculated (**Table 4-1**). It should be mentioned that according to the literature, reverse osmosis recovery varies from 35% to 85% depending on the feed water composition and salinity, pretreatment, concentrate disposal options, and optimum energy design configuration. The overall water of BDW/PW treatment under an applied pressure of 900 psi was 79%. **Table 4Table 4-1-1** also shows that due to higher water recovery at higher applied pressure the unit energy consumption of the system (kWh/L of permeate water) was lower despite higher overall power consumption (kW). At the end of the operation, the concentrate and permeate waters were analyzed for their main characteristics (**Table 4-2**). The concentrations of chemicals in the permeate water were very low and ready for reuse or discharge to surface waters.

Table 4-1. Salt rejection, concentration factor, water recovery, and final TDS concentration of permeate and concentrate after RO treatment of BD/PW under different applied pressures.

BD/PW Mix	Applied Pressure		
	500 psi	700 psi	900 psi
Final TDS concentration of the concentrate (g/L)	28	45	58
Salt rejection	99%	99%	99%
Concentration factor	1.7	2.6	3.4
Operation time (min)	150	145	110
Water recovery	48%	71%	79%
Water recovery of 100-min operation	34%	59%	84%
Water recovery of 60-min operation	22%	40%	63%
Final TDS concentration of the permeate (g/L)	0.64	0.68	0.73
Power (Watt)	896	1128	1307
Unit energy consumption (kWh/L)	0.07	0.05	0.04
Unit energy consumption of 100-min operation (kWh/L)	0.06	0.05	0.04
Unit energy consumption of 60-min operation (kWh/L)	0.06	0.04	0.03

Table 4-2. Chemical characteristics of permeate and concentrate from BDW/PW RO treatment.

BD/PW	Permeate			С	oncentrate	•
	500 psi	700 psi	900 psi	500 psi	700 psi	900 psi
Ca (mg/L)	<0.1	<0.1	<0.1	4.1	7.2	4.3
Mg (mg/L)	<0.04	<0.04	<0.04	<0.04	<0.04	0.07
Ba (mg/L)	<0.007	<0.007	<0.007	0.5	0.9	0.2
Sr (mg/L)	0.009	0.01	0.02	3.1	5.7	2.9
Fe (mg/L)	<0.06	<0.06	<0.06	0.16	0.19	0.12
Si (mg/L)	0.2	0.16	0.19	22.4	27.0	47.6
TOC (mg/L)	0.65	0.45	0.80	3.1	3.5	5.0

BDW alone

Similar to the BDW/PW RO treatment, for BDW treatment, the initial volume was ~70L and the initial pH of the water was adjusted to ~10.5. Three different feed pressures (500, 700, and 900 psi) were applied as well to evaluate the treatment performance.

While the TDS concentration of the feed water for the BDW/PW treatment leveled off to a steady state, the treatment of BD water alone showed a sharp increase in the TDS concentration (**Figure 4-4**). As feed pressure increased, the rate of TDS increment increased with a significantly higher rate at the feed pressures of 900 and 700 psi compared to 500 psi. In all of the RO experiments, the salt rejection was >99% and the concentration factor was ~ 5 under the applied pressure of 700 and 900 psi (**Table 4-3**).

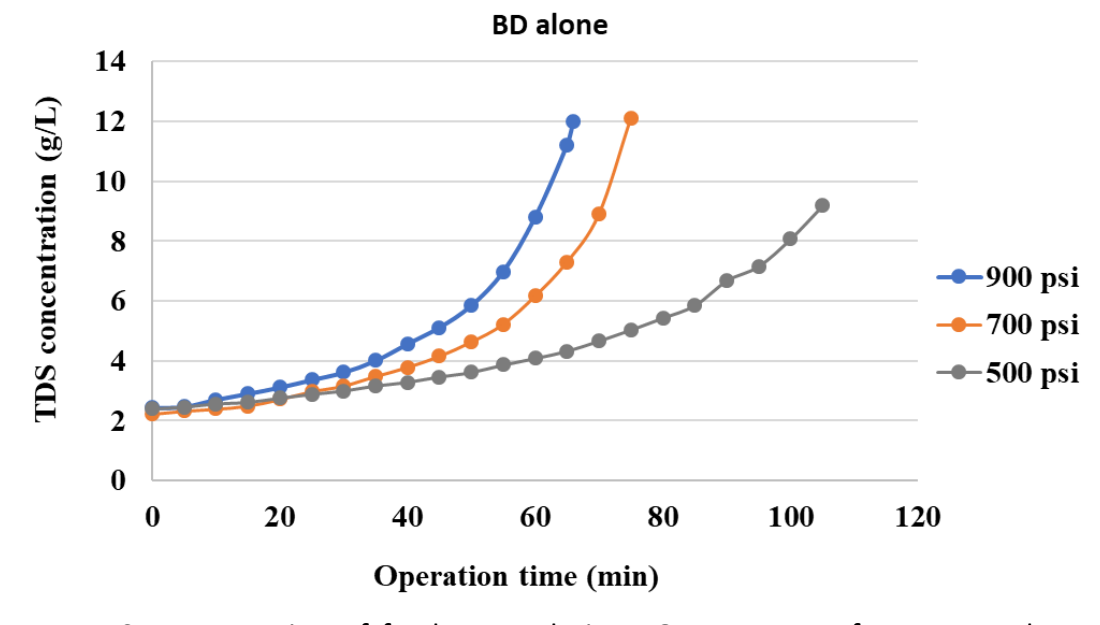


Figure 4-4. TDS concentration of feed water during RO treatment of BD water alone under applied pressures of 500, 700, and 900 psi.

Due to the significantly higher applied pressures than the osmotic pressure of the water, the permeate flow rate remained constant during the operation (**Figure 4-5**). Because of the limited amount of water, the operation continued until the water volume in the feed tank reached $^{\sim}10$ L. At this point, the volume of permeate water was $^{\sim}60$ L corresponding to 85% water recovery. In the case of a large volume of water being available, the membrane treatment of BD water can be pushed to the limit of the RO to generate a concentrate with a TDS concentration of approximately $^{\sim}40$ g/L ($^{\sim}500$ psi). Water recovery in all experiments was 85%. W alone, the permeate flow rate increased with the applied pressure, and consequently, the operation time decreased.

The analysis of permeate water at the end of the treatment showed that the concentration of divalent ions and organic matters was negligible and permeate water was suitable for reuse (**Table 4-4**).

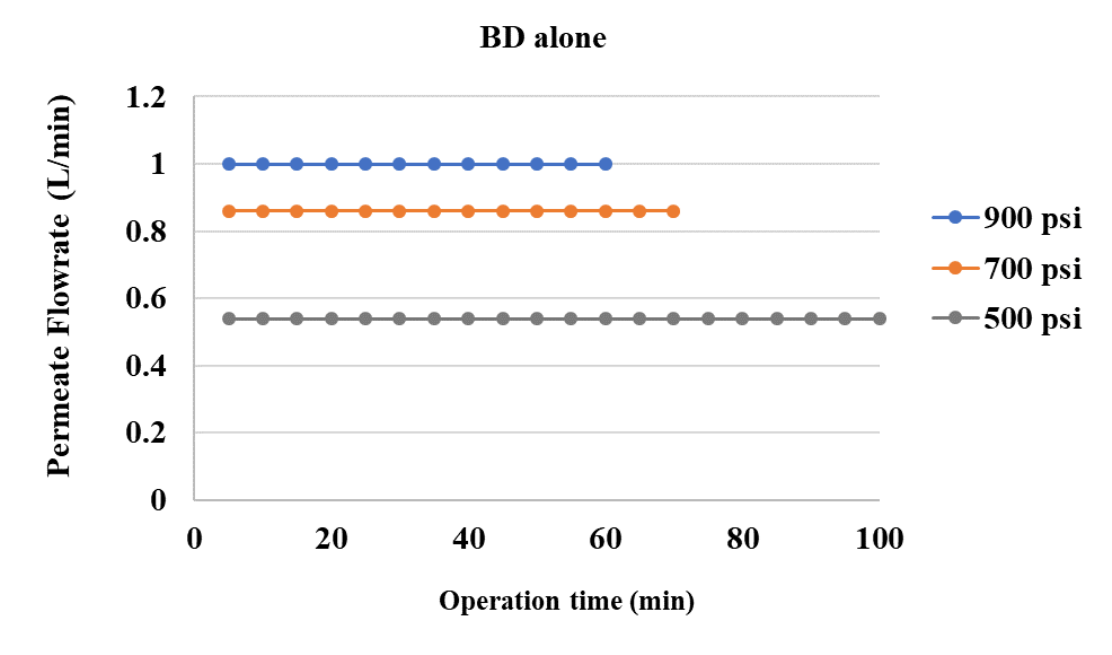


Figure 4-5. Permeate flow rate during RO treatment of BD water under the applied pressures of 500, 700, and 900 psi.

Table 4-3. Salt rejection, concentration factor, water recovery, and final TDS concentration of permeate and rejected streams after RO treatment of BD water under different applied pressures.

BD water	Applied Pressure		
	500 psi	700 psi	900 psi
Final rejected TDS concentration (g/L)	9	12	12
Salt rejection	99%	99%	99%
Concentration factor	3.7	5.4	5
Operation time (min)	105	75	66
Water recovery	85%	85%	85%
Water recovery of 60 min operation	46%	74%	85%
Final permeate TDS concentration (g/L)	0.04	0.04	0.034
Power (Watt)	890	1095	1340
Unit energy consumption (kWh/L)	0.028	0.023	0.025
Unit energy consumption of 60-min operation (kWh/L)	0.027	0.021	0.022

Table 4-4. Characteristics of permeate and rejected water of BD water RO treatment.

BDW/PW	Permeate Water			Rej	ected Wat	ter
	500 psi	700 psi	900 psi	500 psi	700 psi	900 psi
Ca (mg/L)	<0.112	0.2	<0.112	2.4	8.0	3.0
Mg (mg/L)	<0.04	<0.04	<0.04	0.1	0.7	0.1
Ba (mg/L)	<0.007	<0.007	<0.007	0.1	0.3	0.2
Sr (mg/L)	0.002	0.005	<0.002	1.1	4.7	1.8
Fe (mg/L)	<0.061	<0.061	<0.061	<0.061	0.143	0.068
Si (mg/L)	0.16	0.2	0.1	51	65	44
TOC (mg/L)	0.5	0.5	0.2	7.4	10	12

pH Effects

In the case of BDW/PW co-treatment, the TDS concentration of the concentrate was slightly higher at initial pH of 8.5 during the first 60-min operation. However, after that, the two pHs tested did not show any significant difference in TDS of the RO reject (**Figure 4-6**). The effect of pH on the permeate flow rate of BDW/PW was also not consistent with BDW alone and most of the time was higher at the pH of 10.5 (**Figure 4-7**). In contrast, pH effects were more significant in the case of RO treatment of BDW alone than the BDW/PW. Higher TDS concentrations of the RO concentrate and permeate flow rate were observed at pH 8.5 than those at pH 10.5 (**Figures 4-8** and **4-9**).

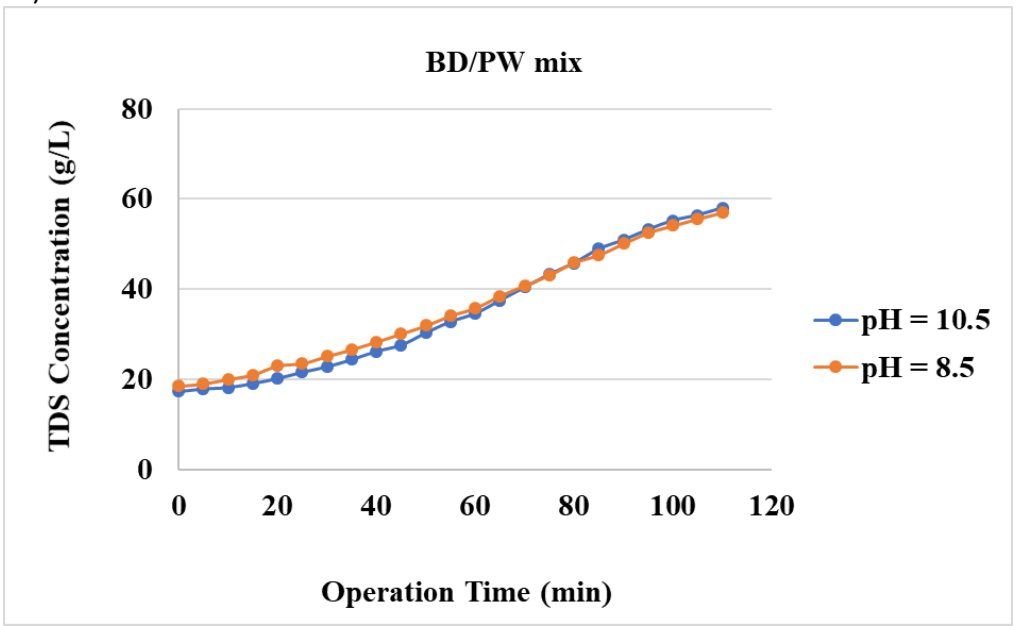


Figure 4-6. TDS concentration of the RO concentrate during BDW/PW membrane treatment under an applied pressure of 900 psi for initial pHs of 10.5 and 8.5.

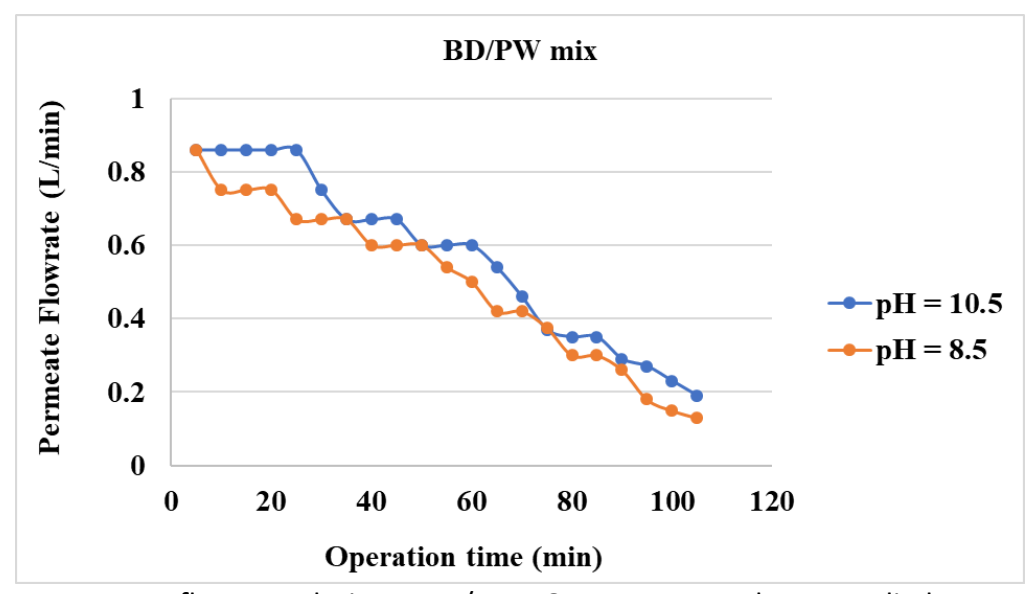


Figure 4-7. Permeate flow rate during BDW/PW RO treatment under an applied pressure of 900 psi for initial pHs of 10.5 and 8.5.

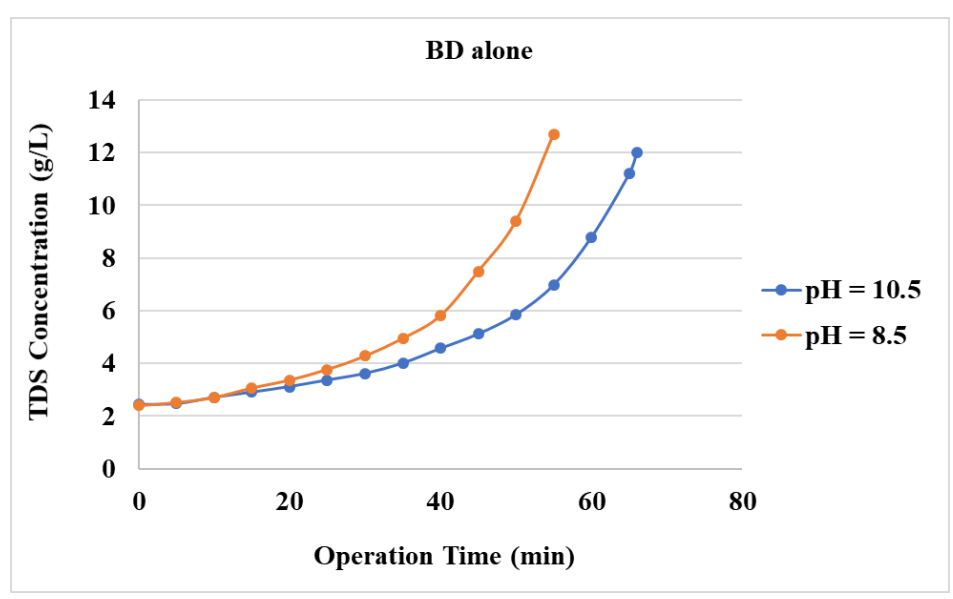


Figure 4-8. TDS concentration of the RO concentrate during BD water RO treatment under an applied pressure of 900 psi for initial pHs of 10.5 and 8.5.

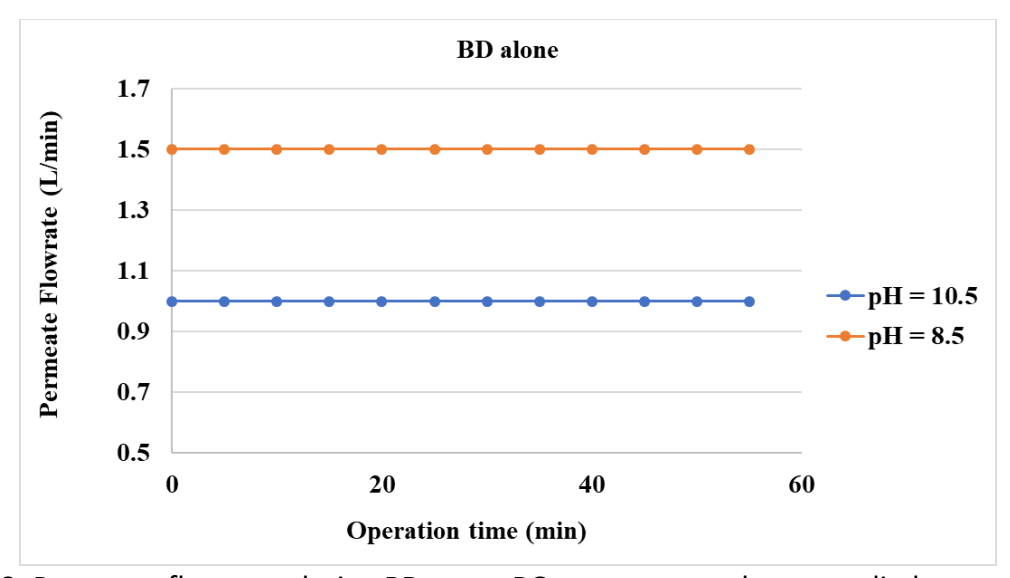


Figure 4-9. Permeate flow rate during BD water RO treatment under an applied pressure of 900 psi for initial pHs of 10.5 and 8.5.

Task 4.1 – Electrodialysis for RO concentrate treatment (additional work beyond the original scope of the project)

In addition to the RO treatment, we explored feasibility of using eletrodialysis (ED) to further concentrate the TDS of the RO concentrate before thermal desalination. The ED system converted the RO concentrate stream (e.g., 50-70 g/L) into a concentrated brine with a target concentration of 200 g/L and a diluate which can be fed into the RO system to further recover

water. The protocol involved use of three stages with intermediate TDS values of 150 and 105 g/L since ED cannot convert 50-70 g/L to 200 g/L in a single pass with reasonable recoveries of diluate and reasonable efficiencies.

The ED system was a PCCell unit with 20 anion-exchange/cation exchange pairs, each with an area of 64 cm² (total area 0.128 m²). The metrics for partial desalination of concentrated brine solutions were determined. Parameters tested included measurement of desalination coulombic efficiency, water recovery, transfer coefficients, specific energies and specific costs of product water for NaCl/NaHCO₃ solutions at concentrations intermediate between 70 and 200 g/L in two stages and at three current densities (~20, 30, and 40 mA/cm²). Sodium bicarbonate was included because the softening step results in excess carbonate present in the solution. ED requires that the pH of the feed solution be less than 9, so carbonate was converted to bicarbonate after adjustment of pH.

Experimental Details

Initial compositions of dilute and concentrate solutions were identical. Electrode rinse solution were 42 g/L NaHCO₃ plus 130 g/L Na₂SO₄. The PCCell system was pre-soaked in the solutions to equilibrate the membranes and the solutions were replaced for the electrolysis. Initial volumes were 500 mL of diluate and 100 mL of concentrate. Electrolysis was performed at constant current (1.2, 1.8 or 2.4 A corresponding to ~20, 30, or 40 mA/cm²) and was stopped at a time required to retain 65-70% of the initial diluate volume. At all three currents, the time was adjusted so that the total charge passed was identical. Electrochemical impedance spectroscopy was used to determine the cell ohmic resistance at open circuit before and after electrolysis. Samples of diluate and concentrate solutions were collected from the diluate and concentrate before and after electrolysis. NaCl and NaHCO₃ concentrations were measured by gravimetry and acid titrations following evaporation of liquid and thermal decomposition of NaHCO₃ to Na₂CO₃.

Results and Discussion

In the first stage, the test solution contained 138 g/L NaCl + 12 g/L NaHCO₃. Voltages remained nearly constant during electrolysis indicating that the cell resistance was dominated by membrane resistances. Ohmic resistance at open circuit decreased after electrolysis, in part because ohmic heating caused the temperature of the cell and solutions to increase by 2 to 4°C.

Figure 4-10 shows the volume of diluate as a function of time and of charge. The plots are not quite linear and the lines are quadratic fits to the data. The curvature indicates that the water transfer coefficient (t_{H2O} = moles of H_2O transferred per mole of electrons) increased with time and charge. This increase was mainly due to increasing rates of osmosis as the diluate concentration decreased and the concentrate concentration increased. Increasing temperature

also contributed to the change in the water transfer coefficient. **Table 4-5** contains the initial, final and average water transfer coefficients.

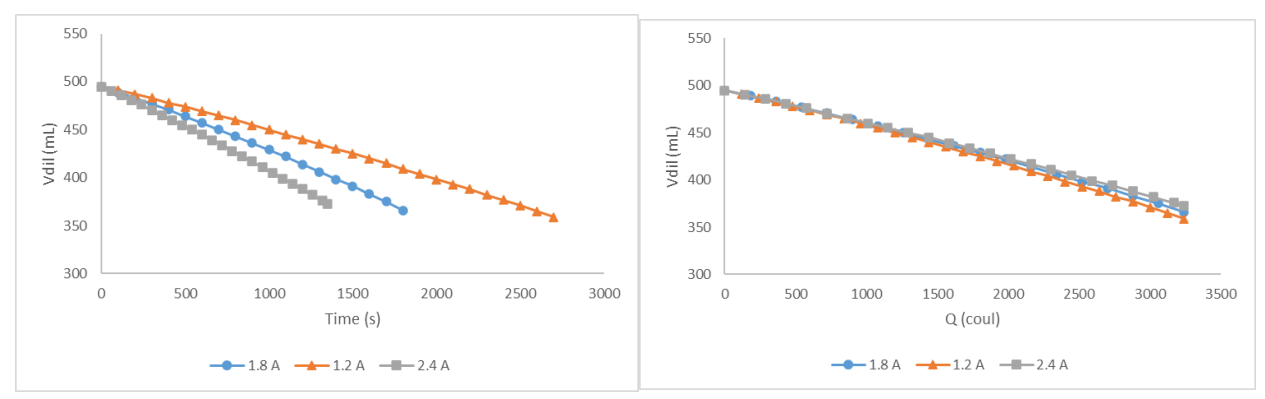


Figure 4-10. Diluate volume vs time (left) and charge passed (right).

Table 4-5. Water transfer coefficients at three currents.

I (A)	initial t	final t	Avg. t
1.2	9.5	13.1	11.3
1.8	8.9	12.5	10.7
2.4	8.9	11.3	10.1

Table 4-6 contains the relevant metrics of desalination for the diluate. Concentrate salinities reached 183, 187 and 196 g/L NaCl and 8.5, 8.8 and 8.9 g/L NaHCO $_3$ for the three currents. As current increased, recovery, faradaic efficiency, and transfer coefficients of Na and Cl all increased slightly and water transfer coefficients and possibly HCO $_3$ transfer coefficients decreased slightly. Specific energy increased almost linearly with respect to current. The transfer coefficients for bicarbonate were anomalously low. Based on electrophoretic mobilities and concentrations, the ratio of t_{Cl}/t_{HCO3} should be 20, whereas the observed ratios were close to 50. Consequently, the concentration of bicarbonate increased in the diluate and decreased in the concentrate relative to the initial concentrations.

Table 4-6. Metrics with respect to current. NaCl and NaHCO₃ final concentrations are in units of g/L, specific energy in kWh/m³ of diluate. Recovery is the final diluate volume relative to the total initial volume of diluate and concentrate (600 mL). Faradaic efficiency is based on the transfer coefficient of Na.

I (A)	NaCl	NaHCO₃	Recovery	SpcEn	FE%	t _{Na}	t _{Cl}	t _{HCO3}
1.2	107.7	14.7	60.3%	17.4	78.0%	0.780	0.764	0.017
1.8	102.1	14.2	60.8%	22.4	79.1%	0.791	0.776	0.015
2.4	102.0	14.3	61.9%	27.2	81.1%	0.811	0.794	0.016

The specific costs of the diluate is tabulated in **Table 4-7**. To determine a specific cost for the diluate, the analyses of the Lienhard group is adopted (McGovern et al., 2014a; 2014b).

 SC_w = specific cost of water in \$/m³.

 $SC_w = C_E + C_C$

 $C_E = cost of energy = K_E * E_w$

 K_E = cost of electricity = \$0.15/kWh.

 E_W = specific energy consumption = $\int V_{ed} I_{ed} dt / V_{fd}$ in kWh/m³

V_{ed} = voltage during electrodialysis, I_{ed} = current during electrodialysis.

 V_{fd} = volume of final diluate.

 C_C = capital cost of equipment = $(\tau)(K_QA_m)/((1/r)(1-(1/(1+r)^T)))$

Tau (τ) = process time for diluate = years/m³

 K_Q = equipment cost per membrane area = \$1500/m² (a guess which does not include the expected cost of installed equipment or the total area of AEM and CEMs; the cost is \$4500/m² according to McGovern et al., 2014a).

 A_m = membrane area of the AEM/CEM pair.

r = annualized cost of capital per year = 10% (0.1)/year

T = estimated plant life = 20 years

With the given values for r and τ , the amortization factor in the C_C denominator = 8.514.

Current 1.2 1.8 2.4 Α m^2 0.128 0.128 0.128 A_{m} \$/kWh K_{E} 0.15 0.15 0.15 \$/m² K_Q 1500 1500 1500 2700 time 1800 1350 8.56x10⁻⁵ 4.28x10⁻⁵ time 5.70x10⁻⁵ year m^3 V_{fd} 3.56x10⁻⁴ 3.59x10⁻⁴ 3.65x10⁻⁴ 0.159 0.240 0.117 years/m³ tau 6.21x10⁻³ 8.03×10^{-3} 9.93×10^{-3} kWh Energy 22.4 kWh/m³ 17.4 27.2 E_{w} \$/m³ CE 2.61 3.36 4.08 CC \$/m³ 5.42 3.58 2.64 \$/m³ Sum 8.03 6.94 6.72

Table 4-7. Specific costs of diluate for the first stage.

Based on the assumptions, an increase in current causes an increase in the energy costs but a decrease in both the capital costs (higher current means that the ED system is smaller) and the total specific costs (**Table 4-7**). Higher currents become more attractive as the equipment

cost per membrane area increases, but it is desirable to avoid reaching limiting current conditions during the electrolysis.

In the second stage, the starting solution was the average composition of the diluate after electrolysis in the first stage (104 g/L NaCl + 14 g/L NaHCO₃). Similar trends in all metrics were observed, with higher recoveries, lower specific energies, higher faradaic efficiencies, and higher transfer coefficients for sodium, chloride, bicarbonate and water. Again, the transfer coefficients for bicarbonate are anomalously low. Final concentrations were 67-70 g/L NaCl + 14 g/L NaHCO₃ for the diluate and 166-179 g/L NaCl + 16 g/L NaHCO₃. **Figure 4-11** shows the specific costs for the second stage using the same assumptions as for the first stage. Overall, it is possible to convert RO reject into 200 g/L brine and recover ~40% of the water for RO processing using three stages of electrodialysis with optimization of conditions for each stage.

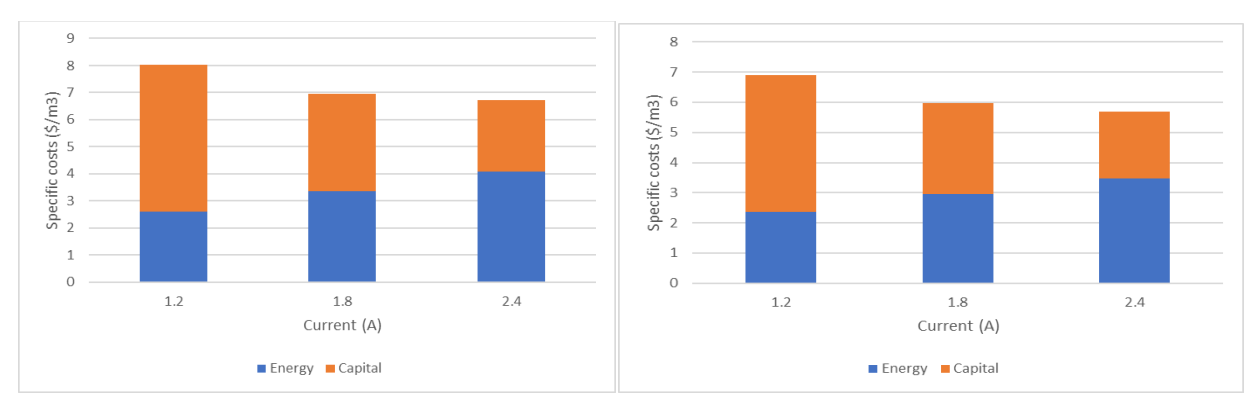


Figure 4-11. Specific costs for the first stage (left) and second stage (right) of desalination as a function of current.

Products

- H. Finklea, L.-S. Lin, and G. Khajouei, Electrodialysis of Softened Produced Water from Shale Gas Development, Journal of Water Process Engineering, 45, 102486, 2022, https://doi.org/10.1016/j.jwpe.2021.102486.
- G. Khajouei, Development of an Innovative Co-treatment Technology for Produced Water and Blowdown Water: A Regional Approach of Water Management for Energy Production, Ph.D. Dissertation, Wadsworth Department of Civil and Environmental Engineering, West Virginia University, July 2022.

Task 5.0 – Waste heat-aided thermal desalination to generate 10-lb brine

Approach

In the task, the TDS concentration of the RO concentrate was further increased through evaporation by heat of low-quality steam from steam engine. The thermal desalination in the cotreatment approach was to further recover water and produce high concentration brine (i.e., 10-lb brine) as products.

5.1. Design and objectives of the thermal desalination system

Figure 5-1 shows the 2-stage thermal desalination system proposed in this project. The key component is a shell-tube heat exchanger with high temperature vapor flows though the tubes as the RO concentrate flows through the shell. The thermal energy heating the feed water in the 1st stage is provided by the low-quality steam extracted from the exit of steam turbine. The thermal energy for the 2nd stage system was provided by the steam at about 100 °C evaporated from the 1st stage system. As shown in **Figure 5-1**, a vacuum pump is needed to create vacuum which helps water to evaporate at lower pressure/temperature in the 2nd stage. This creates a temperature difference for feed water in the shell of the 2nd stage system to evaporate. **Figure 5-2** shows the flow direction and ports for feed water, heating steam, vapor evaporated from the feed water, and the produced brine.

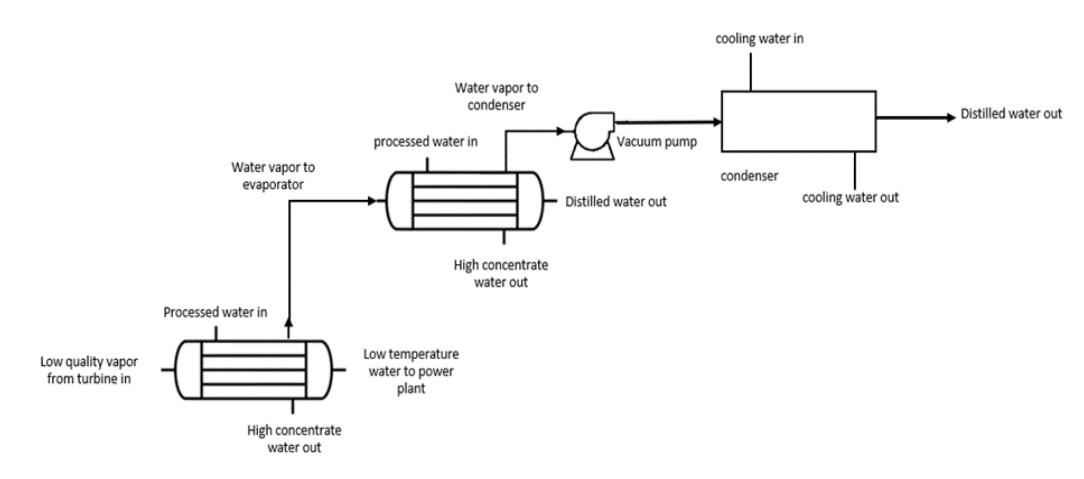


Figure 5-1. The 2-stage process of the thermal desalination system design.

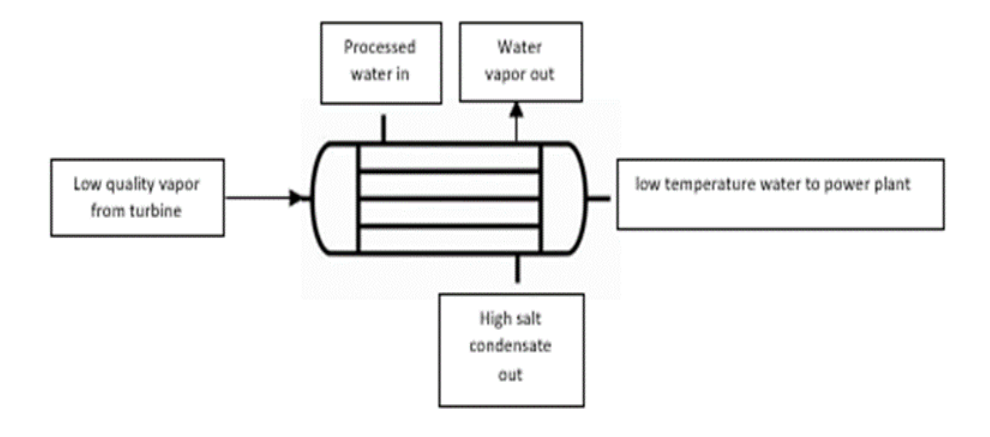


Figure 5-2. The 1st stage process diagram of the desalination system.

The main objective of this work is to design and fabricate a thermal desalination system. The key element to be designed and fabricated is the shell-tube heat exchanger. The primary design work include:

- i. Design and model the heat exchanger in accordance with standard working principles.
- ii. Simulate temperature distribution of the fluids within the shell and tube using CFD.
- iii. Characterize key cost factor and operation parameters such as volume of tube material and pressure drop.

Shell and Tube Heat Exchanger is one of the popular types of heat exchanger due to the flexibility the designer must allow for a wide range of pressures and temperatures. A shell and tube exchanger consists of several tubes mounted inside a cylindrical shell. **Figure 5-3** illustrates a typical unit that may be found in a petrochemical plant, in which one fluid flows over the outside of the tubes in the shell while the second fluid flows through the tubes. The fluids can be either single or two phase and can flow in a parallel or a cross/counter flow arrangement.

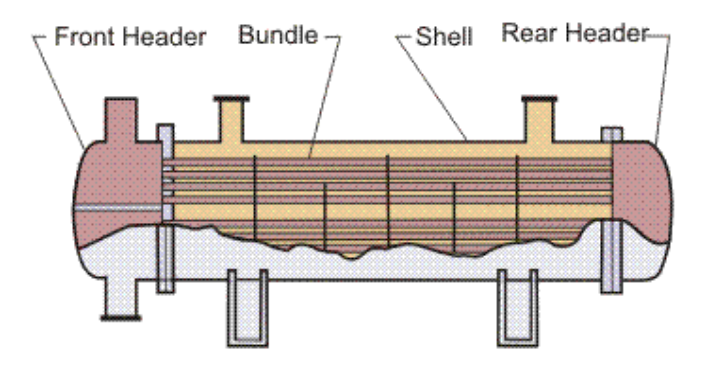


Figure 5-3. Typical shell & tube heat exchanger

The shell and tube exchanger consists of four major parts:

- Front Header—this is where the fluid enters the tube side of the exchanger. It is sometimes referred to as the Stationary Header.
- Rear Header—this is where the tube side fluid leaves the exchanger or where it is returned to the front header in exchangers with multiple tube side passes.
- Tube bundle—this comprises of the tubes, tube sheets, baffles, and tie rods etc. to hold the bundle together.
- Shell—this contains the tube bundle.

The design assumed 2 bar steam at temperature above 120.21 degrees Celsius at the inlet of the heat exchanger. On the shell side the water evaporated at a mass flow rate of 3.6 kg per hour with a power load estimated at around 2 kW. The system was designed with a safety factor no lower than 1.2 while also assuming tube diameter for the calculations. The temperature of the feed water in shell was maintained at 100 °C derived by assuming the evaporation of water

at 100 kPa while the temperature at tube external surface was assumed constant. Upon determining the tube diameter, the working pressure was checked.

5.2. Preliminary examination of thermal desalination system

One of the main concerns of thermal desalination is the deposit of mineral solids on the heat exchanger surface, and its effect on heat transfer due to increased thermal resistance and the flow area of the fluid due to decreased cross section area of the flow channel. An RO concentrate water (82.2 g/L) was used to assess the potential of deposit formation on the surface of heat exchanger is examined evaporating the water at simulated surface temperature. Specifically, the thermal desalination experiments were conducted using the RO concentrate and an electrical heater that has a comparable diameter with the system that would be built by the WVU Innovative Hub (**Figure 5-4**). It was found that the system can generate 10-lb brine without observable deposit on the surface of the electrical heater. **Table 5-1** shows the TDS of the further concentrated through evaporation of water. The maxim TDS observed was 321 g/L.



Figure 5-4. Setup for thermal desalination process demonstration using a stainless-steel pot with water heated by an electrical heating element simulating the tubes in a shell-tube heat exchanger.

Table 5-1. TDS of further concentrated rundown water through thermal evaporation process.

Container (g)	con + TDS (g)	TDS (g/L)	SC (mS/cm)	f = TDS/SC
19.1481	19.6959	110	218	0.50
19.1312	19.8162	137	267	0.51
19.2857	20.892	321	574	0.56

5.3. Preliminary design of the shell-tube heat exchanger

For the preliminary design calculations and simulations, the tubes are made of stainless-steel materials and the shell is made of carbon steel allowing free convection on its outer surface while the shell side fluid is isothermal. It is the aim of the design to make the shell and tube heat exchanger adiabatic for minimized heat loss (**Table 5-2**). **Table 5-3** shows the specifications of the designed shell-tube heat exchanger.

Table 5-2. Design Parameters.

Constraints	Design	Dimensions/Parameter
Tube Pressure		≥ 2bar
Tube inlet temperature		≅100 − 120 deg C
Shell inlet temperature		$\cong 20$ – 25 deg C
	Length	≅ 1 meter
Flowrate		≅ 2 GPH
	Capacity	To be determined
	Shell and tube heat exchanger	To be determined
	surface area	

Table 5-3. Specifications of the designed shell and tube heat exchanger.

Chall Diameter	0.47
Shell Diameter	0.47m
Tube length	0.898m
Tube Diameter	O.D = 16mm, I.D = 10mm
Water Inlet diameter	89.56 mm
Number of tubes	20
Pitch Ratio	1.33, square pitch
Material	Stainless steel, Polished
Shell Material	Carbon steel
Shell side fluid	Produced water
Tube side fluid	Saturated water vapor

5.4. Simulation of the shell-tube heat exchanger using CFD

The designed system was verified by CFD simulations using ANSYS model. Following the design calculations from the Dittus Boelter correlation's, ANSYS Fluent was applied to verify the design of the heat exchanger. A geometry of the fluid zones was generated in Solidworks, and a mesh was created (**Figure 5-5**). The mesh was created with ANSYS Fluent as the solver preference and CFD as the physics preference. For the mesh sizing proximity was selected as the size function with a transition ratio of 0.272 and growth rate of 1. For the assembly mesh method tetrahedrons was used.

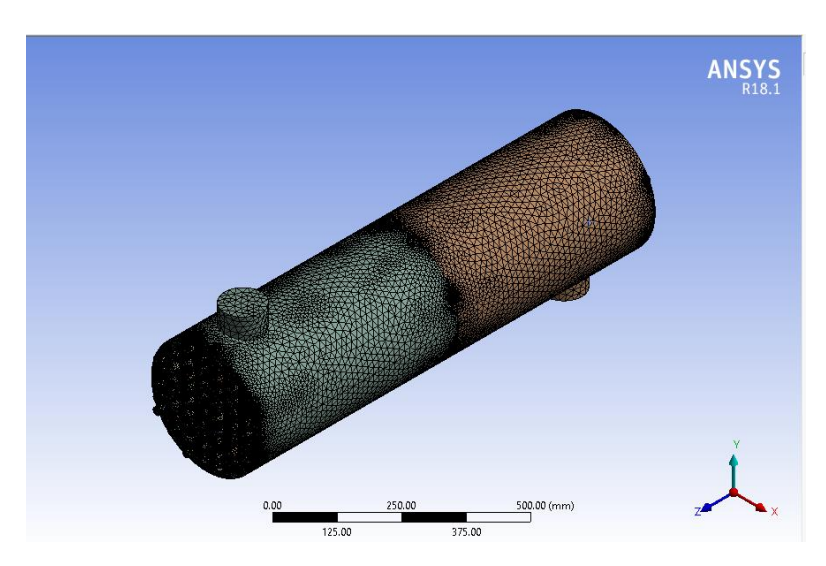


Figure 5-5. Fluid zones in Ansys mesh.

The simulation procedure involved importing the mesh into Fluent, allowing for gravity to be considered, using a pressure-based solver and an absolute velocity formulation, and using steady conditions. Under models the energy equation was employed, and the viscous model was solved using the k-epsilon, realizable with scalable wall functions. **Figure 5-6** shows the longitudinal temperature gradients across of the shell-tube heat exchanger with the outlet temperature at 20 °C. The fluid velocity was fairly uniform in the heat exchanger (**Figure 5-7**). The wall heat flux (**Figure 5-8**) was also simulated to help determine the capacity the heat exchanger. The average heat flux was calculated as 1315 W/m². The heat transfer capacity was calculated as 1290 W given the surface area 0.903 m².

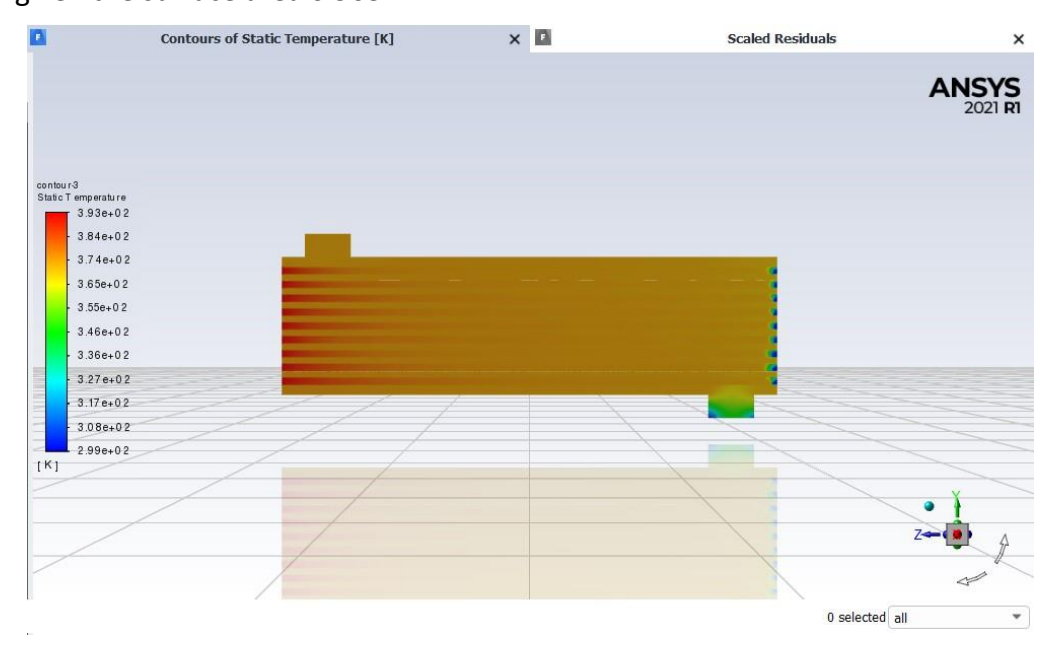


Figure 5-6. Temperature distribution on the cross section of the shell-tube heat exchanger.

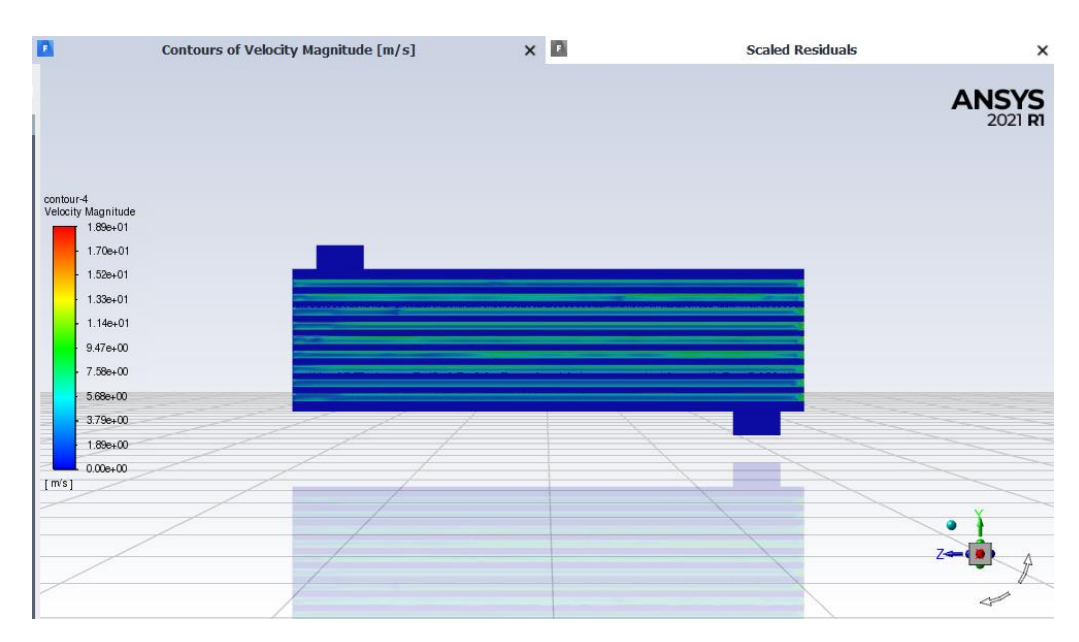


Figure 5-7. Velocity distribution in the designed heat exchanger.

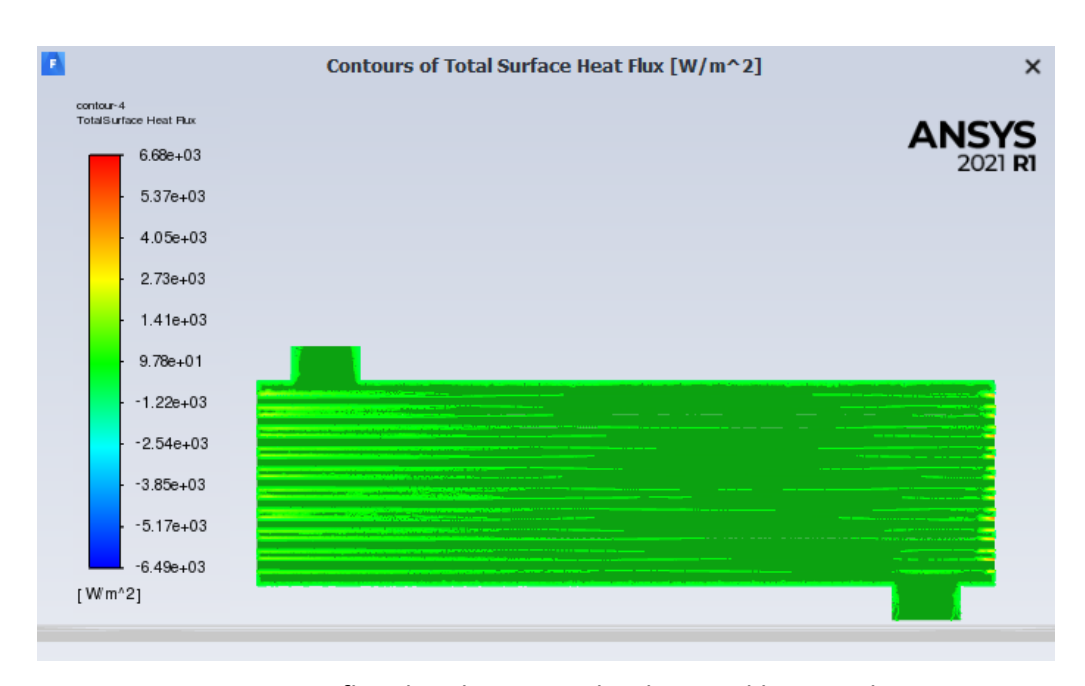


Figure 5-8. Heat flux distribution in the designed heat exchanger.

5.5. Shell-tube heat exchanger fabrication and testing

The fabrication of the 1st stage Heat exchanger was completed with the help of the WVU Innovation Hub. **Figure 5-9** shows the heat exchanger as designed in the Solidworks environment.

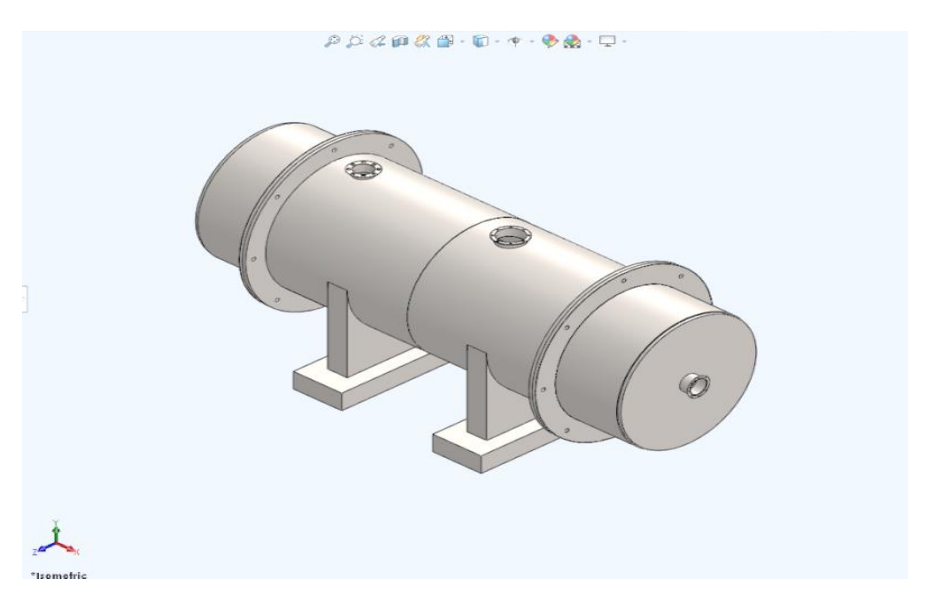


Figure 5-9. Heat Exchanger Design in Solidworks Environment.

The design was fabricated to account for 2 bar saturated steam at 120 °C at the inlet of the heat exchanger at a flowrate of 1 gph. The system was tested to see if it could handle the above tested pressure requirements during fabrication (Figure 5-10). The testing was performed such that the tube side outlet was sealed shut while attached to a pressure gage and the tube side inlet pressure was pumped to about 10 bar. The air resource was shut off once the pressure reached 10 bar. The system filled with air at 10 bar was maintained for over 12 hours to see if any fracture existed or developed, and if the system could maintain the pressure. The test result verified that the system fabricated was able to hold the pressure indicating no leaks at 10 bar, and no fracture was observed.

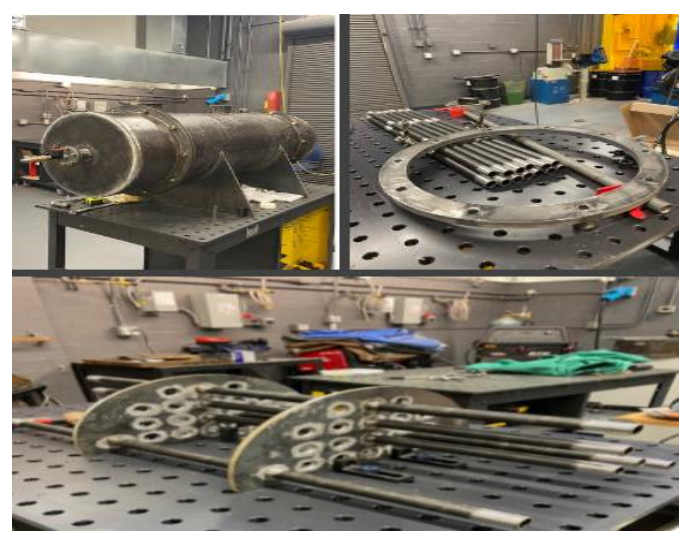


Figure 5-10. Heat exchanger undergoing pressure testing (top left), stainless steel tubes before assembly (top right), and internal frame of the heat exchanger (bottom).

5.6. Thermal desalination system assembling

Additional components were purchased to assemble a thermal desalination system. They include a steam generator, condensing coil, mass flow meter, pressure relieve valve, pressure gauge, and thermal couple.

Steam Generator

The steam generator selected is a steam canner designed work at 2 bar pressure with a pressure maximum limit of 2.5 bar as a safety factor (**Figure 5-11**). The maximum temperature, power and working pressure are summarized in **Table 5-4**.



Figure 5-11. Steam canner for steam generation.

Power Requirement 2.0 kW

Inner Capacity 5.7 QT

Working Pressure 20.6-24.6 psig

Working Temperature 126-129 deg C

Table 5-4. Specifications of the steam canner.

Condensing Coil Bucket

A stainless-steel condensing coil bucket was selected to cool the steam produced from the feed water to liquid water (**Figure 5-12**). **Table 5-5** lists the specifications of coil bucket.



Figure 5-12. Condensing coil bucket.

Table 5-5. Condensing coil bucket specifications.

Material	304 Stainless Steel
Weight	16 lbs
Dimensions	10in x 10in x 10in
Options	3x 1/2in FNPT connection
	3x 1/4in FNPT connection

System integration

The pipes, connectors and other miscellaneous part were fabricated in WVU Innovation Hub for integrating the heat exchanger and the various components into the 1st stage thermal desalination (Figures 5-13 and 5-14).

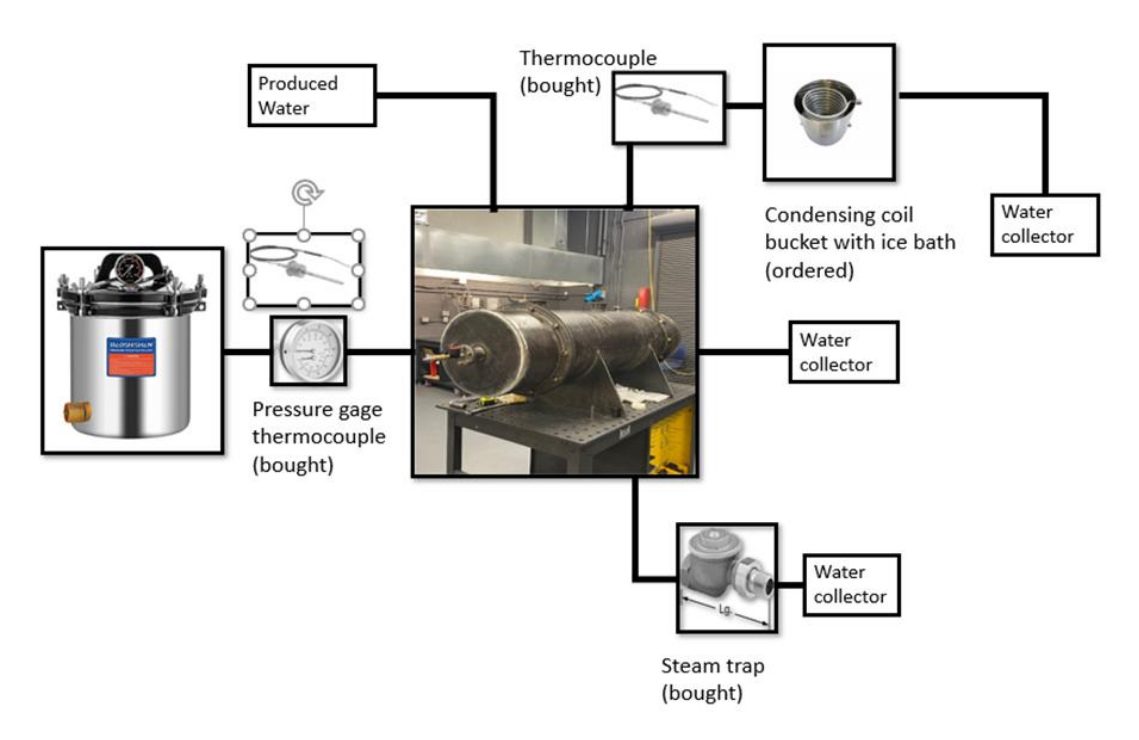


Figure 5-13. Schematic diagram of the integrated thermal desalination system.



Figure 5-14. Photo of the fabricated thermal desalination system.

Products

Takudzwa Chipunza (2022) "Development of a Thermal Desalination System Using Low Quality Thermal Energy," MS Thesis, West Virginia University (To be defensed in Fall 2022).

Task 6.0 – Brine electrolysis for caustic soda and chlorine production Approach

This task was to develop and test a brine electrolysis system for generating caustic soda (NaOH) and chlorine/hypochlorite as useful chemicals for softening and disinfection. To reduce the need for shipping and storing hazardous chemicals for BDW/PW treatment, on-site brine electrolysis is proposed as a means of generating sodium hydroxide and sodium hypochlorite on an as-needed basis. This objective differs from the customary objective of Chlor-alkali process, the commercial production of chlorine and sodium hydroxide. Since the solutions generated become part of the desalination stream, the brine concentrations used in this study (29 g/L & 58 g/L, 0.5 M & 1.0 M) were lower than the typical values used in commercial brine electrolysis (200-300 g/L). Given the often-remote locations of thermoelectric power plants and O&G production wells, such brine electrolysis for on-site generation of useful chemicals for BDW/PW treatment can provide the advantages of a small environmental footprint and minimal chemical transportation.

Experimental Details

A two-cell electrolysis cell was constructed and used to generate sodium hydroxide and chlorine/hypochlorite from brine solutions. The cell contained a dimensionally stabilized anode (DSA), a gas diffusion electrode (GDE) as the cathode, a cation exchange membrane (CEM) which separated the cell into the anode and the cathode compartments. The cell was also equipped with ports for pumping solutions through the two compartments, clamping end plates, spacers and sealing gaskets. The working area of the cell was 24 cm² and the distance between electrodes, including the CEM, was approximately 0.25 cm. The cell was connected to a

peristaltic pump and reservoirs for the catholyte and anolyte. Electrochemical measurements were obtained using a Solartron system (potentiostat/galvanostat and frequency response analyzer). Galvano-dynamic scans were used to determine if the current was limited by mass transfer (formation of depletion layers); galvanostatic experiments generated the products, and electrochemical impedance spectroscopy (EIS) was used to determine the ohmic resistance of the cell at open circuit conditions. All experiments were conducted at room temperature (22-23°C).

The selected catholyte was 0.5 M NaCl (29.2 g/L), and the selected anolyte was 0.5 M NaCl + 0.2 M NaHCO₃ (16.8 g/L). The purpose of the sodium bicarbonate is to neutralize any acid generated in the anolyte, whether from water oxidation or ionization of hypochlorous acid (HOCl), so that H $^+$ does not migrate through the CEM to neutralize generated hydroxide (OH $^-$) in the catholyte. The high pH ($^-$ 8 to 9) of the bicarbonate solution causes chlorine (Cl₂) to convert to HOCl and the HOCl to ionize to hypochlorite (OCl-), which avoids evaporation of volatile chlorine from the anolyte before analysis. Immediately following electrolysis, the anolyte was titrated with thiosulfate in the presence of excess iodide to determine the yield of hypochlorite, and the catholyte was titrated with hydrochloric acid to determine the yield of hydroxide.

The Faradaic efficiency was calculated based on the theoretical yield of these products using the total charge passed through the cell (Faraday's Law: 1 electron generates 1 OH⁻, 2 electrons generates 1 OCl⁻). Four CEMs were donated to the project by Chemours. The electrolysis was performed at a current density of 80 mA/cm² and the time of the electrolysis (1200 s) was selected to generate a catholyte of approximately 0.1 M NaOH. The charge passed through the cell (current x time) was determined by the goal of producing a catholyte with ~0.1 M hydroxide concentration. After the galvanostatic experiment, samples of anolyte and catholyte were collected for analysis. Before and after the galvanodynamic scan and galvanostatic experiments, the electrochemical impedance of the cell was measured between 100 kHz and 100 Hz. The smallest in-phase impedance (which occurs between 100 kHz and 10 kHz) was used as the ohmic resistance of the cell. From the galvano-dynamic scans, this current density did not induce any depletion layers, so cell voltages were dictated by the ohmic resistance of the cell and the electrode overpotential.

The metrics used to evaluate the cell and the membranes included ohmic and polarization resistances of the membrane, faradaic efficiencies for generating hydroxide and hypochlorite, and specific energies for production of hydroxide and hypochlorite. From the titration data, the moles of hydroxide and hypochlorite were calculated and compared to the moles of electrons passed through the cell; for 1200 s at 1.936 A, Q =2323.7 coul = 0.024083 mol e⁻ yielding theoretical concentrations of 0.0963 M NaOH (3.9 g/L) in the catholyte and 0.0482 M NaOCI (3.6 g/L) in the anolyte. Faradaic efficiencies were defined as the yield of product expressed as a

percentage of the theoretical amount.

The work energy is the integral of the product of voltage and current over the period of the galvanostatic experiment. Specific energies were calculated as kilowatt hours (kWh) per mole of product. Specific energies combine both of the factors (faradaic efficiency and work energy) and were used to estimate costs of production from the cost of electricity (\$/kWh).

Results and Discussion

Here we report detailed results for the N2050WX membrane. Then summaries of data and comparisons of membranes are discussed. Additional analyses of membrane resistances and voltages are provided. Galvanodynamic scans for the two solution compositions are shown in **Figure 6-1**. The voltage rose sharply at first and then almost linearly up to the maximum current. On the return scan, the voltage tracked the rising scan values closely. This behavior indicates that depletion layers were not forming at the electrodes or the surfaces of the CEM. To assist analyses, the voltage vs current above 500 mA was fit to a quadratic equation (plotted as the orange line). The slight downward curvature (negative quadratic coefficient) is expected for changes in the electrode voltages with respect to current.

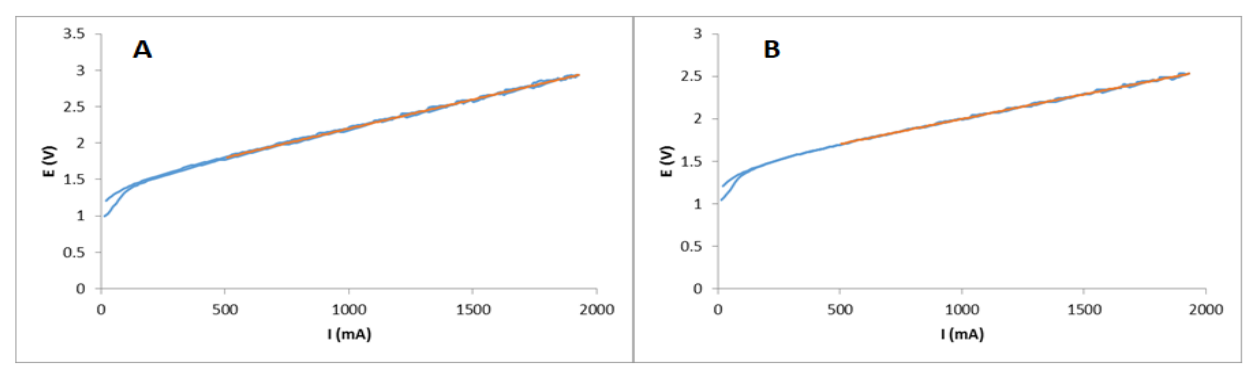


Figure 6-1. Galvanodynamic scans for the cell with the N2050WX membrane. (A) 0.5 M NaCl catholyte, 0.5 M NaCl + 0.2 M NaHCO₃ anolyte; (B) 1.0 M NaCl catholyte, 1.0 M NaCl + 0.2 M NaHCO₃ anolyte. Scan from 0 to 1930 to 0 mA at 20 mA/s. The blue lines are data, and the orange lines are quadratic fits of voltage to current above 500 mA. Quadratic equations are (A) $E(V) = (-0.00328)I^2 + (0.8046)I + (1.398)$ and (B) $E(V) = (-0.01442)I^2 + (0.6137)I + (1.400)$.

Galvanostatic data for the N2050WX memebrane in the two solution compositions are shown in **Figure 6-2**. After an initial rise, the voltages remained nearly constant at ~3.0 V in 0.5 M NaCl and ~2.5 V in 1.0 M NaCl for the N2050WX membrane. Ohmic iR drop and electrode voltages accounted for most of the observed voltage. Faradaic efficiencies in 0.5 M NaCl were 88% for NaOH and 70% for NaOCl; corresponding faradaic efficiencies in 1.0 M NaCl were 96% and 77% (**Table 6-1**). The low values for hypochlorite faradaic efficiency can be explained by a

fraction of the current going into water oxidation and by evaporation of chlorine. Anolyte solutions aged overnight in sealed bottles contained substantially lower concentrations of hypochlorite.

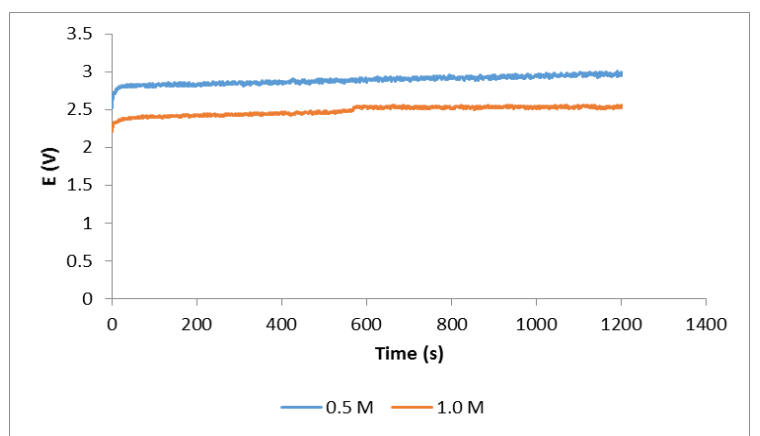


Figure 6-2. Galvanostatic plots of voltage vs time for the N2050WX membrane in two sets of solutions using a current of 1.936 A (80 mA/cm²). Catholyte solution compositions are shown in the legend; the analyte solutions also contain 0.2 M NaHCO₃.

Specific energies in the 0.5 M NaCl solutions were 0.0883 kWh/mol of NaOH and 0.221 kWh/mol of NaOCl (**Table 6-1**). Not surprisingly, they decreased in 1.0 M NaCl solutions due in part to the lower ohmic resistance: 0.0696 kWh/mol of NaOH and 0.173 kWh/mol of NaOCl. **Figure 6-3** displays overlays of the galvanostatic experiments for the four membranes in the two solutions. In all cases, the voltage was nearly constant after an initial rise. Three of the membranes exhibited roughly equivalent voltages vs time. The N966WX membrane exhibited a two-stage voltage rise which may indicate the development of a depletion layer.

Table 6-1. Performance metrics for the four Chemours membranes.

Solution	Membrane	Ohmic Resistance	Faradaic E	fficiencies	Specific Energies (kWh/mol)	
		(ohm cm ²)	NaOH	NaOCl	NaOH	NaOCl
	N2100WX	11.1	93%	70%	0.0892	0.236
0.5 M NaCl	N982WX	10.2	83%	70%	0.0956	0.227
0.5 IVI IVACI	N2050WX	10.1	88%	70%	0.0883	0.221
	N966WX	12.2	72%	67%	0.140	0.303
	N2100WX	7.7	97%	77%	0.0721	0.181
1 0 M NaCl	N982WX	7.0	87%	77%	0.0783	0.177
1.0 M NaCl	N2050WX	6.7	96%	77%	0.0696	0.173
	N966WX	8.2	73%	74%	0.125	0.248

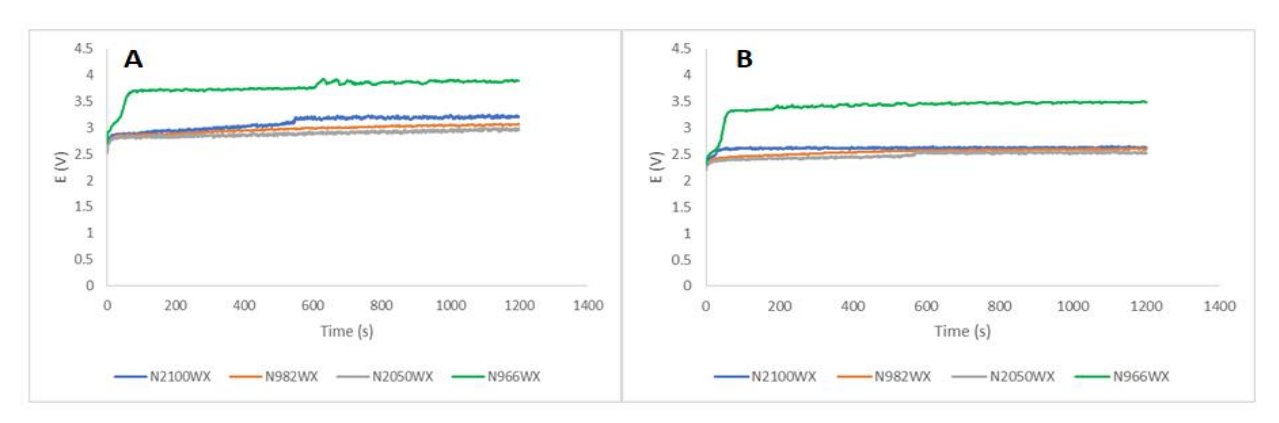


Figure 6-3. Galvanostatic plots of voltage vs time for the four membranes in (A) 0.5 M NaCl and (B) 1.0 M NaCl.

This conclusion is based on the appearance of the galvanodynamic scan for this membrane (**Figure 6-4**). After an initial voltage rise, the voltage increased nearly linearly with current up to 1500 mA, and then showed an upward curvature. The voltage on the return scan was higher. This hysteresis in the voltage was not observed for the other three membranes and not in the membrane-free cells. Therefore, it is not assigned to depletion layers forming at the anode or cathode or in the solutions next to the membrane. It is consistent with a depletion layer forming inside the membrane and then dissipating as the current decreases. Consequently, a lower current density would be better for the N966WX membrane.

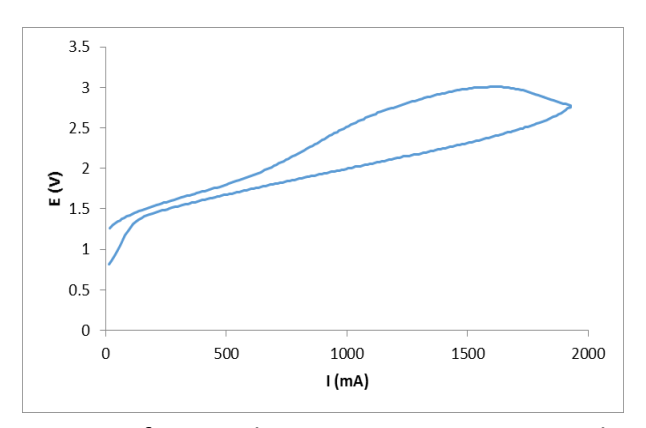


Figure 6-4. Galvanodynamic scan for membrane N966WX in 1 M NaCl. Scan from 0 to 1930 to 0 mA at 20 mA/s.

Figures 6-5 and **6-6** display the data in bar chart form. Ohmic resistances of the cell with each membrane are approximately the same with the exception of slightly higher values for the N966WX membrane (**Table 6-2**).

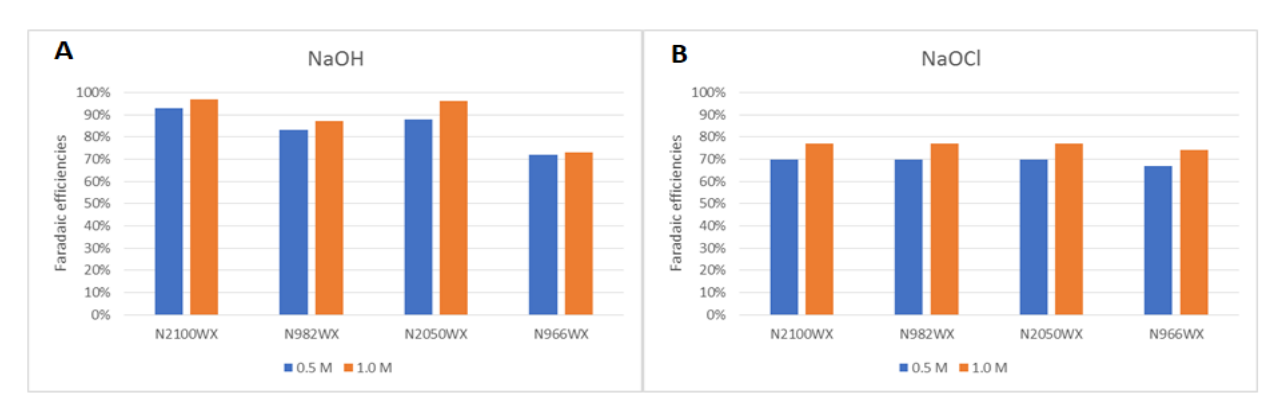


Figure 6-5. Faradaic efficiencies for production of NaOH (A) and NaOCI (B) in two sets of solutions.

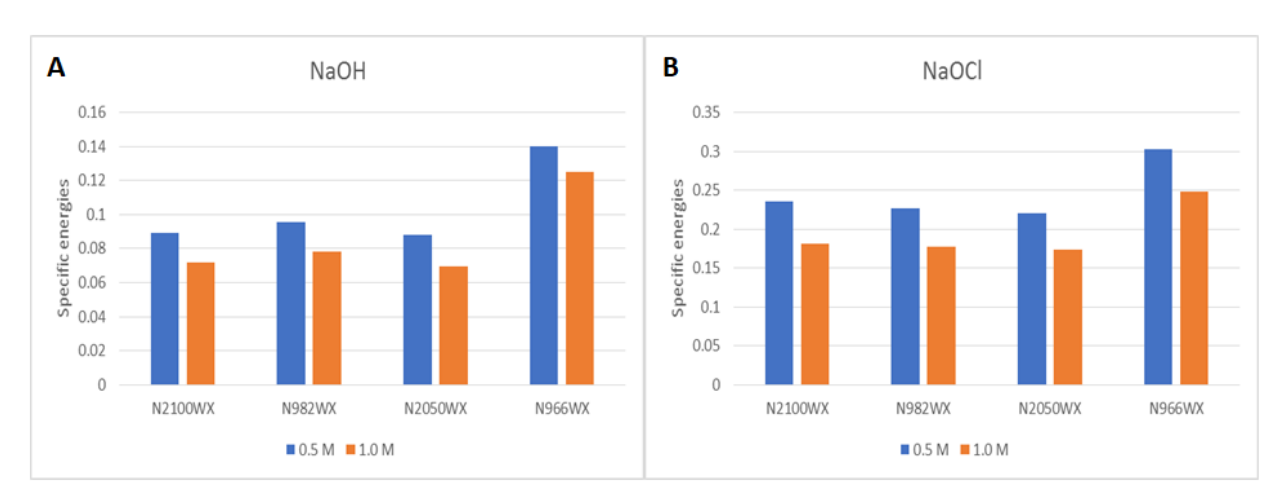


Figure 6-6. Specific energies for the production of NaOH (A) and NaOCl (B) in two sets of solutions.

Table 6-2. Average cell ohmic resistance, membrane resistance and membrane voltage at 80 mA/cm².

Solution	Membrane	Average cell Ohmic resistance	R_{mem}	V_{mem}
	Wiembrane	(ohm cm²)	Nmem	• mem
	N2100WX	10.20	0.61	0.05
0.5 M NaCl	N982WX	11.11	1.52	0.12
0.5 W Naci	N2050WX	10.18	0.59	0.05
	N966WX	12.18	2.59	0.21
1.0 M NaCl	N2100WX	6.69	1.22	0.10
	N982WX	7.71	2.23	0.18
	N2050WX	7.01	1.53	0.12
	N966WX	8.17	2.70	0.22

Faradaic efficiencies are roughly the same for both NaOH and NaOCI production for three of the membranes; N966WX again appears to be an outlier (**Table 6-1**). The faradaic efficiencies for both NaOH and NaOCI production are significantly higher in the 1.0 M NaCI solution. Specific energies are similar for the N2100WX, N982WX and N2050WX membranes and are significantly higher for the N966WX membrane, as expected from the voltages in **Figure 6-3**. Neglecting capital costs and other energy costs such as pumping, and using an estimated price of \$0.15/kWh for distributed electricity (McGovern et al., 2014a), specific energies can be converted to costs in \$/kg (**Table 6-3**). The cost of sodium hydroxide is \$0.26/kg to \$0.53/kg. Bulk NaOH costs at least \$1.50/kg and that does not include shipping and storage. It is harder to find a price for NaOCI powder; most suppliers offer solutions of NaOCI. One supplier quotes a price of \$123 for 50 lbs (equivalent to \$5/kg), well above the \$0.35/kg - \$0.61/kg in **Table 6-3**. The cell used in this study is a simple prototype, and the specific energies and costs per kilogram of future designs are likely to be lower.

Table 6-3. Estimated cost of production in \$/kg for NaOH and NaOCl.

Solution	Membrane	Estimated cost (\$/kg)			
301011011	iviembrane	NaOH	NaOCl		
	N2100WX	\$0.33	\$0.48		
O E M NaCl	N982WX	\$0.36	\$0.46		
0.5 M NaCl	N2050WX	\$0.33	\$0.44		
	N966WX	\$0.53	\$0.61		
	N2100WX	\$0.27	\$0.36		
1.0 M NaCl	N982WX	\$0.29	\$0.36		
1.0 IVI NaCi	N2050WX	\$0.26	\$0.35		
	N966WX	\$0.47	\$0.50		

Three factors contribute to the voltage of the electrolysis cell: the ohmic resistance of the solutions, the potentials developed at the cathode and anode during current flow, and the membrane resistance. Measurements were made in the cell assembled without a membrane using all four solutions (0.5 NaCl with and without 0.2 M NaHCO₃, 1.0 M NaCl with and without 0.2 M NaHCO₃). From the ohmic resistance measurements using impedance spectroscopy and the measured conductivities of the stock solutions, the distance between the anode and cathode was calculated: 0.51+/-0.01 cm. Assuming that the membrane divides this distance equally, the solution resistances were calculated for the cell with the membrane present and 0.2 M NaHCO₃ present in the anolyte. From these values, the ohmic resistance at zero current for each membrane was determined (**Table 6-2**). Membrane resistances in 0.5 M NaCl solutions were lower (0.6 ohm cm²) for N2050WX and N982WX, higher for N2100WX (1.5 ohm cm²) and even higher for N966WX (2.6 ohm cm²). The same pattern was obtained in 1.0 M NaCl solutions.

However, the membrane resistances were consistently higher in 1.0 M NaCl than in 0.5 M NaCl. Currently, we do not have an explanation for this observation. From membrane resistances, estimates of the voltage across the membrane at a current density of 80 mA/cm² are shown in the last column. These results suggest that the voltage across the membrane was small, ranging from 0.05 to 0.22 V. However, the actual values may not be accurate because the ohmic resistance of the membrane-free cell increases after current flow for unknown reasons. The main message of this study is that the voltages and hence the specific energies for the brine electrolysis cells are dominated by the voltages of the electrodes and the iR drop of the solutions for three of the four membranes.

Products

- G. Khajouei, H. I. Park, H. O. Finklea, P. F. Ziemkiewicz, E. F. Peltier, and L.-S. Lin, Produced water softening using high-pH catholyte from brine electrolysis: reducing chemical transportation and environmental footprint, *Journal of Water Process Engineering*, 40, 101911, 2021, https://doi.org/10.1016/j.jwpe.2020.101911.
- G. Khajouei, H. O. Finklea, Lian-Shin Lin, UV/free chlorine advanced oxidation processes for degradation of contaminants in water and wastewater: A comprehensive review, Journal of Environmental Chemical Engineering, 10, 107508, 2022, https://doi.org/10.1016/j.jece.2022.107508.

Task 7.0 – Integration of treatment units Approach

The unit operations developed in the previous tasks were intergated in a process for continuous treatment of BDW/PW. The process was used to treat BDW alone for comparisons of chemical and energy footprints. The process consisted of softening, activated carbon filtration, and RO for continuous treatment operations (**Figure 7-1**). We were not able to build a scaled-up brine electrolysis system for integration due to budget limitation of the project. Due to the supply shortage for some of the components, we only assembled the thermal desalination system (Task 5.0) and were not able to integrate it into the process before the end of the project. Nonetheless, the integrated process was used to treat a continuous flow (0.25-1.2 L/min, or 0.07-0.32 gpm) and successfully generated RO permeate as product water for reuse and a concentrate to be further treated in the thermal desalination unit. These flow rates meet the FOA's criterion of 0.01 -1 gpm.



Figure 7- 1. The integrated process consists of softening treatment (a), activated carbon filtration (b), reverse osmosis (c), and flow diversion from RO concentrate for the thermal desalination unit (d) for continuous treatment.

Experimental Details

Field-collected BDW and PW were mixed and treated with alkaline chemicals in two conebottom tanks (65 gallons each, **Figure 7-1a**) for removing divalent ions (i.e., softening). Specifically, predetermined chemical quantities of $Na_2CO_{3(s)}$ and 5M $NaOH_{(aq)}$ were added to the BDW/PW to raise the pH to ~10.5 based on the results of Task 2. The water mixing was done using a mechanical mixer to promote the chemical precipitates for 20 minutes. The supernatant (i.e., softened water, TDS = ~ 17 g/L) was pumped from the softening tank continuously to four activated carbon filters hydraulically connected in series for organic removal. The effluent of the AC filtration was used as the feed water for the RO treatment. The AC filtration effluent was routed to a feed tank for RO treatment.

Two RO treatment operations were tested. In the first operation, the RO concentrate was continuously recirculated to the RO feed tank to raise the TDS of the AC filtration effluent. A constant volume (*i.e.*, ~5 L) of water was maintained in the feed tank. The ramp-up time of the RO treatment was characterized to assess the time required for the RO to reach a steady state of operation, which is an important factor to consider for intermittent operation of the treatment process. When the TDS concentration in the feed tank reached a steady state, a small flow (*i.e.*, 0.10 L/min) of RO concentrate was diverted for thermal desalination treatment to further concentrate the TDS for 10-lb brine production. The co-treatment performance in terms of ramp-up time, RO feed/permeate flow rate (at the second steady-state), water recovery, and chemical

and energy consumption was compared with the treatment of BDW alone under the same applied pressure of 900 psi. In addition, the co-treatment was tested for a single-pass operation without RO concentrate recirculation under the same operating condition (i.e., RO applied pressure of 900 psi) for comparisons of the treatment performance with recirculation.

Results and Discussion

A BDW:PW mixture (volumetric ratio 10:1) was treated through the softening unit (NaOH and Na₂CO₃), AC filtration, and the RO under 900 psi (6.2 MPa). The RO feed flow rate started from 0.79 L/min and decreased to 0.50 L/min over a 45-min operation with RO concentration recirculation. The corresponding RO permeate flow rate decreased from the initial 0.89 L/min to 0.39 L/min (Figure 7-2a). The decreasing permeate flow was accompanied by increasing TDS concentration in the RO concentrate. The TDS concentration in the RO feed tank increased from the initial 17 g/L to 45.6 g/L after 30 mins. The permeate flow rate corresponding to the RO feed water TDS 45.6 g/L was measured as 0.47 L/min (0.13 gpm). After reaching the RO feed water TDS 45.6 g/L, a small flow rate was diverted from the RO concentrate recirculating loop as a brine stream to be further treated by thermal desalination. The extraction of a fraction of the RO concentrate flow caused a transient state of TDS in the RO feed tank. Results indicated that a diverted flow of 0.10 L/min resulted in the best treatment performance in TDS among the tested diverted flows (Figure 7-2). With a diverted flow of 0.1 L/min starting at 30 mins, the RO feed water TDS initially decreased and reached a secondary steady state at ~42 g/L after 10 mins. The water recovery (i.e., RO permeate/total processed water) at the second steady state using this treatment operation was 76% (Table 7-1). The inclusion of water recovery from thermal desalination to achieve TDS 300 g/L results in an overall water recovery of 92%.

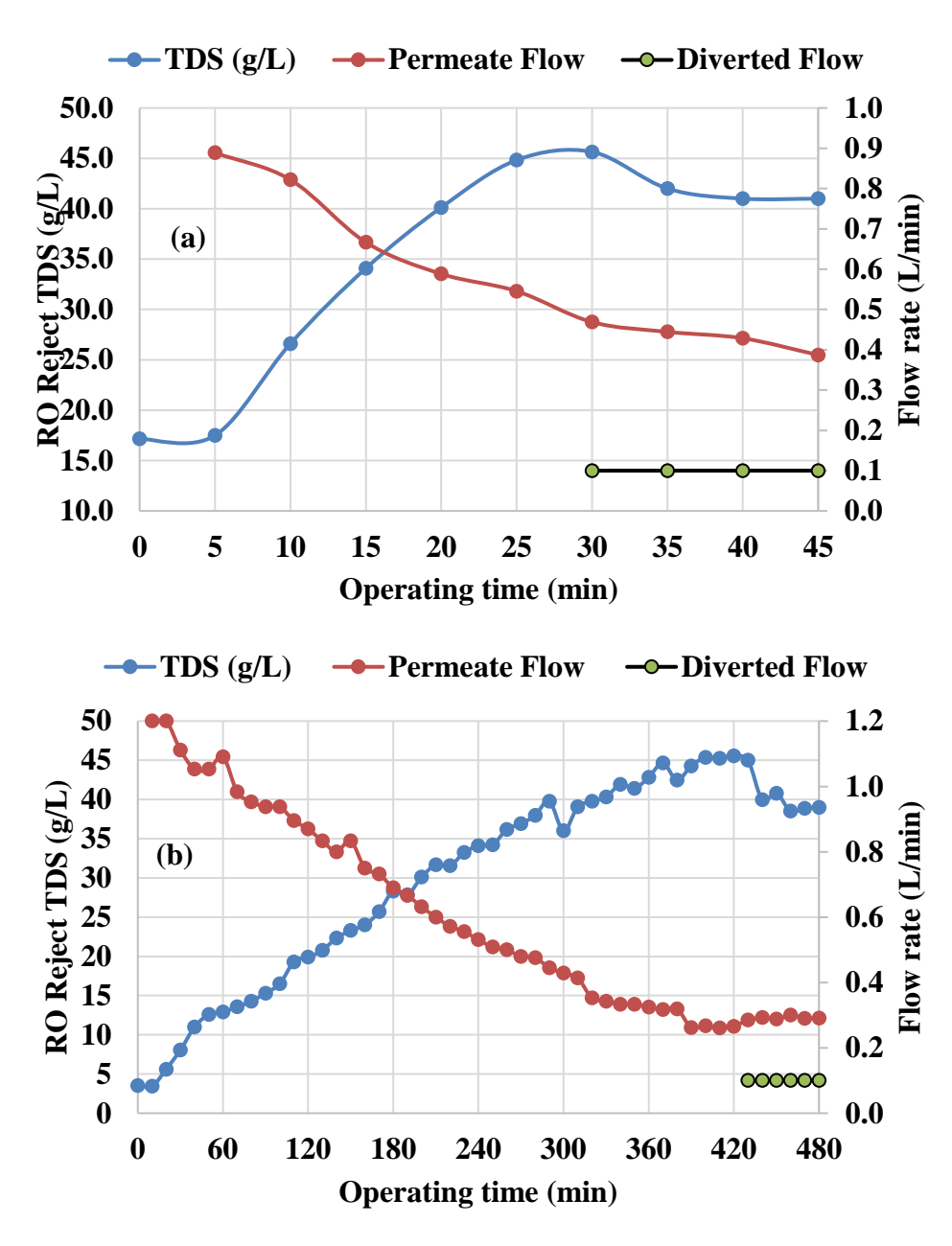


Figure 7-2. TDS concentrations during RO treatment and diverted flow from the RO reject stream (y1-axis); RO permeate and diverted flow rates (y2-axis) under an applied pressure of 900 psi (62 bar) and continuous operation for (a) the co-treatment of BDW and PW, and (b) the BDW alone.

The same treatment operation was conducted for treating the BDW without PW (**Figure 7-2b**). The initial TDS concentration of the softened BD, feed flow rate, and permeate flow rate were 3.5 g/L, 1.2 L/min and 1.2 L/min, respectively. The RO feed water TDS concentration increased to 17 g/L (initial concentration of the BD/PW mixture) after 100 min of operation and reached a steady state TDS concentration at 45 g/L after 420 mins. Similar to the co-treatment operation, a constant water volume of 5 L in the RO feed tank was maintained. Flow diversion

(0.1 L/min) from the RO concentrate at 420 mins of the RO treatment caused a transient period before the TDS reached a second steady state (39 g/L) at 450 min. The average RO feed flow and permeate flow rates at the second steady state were 0.43 L/min and 0.29 L/min, respectively. The water recovery from the RO treatment was estimated as 68%. The inclusion of water recovery from thermal desalination results in an overall water recovery of 88%.

These results show that, under the same applied pressure, the co-treatment of BDW/PW allowed higher RO feed flow and shorter ramp-up time compared to treatment of BDW alone. The co-treatment resulted in slightly higher water recovery rate. In both treatment tests, the recovered permeate water had a low salinity with a TDS < 0.5 g/L, suitable for reuse in cooling operation.

Table 7-1. Continuous treatment performance at the steady-state condition.

•	•	
Parameters	BDW treatment alone	BDW-PW cotreatment
AC effluent TDS, g/L	3.5	17
Steady-state TDS, g/L	39.4	41
Feed flow, L/min	0.43	0.55
Permeate flow, L/min	0.29	0.42
Water recovery (RO)	68%	76%
Energy consumption (kWh/L permeate, AC filtration + RO)	0.047	0.034
Water recovery (RO + thermal desal*.)	88%	92%

Note. *Water evaporation to further increase TDS to ~320 g/L. 'Desal.' stands for desalination.

The Na₂CO₃ (s) requirement for softening of the BD and PW separately (10:1 volume ratio) was estimated as 10.0 g/L based on the total hardness (**Table 7-2**). The Na₂CO₃(s) requirement for the softening of the BDW/PW (10:1) was calculated as 6.0 g/L, resulting in a 40% saving of Na₂CO₃(s). Similarly, the 5M NaOH(aq) requirement to raise the pH to ~12.0 was estimated as 10 mL/L for the mixed water. In contrast, the NaOH_(aq) requirement increased to 22 mL/L if the BDW and PW are to be treated separately (**Table 7-2**), which indicates a ~55% saving of 5M NaOH(aq) with the co-treatment approach.

Table 7-2. Chemicals requirement for the pretreatment of BD-PW mixture and their separate treatments.

Alkaline	BD alone	PW alone	BDW & PW	BDW/PW (10:1)
chemicals			separately (10:1)	mixture
Na ₂ CO ₃ (g/L)	0.6	100.0	9.6	6.0

Energy consumption was calculated for the operating condition at the second steady state in **Figure 7-2** (*i.e.*, with the RO concentrate diversion of 0.1 L/min). Total unit energy consumption which included AC filtration and RO was estimated as 0.034 kWh/L permeate. The unit energy consumption for treating the BD alone was calculated as 0.047 kWh/L permeate, indicating 29% higher energy consumption compared to the BD/PW co-treatment operation. Overall, the cotreatment of the BD and PW at 10:1 ratio could result in ~50% saving of alkaline chemicals and ~29% energy saving compared to the baseline (BD treatment alone) treatment scenario.

In case of the single-pass operation (i.e., no recirculation of RO reject), co-treatment under RO applied pressure of 900 psi quickly (i.e., 25 mins) achieved the steady state TDS concentration of ~20 g/L from the initial TDS concentration of ~17 g/L (**Figure 7-3**). The steady-state permeate flow rates fluctuated within a narrow range between 0.8 L/min and 0.74 L/min with an average of 0.77 L/min. The average energy consumption by the RO unit for this single-pass operation was estimated as ~0.089 kWh/L of permeate, which is ~2.6 times higher than the energy consumption of the co-treatment with recirculation.

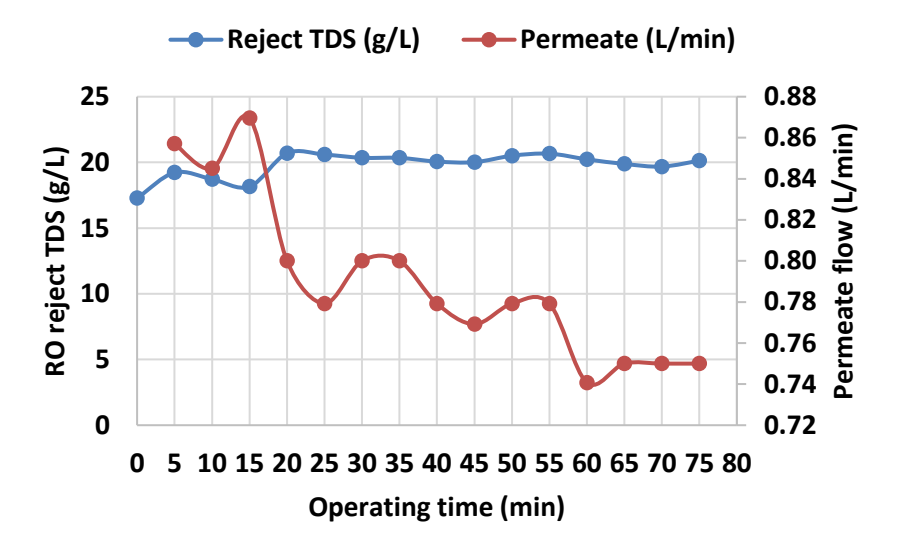


Figure 7-3. RO reject TDS level and permeate flow for a single-pass RO desalination under an applied pressure of 900 psi (62 bar) for the continuous co-treatment of BD and PW.

In summary, the co-treatment of cooling BD and PW is a better treatment scheme compared to the individual treatment of BDW in terms of chemical requirement for softening, shorter ramp-up time, permeate flow, water recovery, and energy saving by the RO treatment. Single-pass RO treatment should be further evaluated under different flow rates to achieve the same level of TDS concentrations as the RO treatment with recirculation to determine optimal RO treatment configuration for the co-treatment approach.

Products

- Mohammad H. Ahmed, G. Khajouei, P. Seats, K. Buzby, H. Finklea, N. Siefert, H. Hunter, and L.-S. Lin, Novel Co-treatment of Cooling Blowdown Water and Produced Water: A Regional Approach for Resource Recovery and Treatment Footprint Reduction, manuscript in preparation.
- Payton Seats, Mohammad H. Ahmed, Golnoosh Khajouei, Hunter Barber, Harry Finklea, Fernando V. Lima, and Lian-Shin Lin, Multi-objective planning for co-managing power plant blowdown water and shale gas produced water for resource recovery, conference paper, 39th IAHR World Congress, Granada, Spain, June 19-24, 2022.
- Mohammad H. Ahmed, Payton Seats, and L.-S. Lin, Produced Water and Waste Heat-aided Blowdown Water Treatment: Using Chemical and Energy Synergisms for Value Creation, 2021 AIChE Annual Meeting, Boston, MA, Nov. 7-11, 2021.
- G. Khajouei, H.I. Park, H. Finklea, P. Ziemkiewicz, and L.-S. Lin, Process selection for produced wateraided blow down water treatment to maximize water reuse and saleable by-product generation and reduce chemical and energy cost, extended abstract submitted to 93rd Annual Technical Exhibition & Conference, New Orleans, Louisiana, Oct. 3-7, 2020.

Task 8.0 – Process Modeling and Simulations

Approach

Commercial software such as OLI Flowsheet (OLI Systems, Inc.) or Aspen Plus (Aspen Tech, Inc.) was used to simulate the proposed process model. Specifically, condenser and cooling tower models were simulated to estimate the water loss by evaporation and drift during different operating scenarios. These models were also employed to calculate the blowdown and makeup water flowrates in order to maintain the appropriate concentration. Different scenarios were considered for acquiring produced water. For example, one scenario is to pay for transportation costs to truck the water from the well and has the produced water available at no cost. Another possible scenario is to pay for water transportation, but also receives compensation for taking the water. For the proposed modular treatment process, the unit model was developed using mass and energy balances based on available experimental data or first-principles models from the commercial software. Also, an economic model was coupled with the process model to estimate the capital and operating costs based on economic assumptions and the Aspen Process Economic Analyzer tool (Aspen Tech, Inc.). With the proposed process and economic models, a MILP (mixed-integer linear programming) optimization problem was formulated to determine the optimal configuration/number of RO (reverse osmosis) units needed and the optimal concentration of the RO reject stream to minimize capital and operating costs. The TEA considered addition of a 4th, higher-pressure RO unit that can handle higher TDS to further concentrate the RO concentrate from a three-stage RO treatment. Disposal options and costs for the generated sludge materials including NORM, if detected, was proposed and included in the TEA. To solve this optimization problem, MILP tools was explored, such as the solvers available in the Optimization toolbox in MATLAB (Mathworks, Inc.) and GAMS (GAMS Development Corporation), if needed for higher complexity. In addition, based on the developed model and optimization algorithm, a TEA was conducted to estimate the manufacturing cost and operating

performance of the proposed modular unit with the ultimate goal of obtaining the most cost-effective modular design.

8.1. Process Modeling and Simulations Objective

In conjunction with the proposed cotreatment process design shown in **Figure 8-1**, the fundamental process modeling objective was to develop a simulation of the treatment train, with notable rigor and validated with experimental data (when available), to perform systematic economic and sustainability assessments. Through the resulting metrics of the assessments, optimization strategies would be formulated to converge toward a design that maximizes water reuse, reduces chemical and energy footprints of treatment, and improves process profitability by generating saleable by-product (10-lb. brine).

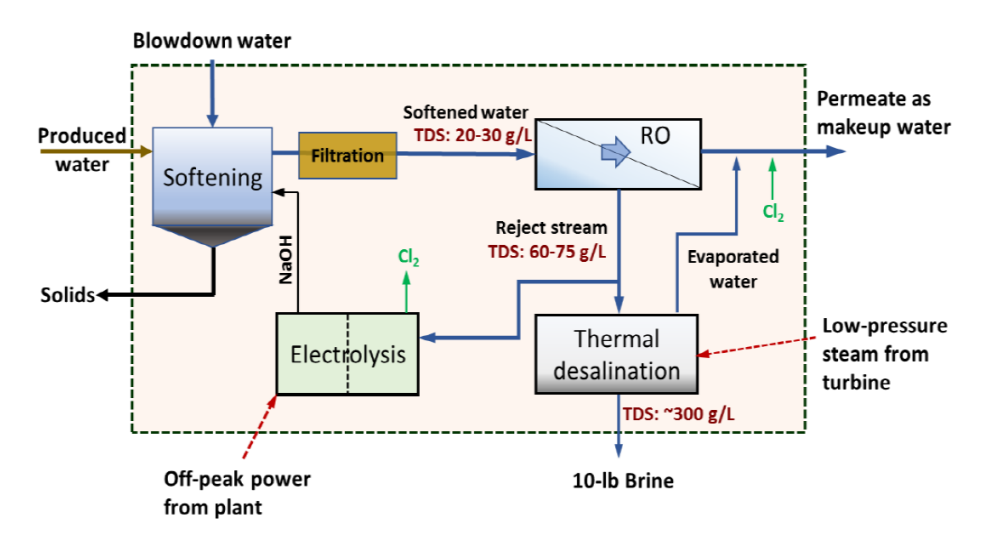


Figure 8-1. Modular process arrangement for water treatment defined in project proposal.

8.2. Solution Approach

For the purposes of this task, the industrial process scale was considered. This would justify the magnitude of process costs, and better inherently evaluate the process in steady-state operation. During the development of the flowsheet design, the strict design constraints as applied to the steady-state process were included.

By reviewing **Figure 8-1**, it was concluded that the process mass balance is nearly zero liquid discharge (ZLD), which lowers the degrees of freedom to meet quality constraints of the product water and 10-lb brine. Considering performance and operational constraints of the equipment, the designs are not feasible at a wide range of conditions. Therefore, the initial goal of the process modeling effort was to develop a physically feasible and solvable process model nearly meeting the design constraints, but not requiring that all conditions were met. The process model structure could then be integrated with economic and sustainability assessment tools to complete the full modeling framework.

Before applying the optimization algorithm, a sensitivity on the decision variables could be conducted. By exploring the input design space, a deviation from the original design where now product quality and equipment constraints are met could be defined as a base case. Initializing from the base case, the process could then be optimized.

8.3. Modeling and Simulation Strategies

8.3.1. Software Implementation

Rigorous simulation of water treatment processes is largely an unconventional application of commercial chemical process simulators. For a suitable chemical process simulator, the phenomena of the process need to be accurately calculated. This includes chemistry, reactivity, and physical properties determined by the thermodynamics and employed process equipment.

An attractive feature of this cotreatment process is the chemical softening by produced and blowdown water mixing. These waters are both diverse in their properties and composition. To accurately simulate the effects of mixing, a rigorous electrolyte thermodynamic package was required.

OLI Systems products were identified as candidates to perform these calculations. These products contain detailed thermodynamic packages to handle complex electrolyte chemistry in waters across a wide range of conditions. OLI Systems had developed a chemical process simulator in OLI Flowsheet ESP, but it lacked all the needed process equipment to model this process. With no means of customization and limited connectivity between OLI Flowsheet ESP and other software for optimization, this simulator could not function as the main tool for the flowsheet simulation. However, another tool in OLI Engine could be imported into Aspen process simulators to utilize the thermodynamic calculations needed for this process. The precipitation of salts when mixing blowdown and produced water at a wide range of mixing ratios was conducted using OLI Engine and had shown good accuracy for modeling the chemistry of the process.

Aspen Plus V9 was the selected chemical process simulator as it could be directly supported by OLI Engine in Aspen Plus 10.0.2 for rigorous thermodynamics (Wang et al., 2002). Aspen Plus still did not contain equipment models for electrolysis and reverse osmosis (RO) units; however, the software connectivity of Aspen Plus was relatively versatile. Aspen products may be used in conjunction and Aspen Custom Modeler V9 (ACM) could address models not included in Aspen Plus' default unit model library. Furthermore, Aspen may be operated through a component object model (COM) interface. MATLAB both has an available library of robust optimization techniques and can communicate with the Aspen Plus flowsheet through the COM connection. Considering the uniqueness of the problem and software solutions available, this overarching software implementation was accepted to move forward as the modeling strategy. A software workflow for the proposed model is shown in **Figure 8-2**.

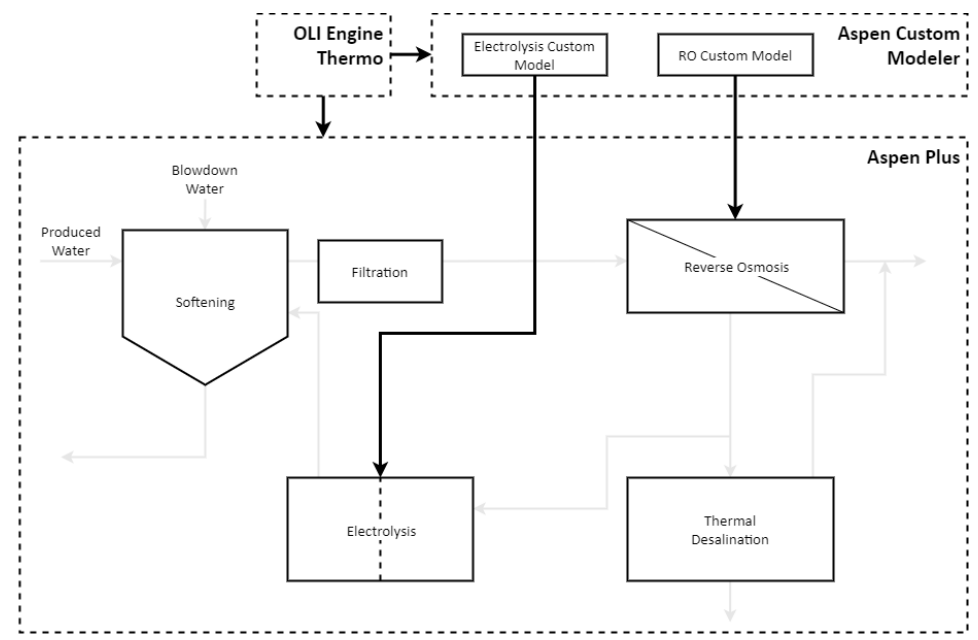


Figure 8-2. Software workflow integrated with the proposed unit designs. Here software packages are outlined in dashed boxes and connectivity is shown by solid black lines.

8.3.2. Process Scale

The quantity of feed water needed was specified to define the scale of the process appropriately. The volume of water fed to this treatment train was matched to simulated data from the supercritical pulverized coal plant model within the 2019 NETL Cost and Performance Baseline Report (James III et al., 2019). This example reported cooling tower blowdown at a normalized rate of 2.89 gpm/MW-net. The assumed power plant size was 700 MW-net (based on Longview Power in Maidsville, WV), resulting in a flow of 2022 gpm (equivalent to 2.91 MGD or 459 m³/hr). This value was then used to fix the design flowrate of the treatment train, which is considered as the sum of blowdown and produced water flows. This sum is used for the following reasons: (i) it guarantees sufficient blowdown water withdrawn on-site at any mixing ratio, bounded by treatment of pure blowdown water; and (ii) it provides a comparable evaluation of economics as designs at any mixing ratio will have identical capacities.

8.3.3. Defining Water Properties

Beginning with the raw industrial wastewaters for the process model, matching these water compositions in a chemical process simulator was critical in accurately assessing downstream performance. The experimentally determined compositions of produced and blowdown water samples were provided from previous tasks in the project.

OLI Chemistry Wizard 10.0 for Aspen Plus was used to generate the property package to be imported into the simulation. The electrolyte species to be included are declared and the tool determines all potential ionic compounds that may form in addition to the chemical and phase equilibrium relations that govern precipitation. Given this effect, including many species in the thermodynamics increases computational complexity significantly.

Next, a set of ions for modeling needed to be determined. It is recognized that the reported compositions are a subset of all the compounds contained in the water, some in trace quantity, and those included may be reported with small error. Exclusion of even trace compounds does affect the charge balance and properties of the water, such as pH, making it difficult to match the real water samples without including an exhaustive set. Species such as OH, Ba⁺², Br⁻, Ca⁺², Cl⁻, ClO⁻, CO3⁻², Fe⁺³, Fe⁺², HCO3⁻, H⁺, HS⁻, MG⁺², NA⁺, SO4⁻², and SR⁺² were selected to meet the specified conditions for simulation. When considering combinations into ionic compounds, this expands the component list to over 200 species in Aspen Plus calculations.

With the thermodynamics generated and imported, the feed streams themselves must then be specified in Aspen Plus as species compositional inputs. Considering that the experimental data provides alkalinity and pH which are bulk measurements of several compounds, further clarification of water composition was required. Water Application Value Engine (WAVE) from DuPont Water Solutions was used namely to translate pH and alkalinity measurements to a water solution that is in charge balance and given in terms of species compositions. Sodium ion concentration was adjusted to satisfy the charge balance conditions. Carbonate, bicarbonate, and carbon dioxide were balanced according to the water alkalinity input provided.

After performing this procedure for both blowdown and produced waters, the adjusted compositions are then inputs in Aspen Plus. The resulting pH of each water type then matched sampled results which was crucial to evaluate the amount of chemical additions for softening, where designs are guided by target pH.

For later process evaluations, the full Aspen Plus flowsheet containing 200 true species is not intuitive to assess the stream conditions. Thus, an algorithm was developed to translate true species into the relevant ions needed for process analysis. The goal of the algorithm is to generate a stream report on a key ion basis, identically to how streams are represented in experimental composition. An equation-based formulation of the algorithm is presented in Equation 2.

$$C_{mass,ion} = MW_{ion} \left[\frac{\dot{n}_{species \ni ion} + \sum_{i=1}^{\alpha_{MAX}} (\alpha - 1) \dot{n}_{species \ni (ion)_{\alpha}}}{\dot{V}} \right]$$
 (2)

The mass concentration of key ions ($C_{mass,ion}$) is calculated using the molecular weight of the ion (MW_{ion}), molar flowrate of the true species (\dot{n}) (where the species text string contains the ion string, $species \ni ion$), and the volumetric flowrate (\dot{V}). In this algorithm, the full component list of true species is searched for the text containing the ion of choice as they appear in the Aspen Plus alias (e.g., searching for "NA", "CL", "OH", "SO4", etc. in each true species alias "NA+", "NAOH","NA2CO3", etc.). Using the stoichiometric ratio (α), the molar flow for each ion can be calculated using the molar flow of the containing compound. Stoichiometric ratios are searched sequentially ("NA" then "NA2" then "NA3"). Ratios greater than one are reduced by one to ensure no duplicate counting. The algorithm was successful when tested with the inlet

streams where the key ion concentration is known.

8.3.4. Softening and Filtration

Chemical softening is performed by water mixing and additions of sodium hydroxide and sodium carbonate to precipitate contaminants. For a steady-state simulation, no batch times or dynamics regarding the chemical additions is needed for this flowsheet. When using Aspen Plus mixer models, the effluent of each block is flashed to equilibrium, employing extensive thermodynamic calculations for the water chemistry. This implies the batch time is long enough such that the water reaches equilibrium. This also ensures that chemicals are not added in excess and removes any time dependencies for this step of the process.

The initial design specifications are made in coordination with approximations provided by the experimental groups. The preliminary simulation is specified at a 10:1 blowdown to produced water volumetric mixing ratio. Sodium hydroxide additions are made to increase the pH of the water to 12. Sodium carbonate is added at equimolar concentration to the remainder of aqueous divalent cations.

To simulate suspended solid removal after softening, the Aspen Plus filter model is used. The filter model is specified for 100% solids-to-solids outlet and 99.5% of liquid-to-liquid outlet separation. This results in a sludge liquid fraction of approximately 30 wt% (Wenzlick & Siefert, 2020).

For adsorption of organic materials, granular activated carbon (GAC) filtration is proceeding this filter. Organic materials in simulation are removed by a simplified component separator. This model is solely a fixed separation where organics are set to be completely removed. For more insight, a GAC Excel tool, as part of a larger pollution control unit (PCU) toolbox, is used externally to the Aspen Plus flowsheet (Li et al., 2018). The process flow, organic properties, and removal specification are matched as much as capabilities allow between the Aspen and Excel software tools. In the decoupled simulation of the GAC model, the Excel tool provides a detailed and comprehensive analysis of the module design and cost.

After filtration, hydrochloric acid is added to act as a pH control system. The selected DuPont FilmTec SW30-4040 RO membrane has an upper pH limit of 11 as defined by DuPont's product data sheet (DuPont, 2020). With this consideration, the pH of 12 must be neutralized to some extent. The pH entering the RO is fixed to 11 for the preliminary simulation. In the same step, air is added to the mixer to simulate aeration for hydrogen sulfide removal. With small amounts of hydrogen sulfide, the air is supplied in excess to remove all vapor before reverse osmosis.

8.3.5. Reverse Osmosis

Reverse osmosis (RO) does not have an Aspen Plus model available in the modeling library and therefore requires custom model development through ACM. The Spiegler-Kedem-Katchalsky (SKK) model for ion transport through a membrane was selected for rigorous reverse

osmosis modeling (Boussouga & Lhassani, 2017). Fundamentally, the transfer across the membrane of the water and salts needed to be determined for the mass balance to be satisfied. In this model, the water flux (J_v) is a function of the water permeability coefficient (L_p) , transmembrane pressure (ΔP) , osmotic pressure $(\Delta \pi)$, and coefficient of reflection (σ) .

$$J_{v} = L_{n}(\Delta P - \sigma \Delta \pi) \tag{3}$$

Similarly, the salt flux (J_s) may be determined from the summation of terms containing the salt permeability coefficient (P_s) , the concentration at the membrane surface (C_m) , and concentration in the permeate (C_n) .

$$J_s = P_s \left(C_m - C_p \right) + (1 - \sigma) J_v C_m \tag{4}$$

To determine the membrane concentration relative to the bulk retentate, the coefficient of mass transfer (k) is introduced. Relating these variables and rearranging to conveniently display the salt rejection of the membrane (R_{obs}) results in Equation 5.

$$R_{obs} = \frac{1}{\frac{(1-\sigma)exp^{(\frac{J_{v}}{k})}}{\sigma(1-exp^{\frac{(1-\sigma)}{P_{s}}J_{v}})}} + 1$$

$$(5)$$

Four parameters are unknown and are a function of the membrane properties. To determine L_p , σ , P_s , and k, experimental data is required to regress data and fit the model equation. To allow for a large set of steady-state data, WAVE was used to generate simulated data using a similar membrane (DuPont FilmTec SW30-4040) to that employed in experimental demonstrations for the project. To limit variability in these parameters across data points, the temperature was fixed at 20°C assuming the process would be operated at ambient conditions.

The SKK model is most accurate when using a finite element model. To mimic the established WAVE tool, the ACM model would also operate using 6 discrete membrane elements housed in the pressure vessel. Therefore, this default option was retained when generating data.

Simulated data using WAVE was generated for a variety of inlet compositions and design pressures. L_p was determined from a simple scenario considering the limiting condition of pure water where the flux equation is reduced to flux induced by pressure differential.

$$J_v = L_p \Delta P \tag{6}$$

The RO element results for all other trials were imported into MATLAB for a least-squares curve fitting function to determine σ , P_s , and k. The results of the fit are shown in **Figure 8-3**.

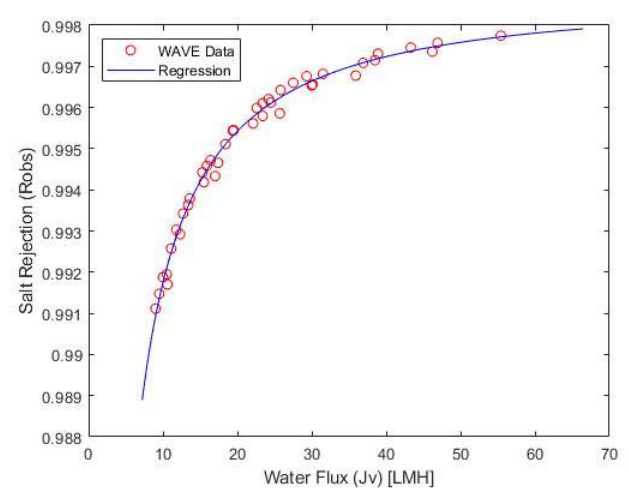


Figure 8-3. Regression results for determining σ , P_s , and k

A method for calculating osmotic pressure is proposed by Lentech and used by Dow/Filmtec (Lentech, n.d.). When writing an isothermal model, this provides a simple and accurate linear osmotic pressure correlation using the molality of components (m_i) .

$$\pi = 1.12(273 + T) \sum m_i \tag{7}$$

The given expressions were coded into an ACM model. Given the equation-oriented solution strategy, the 6 finite elements contained within each pressure vessel are calculated sequentially where no finite difference approximation is necessary. Resulting permeate and retentate streams are the output from the vessel. The model considers the fixed 6 membrane element area of a single pressure vessel and allows for multiple vessels in parallel to handle different amounts of flow. Reverse osmosis membrane and vessel operating limitations are accepted from the product data sheet and the WAVE library and are considered in the feasibility of the model (DuPont, 2020).

8.3.6. Thermal Desalination

Thermal desalination as a multi-effect distillation (MED) unit is not available as a unit model in Aspen Plus. A general schematic of MED is shown in **Figure 8-4**.

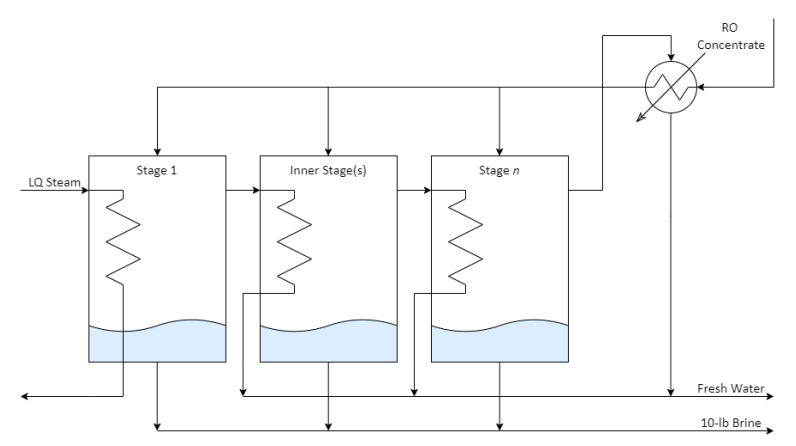


Figure 8-4. General configuration of a 3-stage multi-effect distillation unit.

The phenomena contained within this unit operation can be simply decoupled to heat exchange and flash vessel models. Given this separation, units available in Aspen Plus can be employed given the equipment configuration shown in **Figure 8-5**.

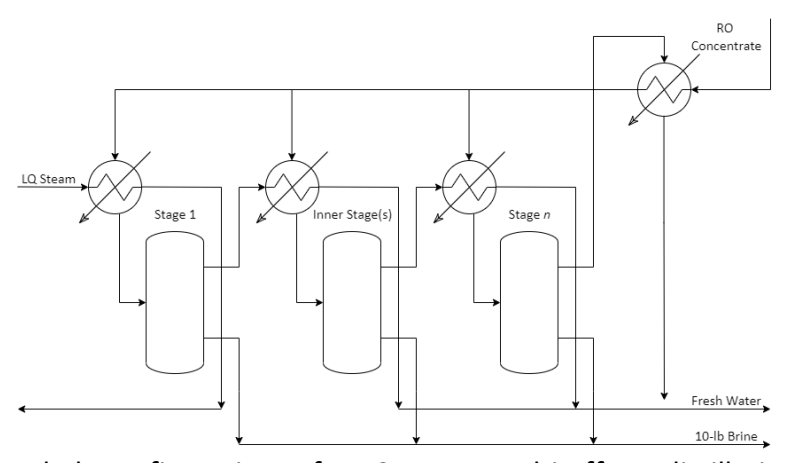


Figure 8-5. Decoupled configuration of a 3-stage multi-effect distillation unit into heat exchangers and flash vessels

Low quality (LQ) steam is used in the first stage of the MED model. For simulation, this steam is assumed to be at atmospheric pressure. Given stream tables from the supercritical pulverized coal plant model within the 2019 NETL Cost and Performance Baseline Report, waste steam may be estimated at 120°C (James III et al., 2019). The 100°C assumption is conservative considering the quality of this steam is largely unknown and MED units are typically run under higher vacuums than simulated. For this process, RO concentrate flow is evenly split between all stages of the unit. Consecutive stages have a fixed drop in operating pressure after the first. With the only degree of freedom present within the first stage, the vapor fraction of the RO concentrate exiting the exchanger is adjusted to result in a 10-lb brine nearly saturated with sodium chloride.

8.3.7. Electrolysis

The unique electrolysis design is not conventionally available in Aspen Plus, and custom modeling would again be necessary for this unit. With limited experimental data available, a simplified model would be needed to estimate the performance in the flowsheet. Novel Aspen Plus approaches using Gibbs reactors to decouple phenomena increase computational complexity for the flowsheet and are not directly applicable with the embedded thermodynamic package (Du et al., 2018).

For electrochemical reactions, the ideal conversion of electricity to moles of product corresponds to Faraday's Law (Du et al., 2018).

$$I = \dot{n}_i v_i F \tag{8}$$

where I is the current, \dot{n}_i is the molar production of component i, v_i is the stoichiometric coefficient of component i in the electrolysis reaction, and F is Faraday's constant (96,485 C/mol).

Under ideal Faradaic conversion, each mole of electron transferred in the form of electricity directly contributes to the stoichiometric amount of targeted product. In the developed model, efficiencies are applied to the ideal conversion to directly represent conversion determined from experimental data. The specific mechanisms that these efficiencies are attributed to are reductions identified by experiments with this electrolysis cell. The conceptual diagram of this model with identification of these mechanisms is provided in **Figure 8-6**.

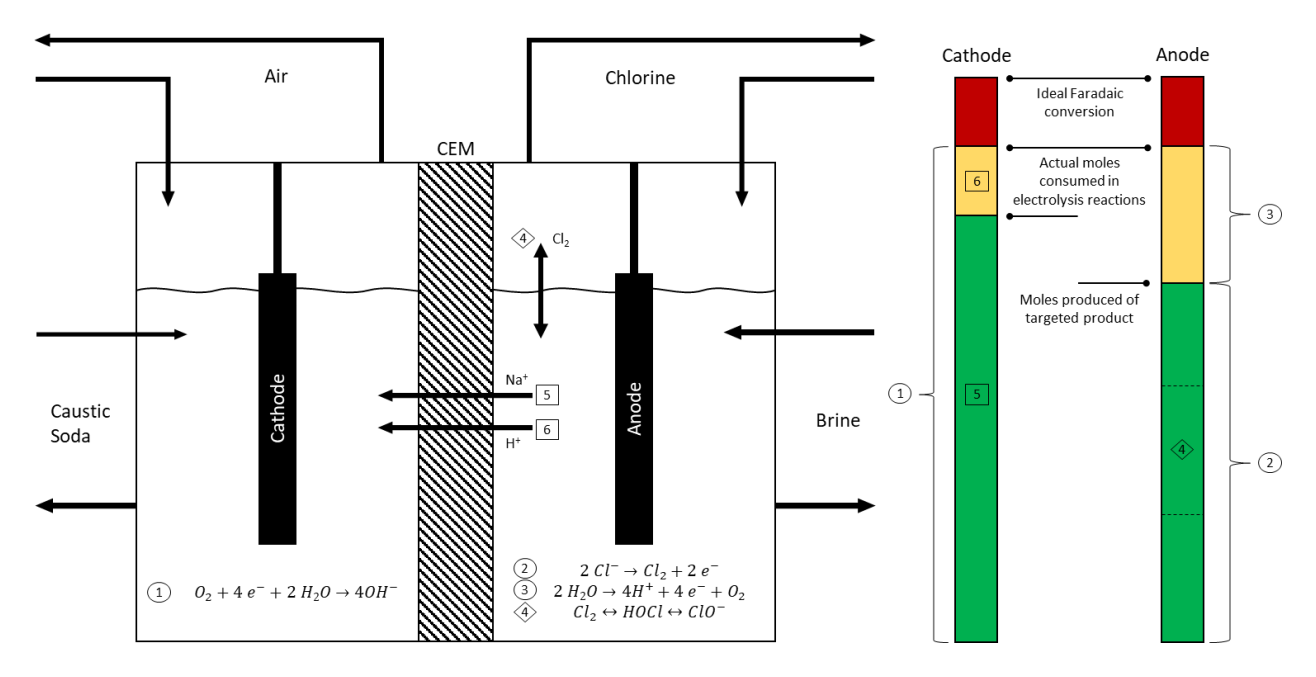


Figure 8-6. Conceptual diagram for the ACM Electrolysis model

In the developed ACM model, an overall system efficiency is applied to account for

generic resistance between the power supply and the reaction site. The model is interpreted to contain distinctive vapor and liquid compartments for the anode and cathode. Within each compartment, the model's order of operations is applied in the following sequence: (i) liquid and vapor inlet streams are mixed; (ii) solution is reacted according to Faraday's law; (iii) ions are exchanged across the CEM; (iv) an ACM electrolyte vapor-liquid-solid flash procedure calculates the mixture equilibrium concentrations; and (v) vapor and liquid-solid constituents leave the unit through their respective ports.

The assumptions considered within the electrolysis model are: (i) constant temperature and pressure; (ii) conversion is stoichiometric according to Faraday's Law with experimentally derived efficiencies applied; (iii) each electrode's efficiency is constant; (iv) cathode efficiency is contributed to migration of H⁺ across the CEM, neutralizing OH⁻; (v) anode efficiency is contributed to undesired oxidation of water, chlorine species are determined by equilibria; and (vi) Na⁺ transport across the membrane is equal to the OH⁻ produced at the cathode.

8.3.8. Summary

Several software packages and experimental data were used to result in the working process flowsheet model described in this section. The fully connected flowsheet is shown by the process workflow in **Figure 8-7**. Distinct steps for data acquisition, external custom modeling requirements from the default Aspen Plus library, and simulation flowsheet are presented.

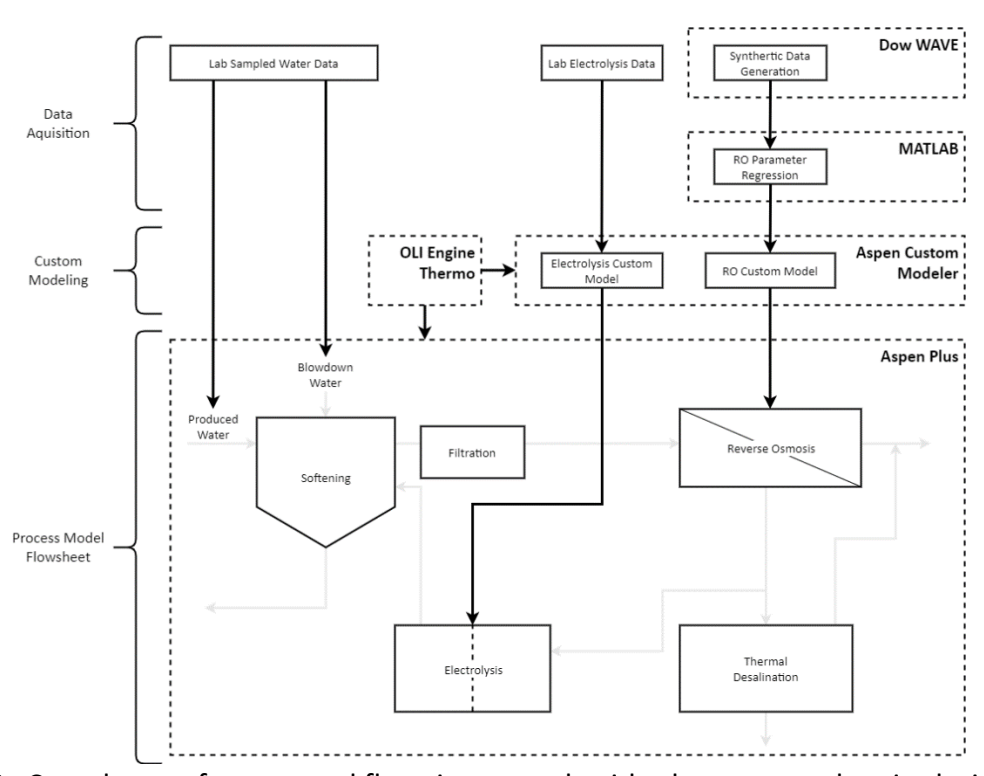


Figure 8-7. Complete software workflow integrated with the proposed unit designs. Here software tools are outlined in dashed boxes and connectivity is shown by black lines.

The resulting Aspen Plus flowsheet shown in **Figure 8-8** is a preliminary design and does

not explicitly meet all the design criteria for the process. It serves as a solvable Aspen Plus model and as basis to form the costing infrastructure. This model shows to be computationally complex, taking several minutes to solve. Later sensitivity studies on the process design are performed to result in a distinctive base case design.

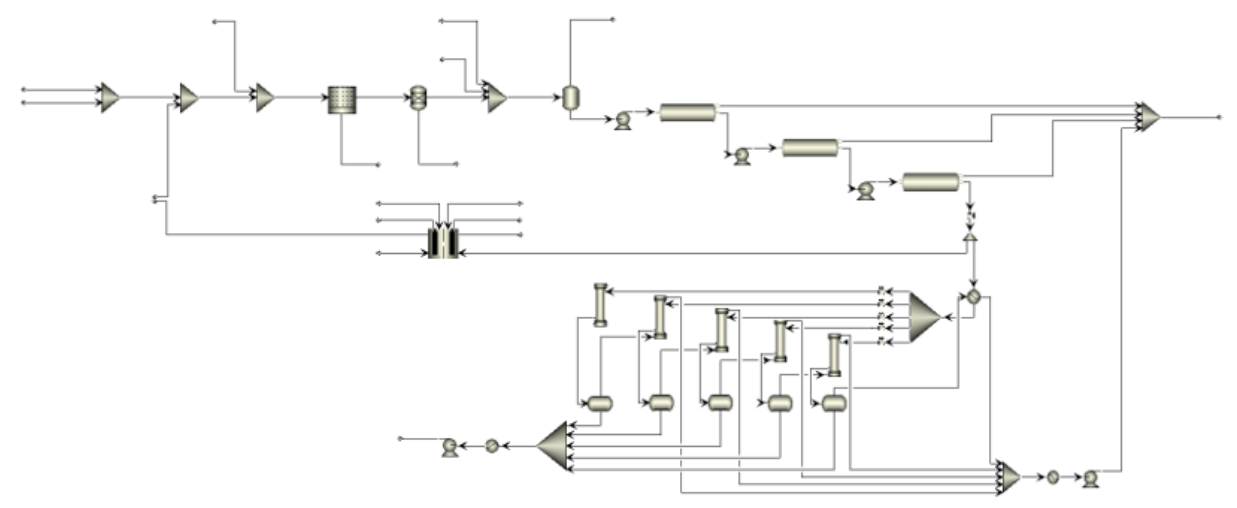


Figure 8-8. Preliminary Aspen Plus flowsheet.

8.4. Process Analysis

8.4.1. Techno-Economic Analysis

For a comprehensive cost assessment, all relevant operational costs were considered. Fixed rate chemical prices for raw materials were obtained from literature (Wenzlick & Siefert, 2020) (U.S. Geological Survey, 2020) (Turton et al., 2018). Similarly, prices of saleable products are obtained from literature (Turton et al., 2018) (Wenzlick & Siefert, 2020) (Sánchez-Aldana et al., 2018) (Wiesner et al., 1994). These prices are paired to the quality of the material at the price point. Prices provided for pure compounds are normalized to the diluted quality used in the process.

From electrolysis, it is assumed that chlorine contained in the outlet anode solution may be chemically manipulated (shifting equilibrium) to result in a targeted compound. For costing purposes, the aqueous chlorine containing compounds are recognized as sodium hypochlorite.

Air used in aeration is costed as utility compressed air (Turton et al., 2018). Nitrogen is costed as a fraction of this cost but ultimately is used in significantly lower quantities compared to the magnitude (for both process flow and unit cost) of other materials that it has negligible effects on process costs.

To standardize the reporting, worst-case scenarios for many cotreatment benefits are considered. Electricity is costed using the 2019 average price in West Virginia available from the 2020 U.S Energy Information Administration annual report (US EIA, 2019). Off-peak power used for sodium hydroxide production via electrolysis is costed as standard electricity usage as its main

attractiveness is a power storage technique for improved sustainability.

Low quality steam used in thermal desalination is costed as low-pressure steam obtained from a conventional steam plant header (Turton et al., 2018). Currently, it is unclear whether the low-quality steam generated from power plants is recycled for any other purpose such as building heating and therefore may be indirectly affecting other costs. Any power plant waste heat able to be utilized freely for water treatment would lower prices further than reported. Cooling water and low-pressure steam costs are determined as a function of the electricity price using a tool in CAPCOST (Turton et al., 2018).

GAC energy consumption, particle regeneration, and other accompanying costs are directly accepted from the PCU tool used to model the unit (Li et al., 2018). Although unmodeled, waste treatment for activated sludge and hydrogen sulfide scrubbing are costed from established waste treatment unit costs.

An aspect directly affecting the economic feasibility of the cotreatment concept is the cost interaction between produced water (PW) and blowdown water owners. To perform an informed assessment of the process, an assumed impartial cost consideration is made. It is assumed that blowdown treatment facilities will pay exclusively for the transportation costs of produced water to the site of the cotreatment facilities. This would eliminate disposal or treatment costs for produced water owners. Ideally, transportation costs may also be lower than the costs of the required chemicals to soften the blowdown water, therefore moderately benefiting both parties.

To estimate transportation costs, a separate analysis was made. Pertaining to the geography of Appalachia, prolonged travel over mountainous regions or to remote well locations may increase transportation costs. To account for this, the estimated value for this analysis was setting transportation costs at 6 cents per 100 km horizontal transport (per m³ of PW), plus 5 cents per 100 m vertical transport (per m³ of PW) (Zhou & Tol, 2005). To further localize the assessment, specific topography of West Virginia was measured to define both the horizontal and vertical distances.

For the horizontal distance, a database available from the West Virginia Department of Environmental Protection (WVDEP) was used. A comprehensive list of over 64,000 well locations with their respective 2019 oil production and water usage was referenced (WV DEP, 2019).

For the mixed treatment facility, it was considered logistically impractical to utilize the low-quantity-producing well locations as a viable resource. Only using high-quantity-producing wells limits the number of required sites to access, ensures easily met maximum capacity of transportation vehicles, and attempts to mitigate the potential for difficult geographic access of smaller well sites. Thus, only the 2,409 wells classified as Horizontal 6A (H6A) wells (653 excluded from lack of reported geographic location) were considered viable as sources to import produced water from. Under the Natural Gas Horizontal Well Control Act, an H6A well is "any well site...which disturbs three acres or more of surface...or utilizes more than two hundred ten

thousand gallons of water in any thirty day period." The locations of the sites are provided using the Universal Transverse Mercator (UTM) coordinates, a gridded system with units of meters.

To maintain independence from a single mixed treatment facility location, all data from the H6A wells were standardized per unit area of land. This provides a more generalized approach to estimating the transportation costs in any area with H6A wells in proximity (as many areas in the Appalachian or more specifically Marcellus Shale region have). To evaluate the total enclosed land area of the H6A wells, a MATLAB function was used. The location spanned approximately 4,400 square miles, with the boundary shown in **Figure 8-9**.

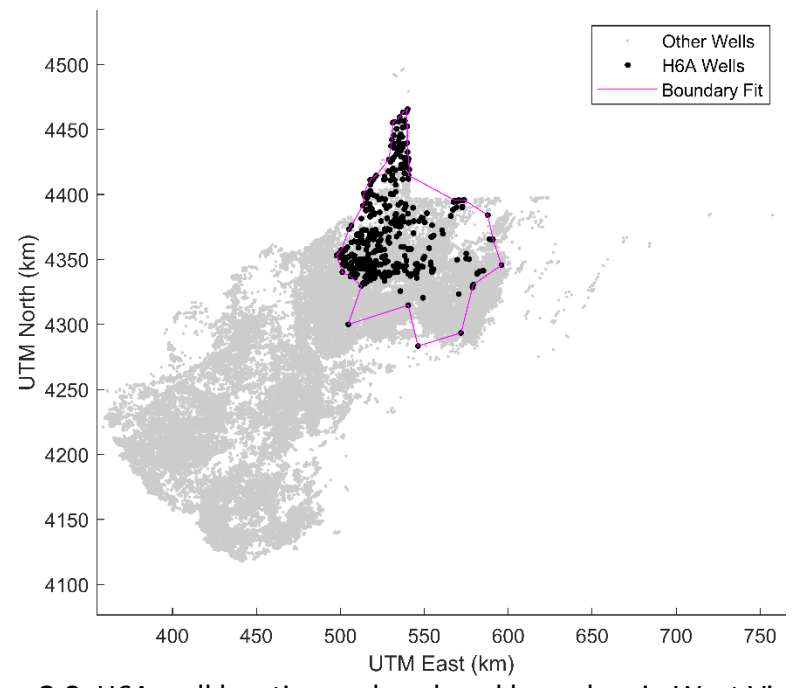


Figure 8-9. H6A well location and enclosed boundary in West Virginia.

The location density, oil production, and water usage are then normalized per unit area (considering the boundary). With these normalized values, all wells are assumed identical for the purpose of resourcing produced water and are reimagined at a constant location density. The outreach area, or spanned area needed to encompass sites which in total source the amount of produced water necessary for a given design, is then constructed as a circle with the power plant and treatment facility at its center. This simplifies calculations as the average distance of all sites in the circle (\bar{d}_{well}) can be obtained by the following equation using the circles radius (r).

$$\bar{d}_{well} = \frac{2r}{3} \tag{9}$$

The outreach area is extended radially to meet the required sites for the simulated design. An example visualization of a plant location that would resource produced water from 594 locations (using over 830,000 m³/year of produced water) is shown in **Figure 8-10**.

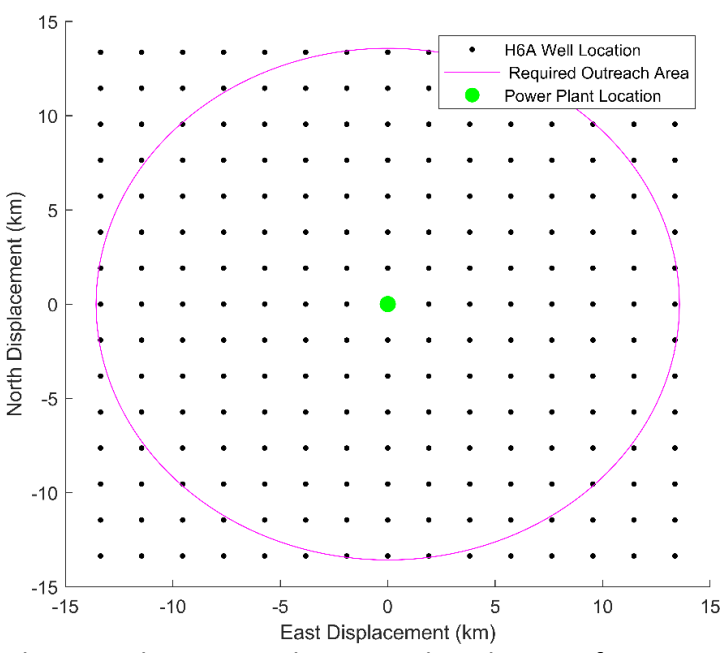


Figure 8-10. Required outreach area to obtain produced water for a centralized cotreatment plant.

When relating this configuration back to cost, the associated transportation costs are calculated assuming the one-way transportation of produced water from each individual site to the power plant location. For added costs, the average elevation gain was estimated at 0.01 vertical meter per horizontal meter using a Google Maps route spanning the longest straight-line distance of the considered bound area in West Virginia. Assuming that the treatment facility will utilize the nearest wells first, it is clear that as a site is designed to use more produced water the outreach area will also expand to include more well locations. By the nature of the problem, these costs identically fit to a power law model and parameters are determined using MATLAB regression (Figure 8-11).

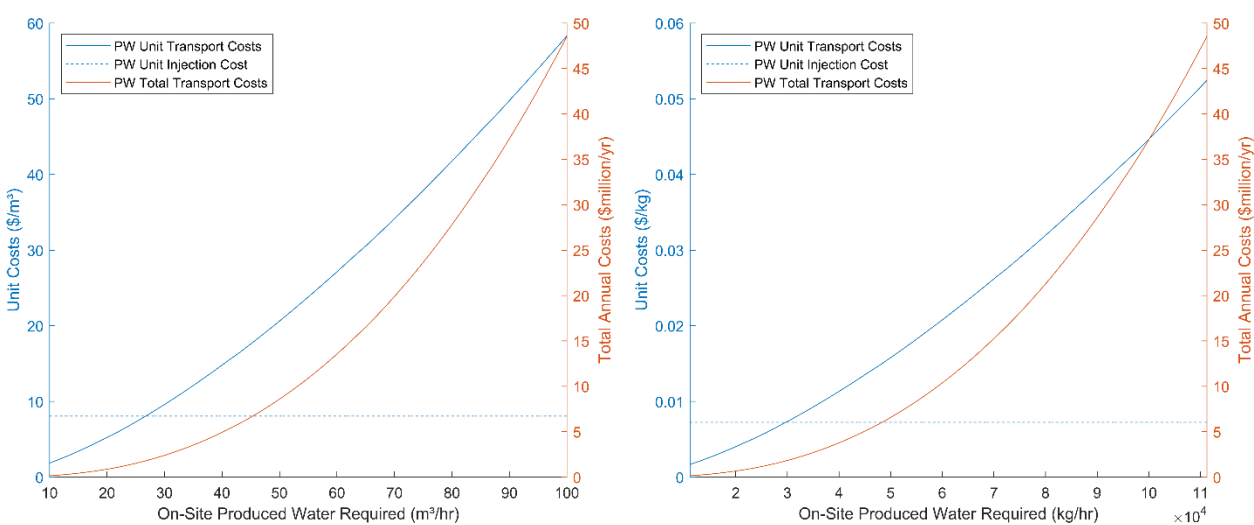


Figure 8-11. The regression of unit costs of importing produced water as a function of the amount of produced water used in the process design.

The unit costs are compared to the average cost of produced water injection and shown in Figure 8-11. These obtained equations are applied for three cases and compared to the benchmark: (i) the unit cost to import 76.87 m³/hr (5:1 mixing ratio) is \$39.28 per m³ of PW; (ii) the unit cost to import 41.93 m³/hr (10:1 mixing ratio) is \$15.87 per m³ of PW; and (iii) the unit cost to import 26.72 m³/hr (16.26:1 mixing ratio) is \$8.06 per m³ of PW, the same price required to inject PW for disposal averaged from literature data (Puder & Veil, 2006).

Unit Cost
$$\left[\frac{\$}{m^3}\right] = 0.05875 \left(Produced\ Water\ Required\ \left[\frac{m^3}{hr}\right]\right)^{1.498}$$
 (10)

Unit Cost
$$\left[\frac{\$}{kg}\right] = 1.44 \times 10^{-9} \left(Produced\ Water\ Required\ \left[\frac{kg}{hr}\right]\right)^{1.498}$$
 (11)

The operating costs for all the considered features are summarized in **Table 8-1**. The quality specified is determined from various sources in literature.

Table 8-1. Operating costs summary.

Material Name	Classification	Quality	Price	Price UOM	Reference
Blowdown Water	Raw Material	-	-	\$/kg	-
Produced Water	Raw Material	-	$1.44 \times 10^{-9} (PW [kg/hr])^{1.498}$	\$/kg	-
Sodium Hydroxide	Raw Material	30 wt%	0.14	\$/kg	(Wenzlick & Siefert, 2020)
Sodium Carbonate	Raw Material	Solid	0.154	\$/kg	(USGS, 2020)
Hydrochloric Acid	Raw Material	20 wt%	0.094	\$/kg	(Turton et al., 2018)
Potable Water	Product	<500 ppm in all other species	0.00053	\$/kg	(Turton et al., 2018)
10-lb Brine	Product	>16.5 wt% NaCl, <100 ppm Mg ²⁺ , <350 ppm Ba ²⁺ + Ca ²⁺ + Sr ²⁺	0.0114	\$/kg	(I.F., n.d.) (Wenzlick & Siefert, 2020)
Sodium Hypochlorite	Product	-	0.045	\$/kg	(Sánchez-Aldana et al., 2018)
Chlorine Gas	Product	-	0.276	\$/kg	(Wiesner et al., 1994)
Utility Air	Utility	3.3 barg	0.0041	\$/kg	(Turton et al., 2018)
Inert Nitrogen	Utility	-	0.0001	\$/kg	-
Electricity	Utility	-	23.583	\$/GJ	(US EIA, 2019)
Cooling Water	Utility	30°C	0.448	\$/GJ	(Turton et al., 2018)
Low Quality Steam	Utility	5 barg (as LPS)	4.68	\$/GJ	(Turton et al., 2018)
GAC Operation and Regeneration	Utility	-	16.617	\$/hr	(Li et al., 2018)
Activated Sludge Treatment	Waste Treatment	~30 wt% liquid	0.007826	\$/kg	(Turton et al., 2018)

Capital costs of all relevant equipment are considered for the economic model. The Excel tool for chemical process techno-economic analysis (TEA), CAPCOST, is employed for the internal calculations available (Turton et al., 2018). Its Visual Basic for Applications (VBA) procedures are augmented to incorporate unconventional process units with unit specific costing correlations.

In this tool, chemical softening would be assumed to be performed within a batch reactor. In accordance with reactor types in the design literature, the vessel was sized as a 40 m³ mixer with agitation (Turton et al., 2018). The size of the reactor was inferred given the inlet flowrate to the softening unit where a 40 m³ reactor allows for a 4-hour residence time under a steady-state assumption (US EPA, 1999). This residence time is selected to reaffirm the assumption that sufficient batch time allows for the water to approach equilibrium. Two identical reactors are costed to allow for alternating operation to maintain a near steady-state rate.

The offline GAC model previously mentioned is also employed at this step to directly import size and cost of the calculated design.

The chemical engineering plant cost index (CEPCI) is used for dated publications to normalize prices to the 2020 USD. The 2020 CEPCI is approximated at 600 (Turton et al., 2018).

These provided costing equations are used to determine the base equipment cost and are provided in **Table 8-2**. This cost is then upscaled based on other important design parameters such as pressure tolerance and materials of construction to reach a base bare module cost (Turton et al., 2018). These capital and operating costs are evaluated for the process design in CAPCOST.

CAPCOST provides further evaluation of cost of land, labor, and other miscellaneous indirect costs. Most notably, the costs of materials, utilities, waste treatment, annuitized capital, and revenue from sales are incorporated into levelized cost of water (LCW) calculations. This metric most holistically encompasses process costs whilst considering water recycling and serves as a valuable reference for process optimization as objective function.

Table 8-2. Capital cost summary.

Equipment	Equation for Page Equipment Cost	Sizing Paran	neter			CEPCI	Reference	
Equipment	Equation for Base Equipment Cost A B	С	D	Ref.	Reference			
Electrolysis	$=\frac{540A}{B}$	Membrane Area	% Cost of Membrane			600	(McGovern et al., 2014a) (Nayar et al., 2019)	
Heat Exchangers	$= 10^{4.8306 - 0.8509\log_{10}(A) + 0.3187(\log_{10}(A))^2}$	Area				397	(Turton et al., 2018)	
MED	$= 24A \left[(1-B)(6291 \times (24A)^{-0.135}) + (B)\left(\frac{c}{8}\right)^{1.277} \left(\frac{70}{D}\right)^{1.048} \right]$	Volumetric Flow	% Cost of Evaporator	# Stages	Heat Source Temp.	600	(Kosmadakis et al., 2018)	
Pumps	= $(B+1) \times 10^{3.3892+0.0536\log_{10}(A)+0.1538(\log_{10}(A))^2}$	Power	Number of Spares			397	(Turton et al., 2018)	
RO	$= (121.35A_{RO} + 7802.6)N_{RO} = 13117.73N_{RO}$	# Vessels	# Elements			600	(Yang et al., 2014)	
Softening Reactor	$= 10^{4.1052 + 0.5320\log_{10}(A) - 0.0005(\log_{10}(A))^2}$	Volume				397	(Turton et al., 2018)	
Flash Vessels	$= 10^{3.4974 + 0.4485\log_{10}(A) - 0.1074(\log_{10}(A))^2}$	Volume				397	(Turton et al., 2018)	
GAC	Costs imported from Excel tool					600	(Li et al., 2018)	

8.4.2. Sustainability Assessment

A comprehensive tool for sustainability analyses, GREENSCOPE (Gauging Reaction Effectiveness for the ENvironmental Sustainability of Chemistries with a Multi-Objective Process Evaluator), was used to provide additional performance metrics (Ruiz-Mercado et al., 2012). When applying simulation results, the framework calculates key performance indicators (KPIs) to evaluate results based on the simulation and sustainability data available. Given an unconventional water treatment application, much of the environmental data input requirements for electrolyte systems were not applicable to the tool. Therefore, a set of economic, energy, and material efficiency KPIs were selected to evaluate. These metrics are shown in **Table 8-3**.

Table 8-3. GREENSCOPE indicators selected for sustainable design assessment (Ruiz-Mercado et al., 2012).

Category	Indicator	Label	Brief Definition
Economic	Net present value (worth)	NPV	NPV is computed by adding the present values of all incomes subtracted by the summation of the present values of all investments.
Economic	Payback period	PBP	PBP is the time required, after start-up, to recover the fixed capital invested, FCI, for the project.
Economic	Equivalent annual cost	C_{eq}	Equivalent annual cost is the sum of the annualized investment cost (AIC) calculated with a specified discount rate and the total annual outcomes after taxes.
Economic	Capital cost	C_TM	The capital cost is the combination of one-time expenditures or fixed capital investments and the working capital investments.
Economic	Manufacturing cost	СОМ	Costs related with the day-to-day operation of a manufacturing plant.
Energy	Total energy consumption	E _{total}	Total energy consumed by the process or process unit as primary fuel equivalent.
Energy	Specific energy intensity	R _{SEI}	Total energy consumed by the process or process operating unit as primary fuel equivalent per unit mass of product.
Energy	Energy intensity	R _{EI}	Measurement of the net fuel-energy consumed to provide the heat and the power requirements for the process per unit of sales revenue or value added.
Material Efficiency	Mass intensity	MI	MI is defined as the ratio between the total mass fed to the unit over the mass of the desired product.
Material Efficiency	Environmental factor	E	E factor is the ratio of the mass of waste per unit of mass of the desired product.

Additional custom indicators were also implemented into the GREENSCOPE tool. The customization is to adhere to making logical decisions with the project objective and also to use in comparison with common wastewater treatment design metrics in other works. The custom indicators are supplied in **Table 8-4**.

Table 8-4. Custom indicators added for sustainable design assessment.

Category	Indicator	Label	Brief Definition
Economic	Levelized cost of water including capital	LCW _{CAP}	Cost of water treatment including annuitized capital per unit volume of the purified water.
Economic	Levelized cost of water	LCW	Cost of water treatment per unit volume of the purified water.
Energy	Specific chemical- energy intensity equivalent	R _{SCEI}	Total energy equivalent of treatment chemicals used in the process as primary fuel equivalent per unit mass of product.
Material Efficiency	Water recovery	WR	Fraction of water recovered as reusable product.
Material Efficiency	Contaminant removal	CR	Fraction of contaminants rejected by the treatment process.

The process simulation results are communicated to the process analysis infrastructure by the workflow shown in **Figure 8-12**.

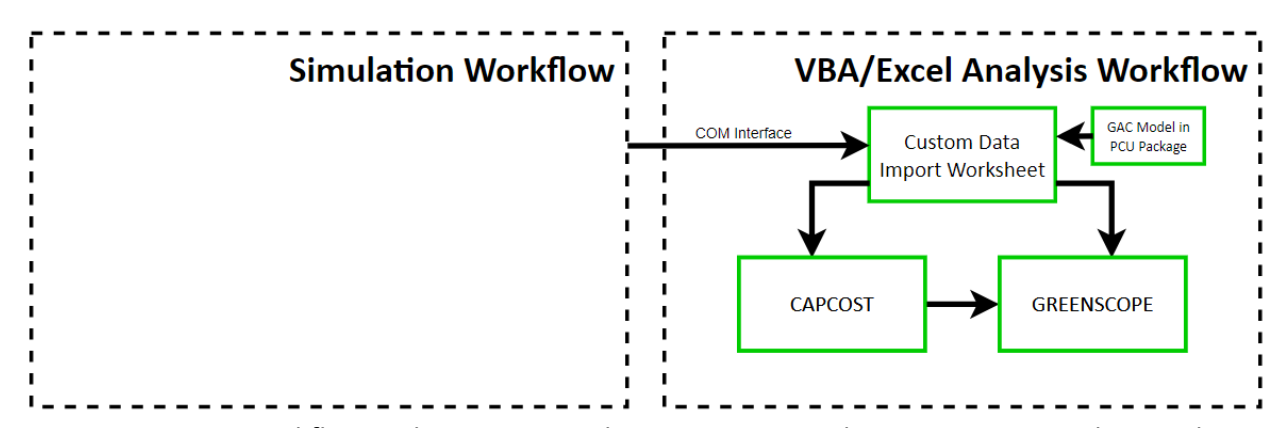


Figure 8-12. VBA workflow with CAPCOST and GREENSCOPE tools as it connects to the simulation workflow presented in full in Figure 8-2.

8.5. Optimization

8.5.1. Optimization Strategy

The optimization goal would be to minimize a single major objective considering added complexity of multi-objective optimization. This objective should largely be an economic metric but also be indirectly relevant to minimizing chemical and energy demands as well as water reuse. Levelized cost of water including capital was selected as the objective function. Treatment costs, chemical and energy demands, resource allocation, water recovery, and product value are captured through costing equivalents within the LCW_{CAP} expression.

The following challenges are present given the problem formulation: (i) the computational complexity (and associated expense) of the process model would need to be reduced to have the optimizer converge within a reasonable amount of time; (ii) the high dimensionality if all decision variables are considered brings inherent challenges to the

optimization; (iii) the model accuracy must be retained within the complex softening unit, but rigorous calculations by the OLI thermodynamics are not easily captured by reduced-order models; and (iv) MED and RO units require topological optimization for their number of stages creating an integer problem not capable of investigation in Aspen Plus, as depicted in **figure 8-13**.

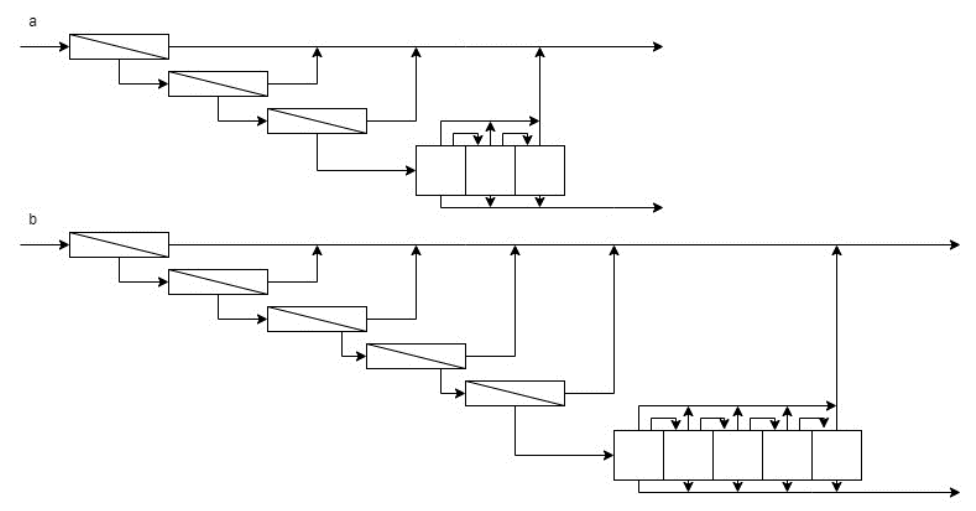


Figure 8-13. (a) a 3-stage RO/3-stage MED; and (b) 5-stage RO/5-stage MED. Each block represents separate equipment models in Aspen Plus. If bound between 3 and 5 stages for both units, 9 possible combinations can exist. If optimizing directly in Aspen Plus, all 9 of these designs would have to be generated and optimized independently. When expanding the bounds between 1 and 10 stages for both units, 100 combinations would become possible that would be exhaustive to optimize.

The strategy that was determined to be compatible and overcome these challenges is a hybrid surrogate optimization. The MATLAB toolbox that has been implemented is an NLP-based surrogate optimizer (Caballero & Grossmann, 2008). In this methodology, Latin hypercube sampling (LHS) is used to generate a decision variable set (of a defined size) that is unbiased and well dispersed throughout the input space. These inputs are applied to the original model and the outputs are recorded. A new machine learning-based model is constructed using Kriging surrogates trained by the initial set. The new surrogate model is optimized using a conventional NLP solver at a lower expense. As iterations within the optimization progress, outputs from the surrogate model are compared with that of the original model. Based on the accuracy of the results, the Kriging surrogate is improved for accuracy as it approaches the optimum design (Alves et al., 2018).

This methodology has been shown to solve computationally expensive Aspen Plus simulations with optimization problems of lower dimensionality (Quirante & Caballero, 2016). This method was selected as it addresses several of the challenges presented and is adapted to satisfy any remaining aspects of the cotreatment process. The surrogate that is to be trained for the optimizer effectively reduces model equations to a black-box that can be efficiently simulated and more easily optimized. The developed solution has allowed for softening to be simulated by

Aspen Plus (to keep its accuracy) and the remaining units and associated costing to be modeled by simplified MATLAB functions.

To reduce the dimensionality of the problem, a smaller subset of decision variables was selected to consider for optimization and are presented in **Table 8-5**. Variables included significantly affect process design. The effects may be used to adjust process costs or meet various product or operating constraints. These constraints are directly imposed in the MATLAB model.

Table 8-5. Decision variables of the process optimization.

Process Unit	Decision Variable		
	Blowdown water volumetric flowrate		
	NaOH mass flowrate		
Softening and Filtration	Na ₂ CO ₃ mass flowrate		
	HCl mass flowrate		
	Air mass flowrate		
Poverse Osmesis (PO)	Number of stages*		
Reverse Osmosis (RO)	Inlet pressure (by stage)		
Electrolysis	Membrane area		
	Stage 1 pressure		
Multi-Effect Distillation (MED)	Stage 1 brine outlet vapor fraction		
	Number of stages*		

^{*}Integer variables

With challenges to the model being addressed, the optimization strategy would still need to be adapted considering that this mixed integer nonlinear programming (MINLP) problem is to be applied to a nonlinear programming (NLP) solution strategy. For integer decision variables, the values generated by the LHS and later the optimizer are relaxed.

The simplified model can output an LCW_{CAP} provided a set of decision variables in approximately 20-40 seconds (**Figure 8-14**). This compares to the full process infrastructure taking over 20 minutes to complete. The simplified model thus provides a more practical simulation model to run a large number of iterations for optimization purposes.

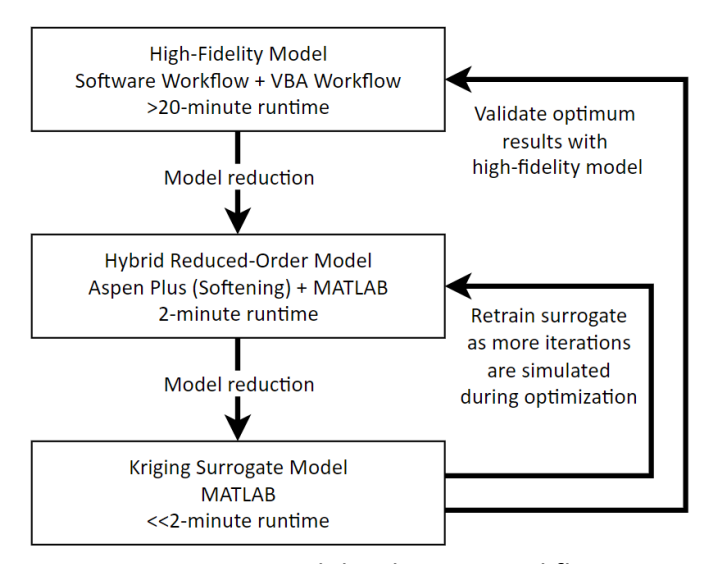


Figure 8-14. Model reduction workflow.

Using the LHS, sensitivity of decision variables was performed from the preliminary case. Feasibility flags placed in the optimization routine allowed for a feasible base case to be determined where all constraints were met. Beginning the optimization from this point, decision variables were sampled at small ±1% margins to create the training set. This was required to retain as many feasible points as possible in the tightly constrained problem. As the optimizer converged to a local minimum, the local optimum point was defined as the new centralized point for the next iteration. The decision variable bounds were again sampled at small margins and the optimization repeated until no variables converged to their bounds. This methodology may not fully explore nonconvex regions but was required to have sufficient data points simulated for a training set at a targeted range of conditions to produce an accurate and timely simulated surrogate model.

8.6. Results and Conclusions

Once obtained the optimized conditions, the solution of decision variables is reapplied to the rigorous flowsheet in **Figure 8-15** for more detailed results.

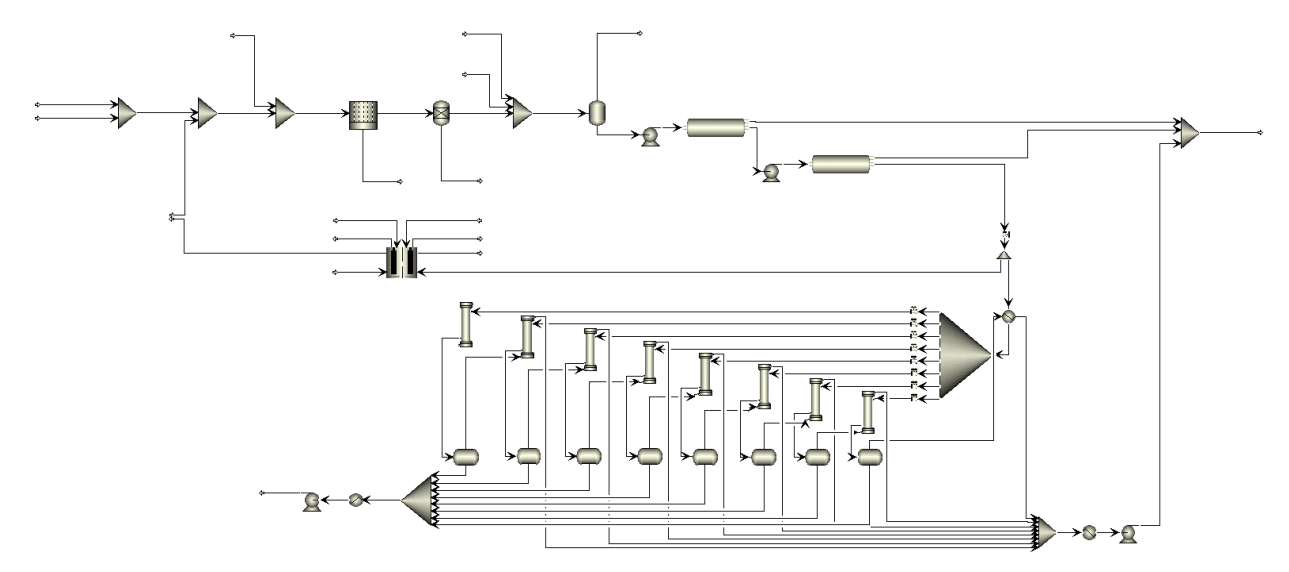


Figure 8-15. Aspen Plus flowsheet design of the optimization cotreatment process.

Notable optimized variables include a mixing ratio of approximately 25:1, 2 stage reverse osmosis, and 8 stage MED. The optimized design configuration resulted in a LCW_{CAP} of $3.81 \mbox{ } / \mbox{m}^{3}$ and LCW of $2.08 \mbox{ } / \mbox{m}^{3}$ when omitting annuitized capital.

The GREENSCOPE results for the preliminary design, optimized cotreatment design, exclusive blowdown treatment variation design (not optimized) using the softening and MED and produced water disposal by injection are compared in **Figure 8-16**. In this visualization, KPIs are normalized between 0 (least) and 100% (most sustainable), where an expanded plot indicates a more holistically sustainable process.

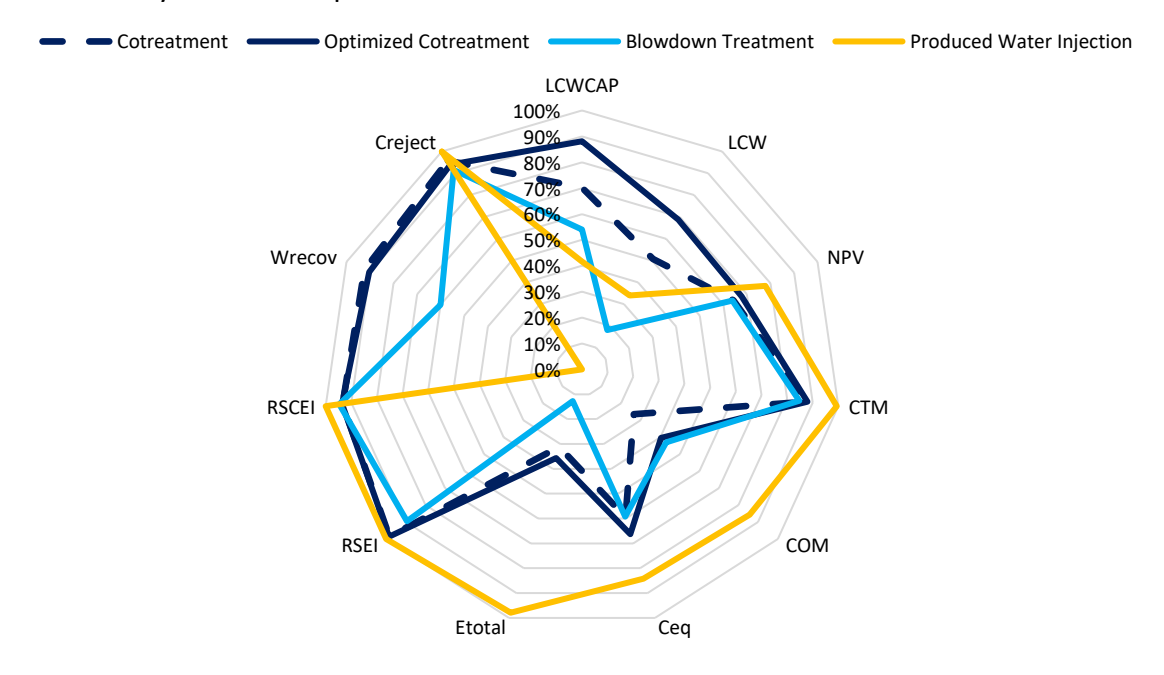


Figure 8-16. Radar plot comparing selected GREENSCOPE KPI's for the water treatment designs

considered

From the process designs, conclusions based on the optimization can be made. To meet both potable water and 10-lb brine constraints, unwanted ions must be completely removed or have their feed limited in the process. Produced water, by composition, introduces many of the ions restricted in RO and electrolysis operation, as well as in potable water and brine composition. The optimization solution converged to using lower amounts of produced water given these restrictions. Produced water for mixing is still advantageous in low quantities. At these mixing ratios, the transportation cost for importing produced water becomes significantly lower than the use of other softening chemicals. As more produced water is used, unwanted ions difficult to remove are introduced in higher quantities and leads to design infeasibility.

The optimum solution approaches a LCW of 2 \$/m³ which becomes cost competitive with nominal water treatment prices. The costing for this process was performed assuming all worst-case scenarios. Considering this, if features of the complimentary power plant process may be utilized, this process shows attractive potential for blowdown treatment processes in specific localized regions.

Reviewing the sustainability features of this process, the optimized cotreatment holistically outperforms other analyzed designs. Produced water injection proves best economically but fails in most sustainability metrics. Of the other designs, the optimized cotreatment process performs best in economic KPI's. Water recovery, specific energy and chemical-energy equivalent intensity of the cotreatment process are also improved when compared to standalone blowdown treatment.

Products

- H. Barber and F. V. Lima. Modeling, Simulation and Optimization of a Synergistically Mixed Blowdown Water and Produced Water Wastewater Treatment Process. Presented at 2021 AIChE Annual Meeting, Boston, MA, Nov. 7-9, 2021.
- H. Barber and F. V. Lima. Optimization of a Wastewater Cotreatment Process for Blowdown and Produced Waters with Economic and Sustainability Analyses. Submitted for presentation at 2022 AIChE Annual Meeting, Phoenix, AZ, Nov. 13-18, 2022.
- Synergistically Mixed Blowdown Water and Produced Water Wastewater Treatment Process: Modeling and Software Approaches for Rigorous Water Treatment Simulation (Working title and manuscript in progress).
- Synergistically Mixed Blowdown Water and Produced Water Wastewater Treatment Process: Surrogate Optimization for Complex Wastewater Treatment Flowsheets with Economic and Sustainability Assessment (Working title and manuscript in progress).

References

- Alves, V. M. C., Lima, F. S., Silva, S. K., & Araujo, A. C. B. (2018). Metamodel-Based Numerical Techniques for Self-Optimizing Control. *Industrial & Engineering Chemistry Research*, *57*(49), 16817–16840. https://doi.org/10.1021/acs.iecr.8b04337.
- Boussouga, Y. A., & Lhassani, A. (2017). Study of mass transfer mechanisms for reverse osmosis and nanofiltration membranes intended for desalination. *Journal of Materials and Environmental Sciences*, 8(3), 1128–1138.
- Caballero, J. A., & Grossmann, I. E. (2008). An algorithm for the use of surrogate models in modular flowsheet optimization. *AIChE Journal*, *54*(10), 2633–2650. https://doi.org/10.1002/aic.11579.
- Du, F., Warsinger, D. M., Urmi, T. I., Thiel, G. P., Kumar, A., & Lienhard V, J. H. (2018). Sodium Hydroxide Production from Seawater Desalination Brine: Process Design and Energy Efficiency. *Environmental Science & Technology*, 52(10), 5949–5958. https://doi.org/10.1021/acs.est.8b01195.
- DuPont Water Solutions. (2020). *Product Data Sheet: FilmTec™ Membranes* (Issue Form No. 45-D01519-en Rev. 2). https://www.dupont.com/content/dam/dupont/amer/us/en/water-solutions/public/documents/en/RO-FilmTec-SW30-Seawater-PDS-45-D01519-en.pdf.
- Intrepid Fluids. (n.d.). *10 LB BRINE with K-Control*. Intrepid. http://www.intrepidpotash.com/wp-content/uploads/2017/02/Spec-Sheet-10-LB-Brine-8-3-17.pdf.
- James III, R. E., Kearins, D., Turner, M., Woods, M., Kuehn, N., & Zoelle, A. (2019). *Cost and Performance Baseline for Fossil Energy Plants Volume 1: Bituminous Coal and Natural Gas to Electricity*. https://doi.org/10.2172/1569246.
- Kosmadakis, G., Papapetrou, M., Ortega-Delgado, B., Cipollina, A., & Alarcón-Padilla, D. C. (2018). Correlations for estimating the specific capital cost of multi-effect distillation plants considering the main design trends and operating conditions. *Desalination*, *447*, 74–83. https://doi.org/10.1016/j.desal.2018.09.011.
- Lenntech. (n.d.). Osmotic pressure calculator. https://www.lenntech.com/calculators/osmotic-pressure.htm.
- Li, S., Feliachi, Y., Agbleze, S., Ruiz-Mercado, G. J., Smith, R. L., Meyer, D. E., Gonzalez, M. A., & Lima, F. v. (2018). A process systems framework for rapid generation of life cycle inventories for pollution control and sustainability evaluation. *Clean Technologies and Environmental Policy*, 20(7), 1543–1561. https://doi.org/10.1007/s10098-018-1530-6.
- McGovern, R. K., Weiner, A. M., Sun, L., Chambers, C. G., Zubair, S. M., & Lienhard V, J. H. (2014a). On the cost of electrodialysis for the desalination of high salinity feeds. *Applied Energy*, *136*, 649–661. https://doi.org/10.1016/j.apenergy.2014.09.050.
- McGovern, R.K., Zubair, S.M., Lienhard, J.H. (2014b). The benefits of hybridising electrodialysis with reverse osmosis, *J. Membr. Sci.*, 469, 326-335.
- Nayar, K. G., Fernandes, J., McGovern, R. K., Al-Anzi, B. S., & Lienhard, J. H. (2019). Cost and energy needs of RO-ED-crystallizer systems for zero brine discharge seawater desalination. *Desalination*, 457, 115–132. https://doi.org/10.1016/j.desal.2019.01.015.
- Puder, M. G., & Veil, J. A. (2006). Offsite commercial disposal of oil and gas exploration and production waste: availability, options, and cost. https://doi.org/10.2172/898533.
- Quirante, N., & Caballero, J. A. (2016). Large scale optimization of a sour water stripping plant using surrogate models. *Computers & Chemical Engineering*, *92*, 143–162.

- https://doi.org/10.1016/j.compchemeng.2016.04.039.
- Ruiz-Mercado, G. J., Smith, R. L., & Gonzalez, M. A. (2012). Sustainability Indicators for Chemical Processes: I. Taxonomy. *Industrial & Engineering Chemistry Research*, *51*(5), 2309–2328. https://doi.org/10.1021/ie102116e.
- Sánchez-Aldana, D., Ortega-Corral, N., Rocha-Gutiérrez, B., Ballinas-Casarrubias, L., Pérez-Domínguez, E., Nevárez-Moorillon, G., Soto-Salcido, L., Ortega-Hernández, S., Cardenas-Félix, G., & González-Sánchez, G. (2018). Hypochlorite Generation from a Water Softener Spent Brine. *Water*, *10*(12), 1733. https://doi.org/10.3390/w10121733.
- Survey, U. S. G. (2020). Mineral Commodity Summaries. In *U.S Department OF The Interior, U.S Geological Survey* (Issue 703). https://doi.org/10.3133/mcs2020.
- Turton, R. A., Shaeiwitz, J. A., Bhattacharyya, D., & Whiting, W. B. (2018). *Analysis Synthesis and Design of Chemical Processes* (5th Edition). Pearson Education.
- United States Environmental Protection Agency, O. of W. (1999). Sequencing batch reactors. In WastewaterTechnology Fact Sheet: Sequencing Batch Reactors, EPA 932-F-99-073.
- U.S. Energy Information Administration. (2019). Form EIA-860, Annual Electric Generator Report, Form EIA-861, Annual Electric Power Industry Report, Form EIA-923, Power Plant Operations Report and predecessor forms.
- Wang, P., Anderko, A., & Young, R. D. (2002). A speciation-based model for mixed-solvent electrolyte systems. *Fluid Phase Equilibria*, 203(1–2), 141–176. https://doi.org/10.1016/S0378-3812(02)00178-4.
- Wenzlick, M., & Siefert, N. S. (2020). Techno-economic analysis of converting oil & produced water into valuable resources. *Desalination*, *481*(November 2019), 114381. https://doi.org/10.1016/j.desal.2020.114381.
- West Virginia Department of Environmental Protection, D. of O. and G. (2019). *Database and Map Information*. 2019 Production Data. https://dep.wv.gov/oil-and-gas/databaseinfo/Pages/default.aspx.
- Wiesner, M. R., Hackney, J., Sethi, S., Jacangelo, J. G., & Laîé, J.-M. (1994). Cost estimates for membrane filtration and conventional treatment. *Journal American Water Works Association*, 86(12), 33–41. https://doi.org/10.1002/j.1551-8833.1994.tb06284.x.
- Yang, L., Salcedo-Diaz, R., & Grossmann, I. E. (2014). Water Network Optimization with Wastewater Regeneration Models. *Industrial & Engineering Chemistry Research*, *53*(45), 17680–17695. https://doi.org/10.1021/ie500978h.
- Zhou, Y., & Tol, R. S. J. (2005). Evaluating the costs of desalination and water transport. *Water Resources Research*, 41(3), 1–10. https://doi.org/10.1029/2004WR003749.